Authors' response document bg-2017-181. Tom Jilbert 19.11.2017

Contents

1.Responses to online discussion Referee #1 (Peter Kraal)

The following document contains both the responses given during the Open Discussion of "Flocculation of dissolved organic matter controls the distribution of iron in boreal estuarine sediments" and a description of the subsequent revisions leading to the submission of "Impacts of flocculation on the distribution and diagenesis of iron in boreal estuarine sediments".

[Referee comments in bold]

[Responses in italics]

[Indication of subsequent revisions in regular text]

With interest I have read this manuscript, in which the authors explore the role of salinity-driven flocculation of DOM and dFe in controlling the settling and diagenetic fate of riverine Fe along a salinity transect in a Baltic Sea estuary. The authors suggest a key role for flocculation in transferring Fe(III) in the form of Fe(III)-OM complexes and Fe(III) (oxyhydr)oxides from the water column to the sediment. Moreover, the Fe-OM pool is relatively stable and this Fe does not seem to participate in the "normal" reductive diagenetic pathways in organic-rich sediments. The manuscript is well-written, well-structured and an interesting addition to the flourishing research field of Fe-OM interactions in marine and terrestrial systems.

Together with this review, I have uploaded an annotated pdf document with all my questions and comments. Below, I highlight the main questions that arose while reading the manuscript.

We thank the referee for the careful consideration of our manuscript. Below, we respond to each of the major comments followed by the line-by-line comments extracted from the referee's annotated pdf.

1. On a technical note: If I understand correctly, relative errors for all solid-phase analyses were calculated from replicate analysis of "regular" (powdered) reference materials. I wonder whether this gives relative errors that are also representative for analysis of suspended material on filters. As far as I am aware, such samples are somewhat harder to process and I am curious to know if the authors can comment on how/whether they specifically assessed analytical precision and accuracy associated with filter samples (or why not).

For the analysis of suspended organic matter, complete filters were combusted after packing and compression in tin cups. This avoids issues of heterogeneity within individual filters and this detail will be added to the methods section. We did not take systematic replicates for all GF/F filters due to limitations of sample volume and processing time. However for each site we did take an additional

water column sample from <1m above the seafloor. At the stations where this sample is close to (within 2 vertical meters of) the deepest 5m depth interval sample, we suggest it may be used as a replicate to assess precision between filters (with the added value of coming from a separate sampling cast rather than simply being a duplicate from the same Limnos bottle). When this is done we see that the $\delta^{13}C$ and N/C values for the extra sample are within the analytical error of the sample from the deepest 5m depth interval (see Fig. R1). Hence we conclude that precision for this data is in fact limited by the analysis and not by the sampling procedure. In terms of accuracy, this can only be determined by reference materials analyzed in parallel to the samples. This was done routinely (two standards for every ten samples) and showed accuracy to be <2.5% as stated in the manuscript.

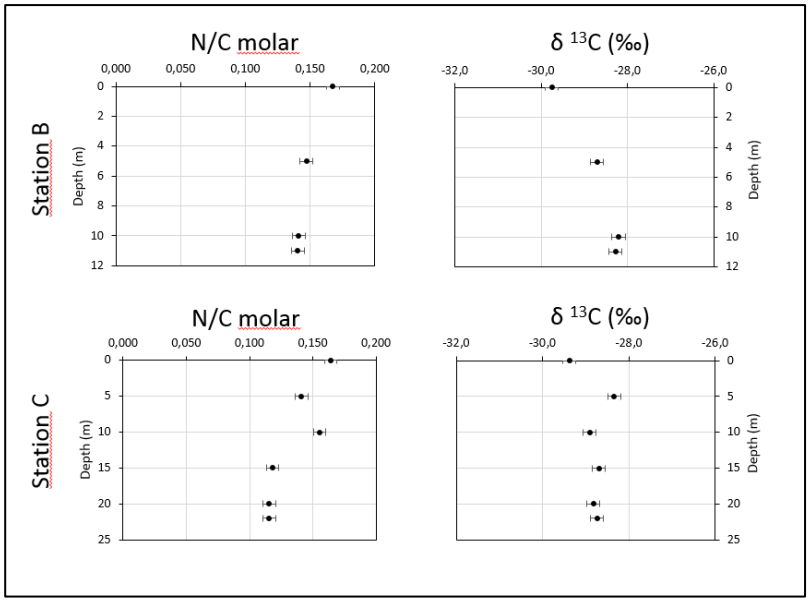

Figure R1: N/C (mol) and $\delta^{13}C$ of suspended particulate matter at Stations B and C. All data presented here, except for the deepest sample at each station (taken from <1 m above the seafloor), are included in Fig. 3 of the manuscript. Here, the sample from <1 m above the seafloor is treated as a replicate for the deepest 5m sampling interval for each station (depth offset = approx. 1 m for Station B, approx. 2 m for Station C). Horizontal error bars indicate analytical precision, reported as one standard deviation, as determined by 10 repeated measurements of standard materials (N/C =0.005, $\delta^{13}C$ = 0.15 ‰).

When the corresponding exercise is carried out for $Fe_{part.}$ from the polycarbonate filters we observe relative standard deviation (RSD) of up to 15% for "replicate" deep water samples. This is substantially greater than the RSD values for $\delta^{13}C$ and N/C (both less than 1 % in Fig. R1). We interpret this as a consequence of the fact that $\delta^{13}C$ and N/C describe the characteristics of the suspended organic material, but are largely insensitive to variations in its total concentration at a given location. $Fe_{part.}$, on the other hand, describes the absolute concentration of particulate Fe in µmol/L, which (similarly to the absolute concentration of organic matter) is likely to vary on small spatial and temporal scales and may well change in the 10–15 minute interval between Limnos casts at a given location. It should however be noted that the error associated with an RSD of 15%, particularly for low-Fe samples, is several orders of magnitude less than the large-scale changes in $Fe_{part.}$ observed along the salinity gradient which are discussed in the manuscript (Mean value at Station A = 2.54 µmol/L, σ = 1.98 (n = 2); mean value at Station K = 0.30 µmol/L, σ = 0.10 (n = 10)). The concentration of $Fe_{part.}$ at Station A is thus 25 times greater than at Station K.

The revised manuscript makes reference to the above clarifications (Section 3.2).

2. There is no information provided on which standards were analyzed with Mössbauer spectroscopy (or whether reference spectra collected previously were included) and how the selection of (number of) standards for LCF was performed. The LCF fitting routine was only explicitly mentioned in the caption to Fig. 5; it should also feature in the main methods section.

The key statement "Quantification of iron-bearing phases and iron oxidation states is based on relative subspectral areas" may be expanded a bit (as it is to some extent in the notes of Table 3). Overall, the procedure of obtaining relative proportions, including that of the "undocumented" Fe phase (in my opinion an awkward term, perhaps "unknown" is more appropriate?), should be more clear, as this phase plays a rather crucial role in the manuscript. Goodness-of-fit is also an important parameter in this respect, as it is basically the (areal) mismatch between the fit and the actual spectrum that is used as a measure of "undocumented" Fe. I think it would be good if all (relevant) reference spectra (perhaps including likely candidates that were not present such as siderite) are clearly presented (they are somewhat hard to discern in the current Figure 5: perhaps a stack plot with offset would work).

We thank the referee for highlighting the need for a more detailed presentation of the Mössbauer approach. To clarify, the LCF fitting was performed using reference spectra rather than freshly prepared and analyzed standards. In the revised version, we will list the reference materials considered, present their spectra, describe how the selection for the LCF was performed, and expand the discussion of the LCF fitting procedure itself including goodness of fit. Furthermore we are in the process of generating Mössbauer spectra of additional sediment samples from the estuarine transect. When presenting these results in the revised manuscript we will consider the referee's terminological suggestions regarding the use of the terms "undocumented" vs. "unknown" Fe phases.

The revised manuscript includes substantially expanded sections on Mössbauer spectroscopy, including further details of the methodology (Section 3.10), and new results and revised interpretations of the spectra (Section 4.7).

3. The authors assign the "undocumented" Fe phase fully to complexes of non-sulfidized Fe(II) with organic matter (p 12, L 17-19). They base this on the study of Yu et al. (2015), who found Fe(II)-OM phase "to be a major component of sedimentary Fe in a nearby boreal estuary." In the Yu et al. study, OM-complexed Fe(II) was identified by Fe X-ray absorption spectroscopy using standards of Fe(II) and Fe(III) complexed with organic matter. As far as I could see, no empirical data in support of the assumption of OM-Fe(II) is provided in this manuscript. Because the Fe(II)-OM phase plays such an important role in the discussion, I wonder whether the authors can further substantiate their assumption that all the "undocumented" Fe, that could not be assigned to their (to the reader unknown) library of standards, was present as Fe(II)-OM? It should be clear exactly which Fe phases could be ruled out based on LCF with reference spectra. Some more focus on which spectral features could not be explained by the available reference standards, and how these may point to OM-associated Fe, would also be welcome. In the absence of a "smoking" gun, perhaps some more consideration should be given to the fact that OM-Fe(II) may not necessarily account for all "undocumented" Fe (to what extent do fitting uncertainties play a role?). In particular, the authors may want to address the validity of extrapolating Mössbauer data (key for assigning Stage 3 and 4 Fe to OM-Fe(II)) for the uppermost sample (0-1 cm) to the whole sediment record (up to 60 cm) at all sites (see also Comment 7).

Our detailed response to this comment is partly dependent on the ongoing Mössbauer analysis of an additional five sediment samples from the estuarine transect. In total, the new dataset will comprise seven samples (riverbed sediment, shallow + deep sediment from Station A, shallow + deep sediment from Station D, shallow + deep sediment from Station J). At the time of writing, four of the additional 5 samples have been measured and the fifth is in progress. Analysis of these spectra will be performed by LCF using references, and as stated in the response to the previous comment, the references used

in the LCF (and the rationale for their selection) will be explicitly stated in the manuscript, complete with presentation of spectra.

See previous. The revised manuscript includes substantially expanded sections on Mössbauer spectroscopy, including further details of the methodology (Section 3.10), and new results and revised interpretations of the spectra (Section 4.7).

We have also performed additional sediment extractions on 15 samples from Stations A, D and J to investigate the robustness of our initial conclusions concerning the dominance of OM-Fe(II) in Stages 3 and 4 of the Poulton and Canfield (2005) method. These results will be included in the revised manuscript and considered alongside the new Mössbauer data. In brief, we carried out parallel extractions of subsamples dried under N_2 after frozen storage, and treated under anoxic conditions as follows:

Subsample 1: 1M HCl, 1 hr (including trap for H_2S evolved from Acid Volatile Sulfur)
Subsample 2: 1 M HCl + 1 M hydroxylamine-HCl, 1 hr
Subsample 3: 0.2 M Sodium citrate at pH 4.8, 2 hr

Fe (II) in each extract was then determined by spectrophotometry after complexation with 1,10 phenanthroline, while AVS was determined by iodometric titration. This approach is similar to that used by Yu et al. (2015) to determine sulfidized vs. unsulfidized Fe (II), and Fe(II) /Fe(III), in the cold 1M HCl-soluble fraction of boreal estuarine sediments. However we also included Subsample 3 to mimick Stage 3 of the Poulton and Canfield extraction – but excluding dithionite – to test the hypothesis that the citrate ligand alone may be able to extract Fe (II) direct from OM-complexes. This specifically addresses a comment of Referee #2 concerning our interpretations of citrate-dithionite-soluble (i.e. nominally reducible) Fe as Fe (II).

The results of the additional extractions suggest that our initial assumptions concerning the solubility of OM-Fe (II) in Stages 3 and 4 may indeed require modification. We do detect unsulfidized Fe(II) in the HCl extracts, and its concentration in most samples is higher than both sulfidized Fe (II) (AVS) and HCl-soluble Fe (III) (derived from the difference between Subsamples 1 and 2, see Figs. R2 and R3). Furthermore the parallel citrate-only extraction does appear to dissolve approximately 60% of the unsulfidized Fe (II) pool (see Fig. R4). While these observations support our claim that OM-Fe(II) complexes are present in the sediments and suggest that at least a fraction of this material is citrate-soluble, the total amount of Fe dissolved in the additional extracts is equivalent to (only) the combined total from Stages 1 and 2 of the Poulton and Canfield (2005) procedure (Fig. R5). Hence, the Fe phases dissolved by 1M HCl are likely identical to those dissolved by sodium acetate and hydroxylamine-HCl, while the Stage 3- (citrate-dithionite) soluble Fe fractions remain largely intact during the 1M HCl extraction.

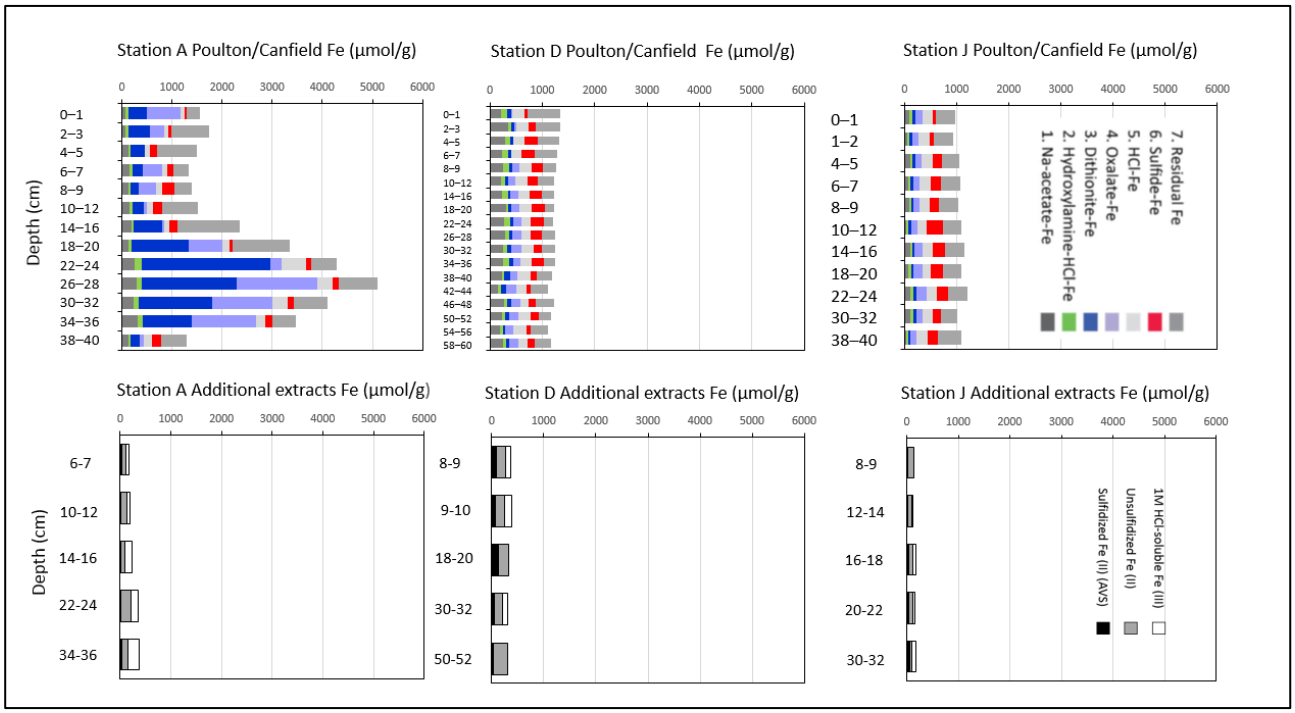

191
192
193

<u>Fig. R2:</u> Comparison of Fe extraction data for the Poulton and Canfield (2005) method reported in the original manuscript (upper panels), and additional extractions with 1M HCl performed in response to the interactive discussion comments (lower panels). All panels are plotted on the same scales for comparability. Where possible, samples for the additional extractions were selected from the set originally extracted by the Poulton and Canfield method. When no sample material was remaining, adjacent samples were taken (n=4).

194
195

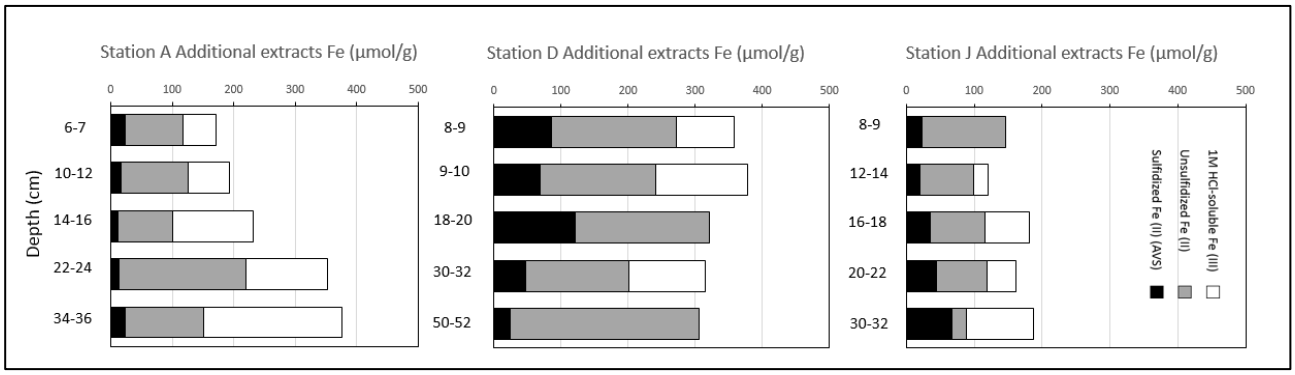

196

<u>Fig. R3:</u> Zoom of lower panels of Fig. R2 for clarity.

197
198
199

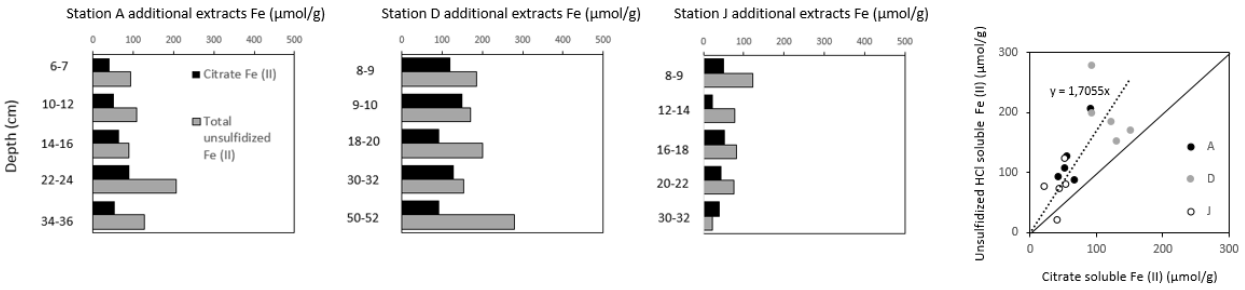

Fig. R4: Comparison of citrate-soluble Fe (II) (Subsample 3) and total unsulfidized Fe (II) (derived from Subsample 1) for the additional extraction samples. Note that approximately 60% of total 1M HCl-soluble unsulfidized Fe (II) is extracted by the citrate solution, as given by the relationship in the final panel (solid line in this panel indicates 1:1).

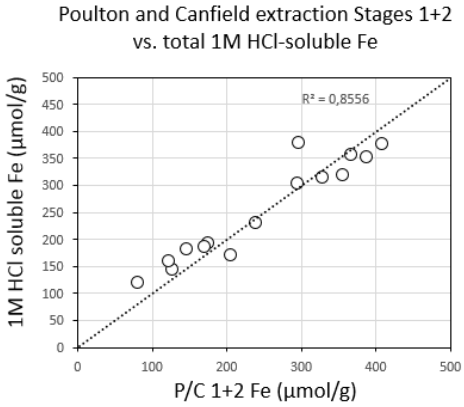

Fig. R5. Relationship between Fe extracted in Stages 1+2 of the Poulton and Canfield method, and total 1M HCl-extractable Fe in the additional extractions. Where no equivalent sample was available, adjacent samples have been compared (n =4). Dashed line represents 1:1 and the least-squares regression is performed against this line.

Therefore, assuming the 1M HCl extraction to be a reliable determinant for OM-Fe(II) as suggested by Yu et al., 2015, we should modify our interpretation of the composition of the phases dissolved in Stages 3 and 4 of the Poulton and Canfield method. We hope that the forthcoming Mössbauer data will clarify this issue, especially the deep sample from Station A, whose combined Stage 3 and Stage 4-soluble Fe pool is in excess of 3000 µmol/g sediment (i.e. 16.8% of the sediment by weight).

We have revised our interpretations of the Fe speciation substantially on the basis of both the additional extraction results and the new Mössbauer data. Figures R2 , R3 and R5 are incorporated into the revised manuscript (in Figures 5, 6a and 6b respectively) and an extensive new interpretation of Fe phases in the sediments is given (Table 3, Sections 4.6, 4.7).

4. p 14, L 13-19. The authors attribute the excess removal of Fediss relative to DOC to "preferred association of Fe with higher molecular weight compounds, which are more sensitive to flocculation (Asmala et al., 2014) or a mechanistic enhancement of flocculation by the presence of Fe (Forsgren et al., 1996)." Firstly, the second mechanism deserves some explanation (it now implies enhancement of flocculation of Fe by Fe?). Secondly, as the authors

also observe a ferrihydrite signal in their Fe flux to the sediment, could flocculation of Fe independent of DOM -> POM dynamics play a role in the removal of Fe from the water column (driven by salinity, pH, perhaps DO)? The authors mention that "Flocculated material in the oxic estuarine water column is likely present as Fe (III) partitioned between organic-Fe (III) complexes and ferrihydrite (Neubauer et al., 2013)." (p 16, L 20-21). Changes in surface charge of Fe(III) particles due to adsorption of ions at higher salinity may also affect the solubility/flocculation of Fe(III) particles?

We will clarify these statements in the revised manuscript. Several authors have noted that the respective behavior of Fe and bulk OM along salinity gradients in Baltic Sea estuaries differ significantly, with non-conservative behavior being much more apparent for Fe. This may indeed imply additional mechanisms for flocculation that are specific to Fe, rather than simply to the fraction of OM to which Fe is associated (the context within which this statement was written). These include, as the referee suggests, direct flocculation of Fe oxides in response to pH changes. Typically, pH of the the Mustionjoki river drainage is in the order 6.0–6.5 (Lahermo et al., Geochemical Atlas of Finland, 1996). Along the salinity gradient in the surface waters of the estuary, pH indeed rises, towards the offshore value of 8.0–8.4 in the open Gulf of Finland (exact value depends on season, e.g., Omstedt et al., Tellus B, 62B, 2010), due to mixing between fresh and brackish water masses. As outlined in Neubauer et al., ES&T 47, 2013, pH – independent of salinity – may determine the partitioning of Fe between NOM-Fe complexes and ferrihydrite, and between different size classes of ferrihydrite in natural waters (their Figure 1e). In their model, freshwater at pH 6 should already contain a substantial fraction of Fe oxides that would not pass through a 0.2µm filter. We used 0.4µm filters, but nevertheless measured a majority of Fe in the particulate phase in the freshwater endmember sample (surface water of Station A, Fig. 2) which supports the Neubauer et al. model for a pH 6.0–6.5 river. However we see an immediate loss of particulate Fe between Stations A and B, despite the onset of the salinity gradient and hence the rise in pH. This suggests that also current strength influences the concentration of this material in the water column, due to its susceptibility to sedimentation. Further offshore, we observe a second maximum in particulate Fe (Fig. 2) which we attribute to flocculated formerly dissolved material. We cannot discount that pH, increasing in tandem with salinity, influences this process. The density of minerogenic matter such as clays may also influence the likelihood of flocculation in boreal estuaries (as discussed in Forsgren et al., 1996).

In the revised manuscript we emphasize the partial decoupling of Fe from DOM during flocculation (see revised Title, Abstract, Introduction paragraph 4, Section 5.2).

5. The reasoning behind the conclusion "that flocculation of DOM to POM in the estuarine environment may provide the second fraction of POM detected in the N/CPOM and 13CPOM data." is somewhat unclear to this non-expert in that field (Fig. 3 and 4 and section 5.3). The authors state that the POM signal in surface waters is dominated by phytoplankton and therefore DOM-POM transitions cannot be discerned in N/CPOM vs 13CPOM signature of surface water-DOM from a previous study plot in the field of C3 plant material, suggesting that phytoplankton is not an important component of surface water DOM? I found this in itself surprising, as I would expect the DOM to be impacted by decomposition (POM -> DOM) of fresh algal material.

To answer this point first: It is true that degradation of phytoplankton material may theoretically impact on DOM content (and therefore net composition). However in this system the mass balance argues against such a hypothesis. Concentrations of river-derived DOM in the estuary are an order of magnitude greater than the potential supply from degrading phytoplankton. In the study of Asmala et al., Biogeosciences 10, 2013, DOM concentrations along the salinity transect of the Mustionjoki

estuary declined from 585 µmol/L in river water to 363 µmol/L in the offshore endmember (average of three seasons). As shown in the same study (and in our Fig. 3), despite transformations in the estuarine environment including flocculation and utilization of DOM in foodwebs, bulk DOM retains a strongly "terrestrial" C/N (or (N/C) ratio even in the offshore region. In this study, we measured POC in the range of 20–60 µmol/L for most stations (see Fig. R7 and convert to molar units). Hence, complete degradation of this material to DOM would yield only minor changes in the C/N (or (N/C) ratio. We will rephrase the text to emphasize this.

In the revised manuscript we emphasize the magnitude of the DOM pool in this system and its persistent terrestrial character as determined by N/C and $\delta^{13}C$ (Section 5.1).

The POM data from deeper waters from this study plot towards the C3 plant signature. The authors use this trend as an indication that the second OM source besides phytoplankton, i.e. C3 plant material, is transferred from DOM to POM through flocculation. I wonder whether the POM N/CPOM vs 13CPOM plots cannot also be determined/impacted by magnification of the C3 signal in the POM reservoir below the phytoplankton-dominated surface waters? I guess this strongly depends on the "rapid remineralization of fresh phytoplankton material during settling" (p 15, L8-9) which would remove the phytoplankton signal from POM and DOM and the persistence of the phytoplankton POM signal.

Our conceptual model for interpreting the plots in Fig. 3 is that there are essentially two end-members of POM in the estuarine water column: phytoplankton and (C3) terrestrial plant material. At any given location (water depth, distance from river mouth), we then observe a mixture of phytoplankton and terrestrial material whose proportions determine the bulk N/C_{POM} and $\delta^{13}C_{POM}$. In deeper waters, these bulk signals are closer to those of the plant material, partly because remineralization of sinking phytoplankton detritus depletes the contribution of this end-member. If we understand the referee's question correctly, it concerns the possibility that plant material in the bulk POM may derive from a direct POM input to the estuary (rather than from flocculated DOM). This is indeed a possibility which cannot be ruled out with the data presented. However as demonstrated by Mattsson et al., Biogeochemistry 76, 2005 in a study of 86 Finnish river catchments, 94% of TOC in river water is present as DOC. This implies that transformations of DOC in the estuarine water column are a more likely source of plant matter-derived POC than a direct POC input from the catchment. Furthermore DOM in the Mustionjoki estuary is known to undergo non-conservative mixing at low salinities (considered mainly to be due to flocculation of DOC to POC as outlined in Asmala et al., JGR Biogeosciences 10.1002, 2014). Hence we stand by the initial interpretation that the terrestrial plant material end-member of POM is likely derived from flocculated DOM.

See previous. In the revised manuscript we emphasize the magnitude of the DOM pool in this system and its persistent terrestrial character as determined by N/C and $\delta^{13}C$ (Section 5.1).

6. p16, L18-27. The authors interpret dithionite- and oxalate-extractable Fe as OMFe(II), and state that this is formed in the water column rather than the sediment. As far as I can see, this is again based on the findings of Yu et al. (2015) for a nearby boreal estuary. It may be good if the authors highlight data from this study or further literature besides Yu et al. (2015) in support of the conclusion that OM-Fe(II) is exclusively formed in the water column and is not of diagenetic origin.

As outlined in the response to comment 3, our interpretations concerning the role of OM-Fe(II) will require modification. The additional 1M HCl extraction data confirm that unsulfidized Fe (II) is present in all measured samples (n=15) but the comparison in Fig. R5 shows that it likely contributes

to Stages 1+2-soluble Fe (rather than Stages 3+4-soluble Fe) in the Poulton and Canfield method. In fact we did not claim that the OM-Fe(II) complexes were formed in the water column, rather that the association between Fe and OM may initially occur in the water column (where Fe is present as Fe(III)) and persist in the sediments (where Fe is then reduced to Fe(II)). In any case we will rewrite this section based on the new information from the additional extractions and Mössbauer analyses.

In the revised manuscript, we have updated our interpretations of the Fe speciation substantially on the basis of both the additional extraction results and the new Mössbauer data (Figures 6, 7, Table 3) With respect to Fe (II)-OM, we infer the presence of this component from persistent detection of unsulfidized Fe (II), including in depth horizons where the presence of H_2S should prevent accumulation of unsulfidized Fe (II) mineral phases such as siderite and vivianite (Section 4.6).

7. p 17, L 4-7. The maximum accumulation of ferrihydrite in a (seasonally oxygen depleted) "pit" of Station D is interesting, in that redox shuttling apparently causes maximum accumulation Fh (the most labile and easily reduced Fe(III) phase) in the surface sediment (Fig. 6), where H2S already seems to accumulate (Fig. 7). Striking is also the persistence of Stage 1 and 2 Fe ("ferrihydrite") with depth through sulfidic depth intervals at Station D and to a lesser extent Station J. Could ferrihydrite perhaps be only part of the answer? The authors assign all Fe extracted by Na acetate at pH 4.5 to ferrihydrite, while this mineral is very slow to dissolve at that pH. Iron monosulfide was not specifically quantified in this study, could the presence of FeS help explain the Na acetate-extractable Fe pool and the persistence of Stage 1 and 2 Fe with depth? Egger et al. 2014, ES&T, mention that FeS in Baltic surface sediments is extracted in Stage 1 and especially Stage 2 of the same Fe extraction scheme as used in this study.

To answer this point first: As outlined in the response to comment 3 we now have a more detailed picture of the likely composition of the Na-acetate- and hydroxylamine-HCl-soluble fractions, which helps to answer these questions. First we recall that total 1M HCl-soluble Fe is equivalent to total Stage 1+2-soluble Fe from the Poulton and Canfield method (Fig. R5), implying that the same phases are dissolved in both approaches. The results of the 1M HCl extractions therefore confirm the referee's suggestion that FeS accounts for a portion of total Na-acetate- and/or hydroxylamine-HCl-soluble Fe (Fig. R3). The remainder is made up of unsulfidized Fe (II) and HCl-soluble Fe (III). It is notable, as the referee also states, that Station D is characterized by the highest total proportions of these "labile" phases (Figs. R2 and R3) which is very likely a consequence of lateral Fe shuttling into the bathymetric depression, followed by diagenetic cycling of Fe in the sediment. This diagenetic cycling may include reduction of ferrihydrite and precipitation as FeS.

Although the additional extractions were performed on only 5 samples per station – and therefore trends with depth in the relative proportions of FeS, unsulfidized Fe(II) and HCl-soluble Fe(III) are difficult to discern – the data suggests that HCl-soluble Fe (III) is indeed present in most samples. This implies a persistent occurrence of ferrihydrite at depth in the sediments throughout the transect, as originally suggested in the manuscript. An alternative theory would be that the HCl-soluble Fe (III) is contributed by labile OM-Fe(III) complexes, which may be less susceptible than ferrihydrite to reaction with H_2S. These possibilities will be discussed in more detail in the revised version. (We note that three of the 15 samples appear not to yield any HCl-soluble Fe(III) (Fig. R3), but that this may be an artefact caused by heterogeneity between Subsamples 1 and 2, which were used to estimate HCl-soluble Fe (III) from the difference between HCl-soluble Fe (II) and HCl-soluble $Fe_{tot.}$).

The roles of ferrihydrite and iron monosulfide, as well as other labile Fe phases, are discussed at length in the revised manuscript in the context of the new extraction data (Section 4.6).

The Mössbauer data indicate abundant superparamagnetic Fe(III) at Stations A and to a lesser extent Station D, but these are data from the uppermost sample (0-1 cm) that was in contact with bottom water O2 that was still 75 % (Station A) to 30 % (Station D) of saturation, eyeballing Fig. 1. FeS persistence far below the zone of H2S accumulation may be unlikely (unless the system is very dynamic and far from any steady state). This zone, characterized by abundant Fe2+ but no sulfide, is often associated with formation of reduced Fe minerals such as vivianite and siderite. Could these also be present here and extracted in the low pH Stage 1 and 2 of the extraction scheme? The fact that these phases were not observed in the Mössbauer data from the surface sample does not rule out their presence at depth. Overall, some more words (beyond "seasonally oxygen depleted") can be spent regarding the steadiness of a geochemical state with apparently co-occurring "Fh" and H2S accumulation, and the nature of Fe extracted from anoxic non-sulfidic and sulfidic sediments during Stages 1 and 2 of the Fe extraction scheme.

We are currently analyzing five additional samples by Mössbauer, including one sample from the deeper part of the core from Station D (26–28 cm), below the H_2S zone. As indicated above, these data will be included in the revised version of the manuscript along with the relevant reference spectra and expanded details of the LCF procedure. The referee is correct that precipitation of Fe(II) phosphates and carbonates is theoretically possible in this depth interval, as shown for example for Bothnian Sea sediments in Egger et al., GCA 169, 2015. We will acknowledge this in the text as well considering these phases in the interpretation of the Mössbauer data. It is also indeed noteworthy that Station D appears to display co-occurrence of "ferrihydrite" and H_2S in the depth interval 5–20 cm, whereas ferrihydrite is expected to react with H_2S with a half-life measured in hours (Table 4.1 in Raiswell and Canfield, Geochemical Perspectives 1, 2012). Although we have only sampled Station D pore waters on one occasion, we expect from nearby – repeatedly sampled – stations that the H_2S peak will be persistent throughout the year, which supports the need for an explanation why "ferrihydrite" should survive in the sediments. As outlined in the previous response, one possibility is that the HCl-soluble Fe(III) is in fact labile OM-Fe(III), which may be less susceptible than ferrihydrite to reaction with H_2S. Another is that ferrihydrite is indeed present, but somehow protected from reaction with H_2S by surface sorption processes. We note the referee's own recent conference abstract (Kraal et al., Goldschmidt 2017) which suggests a greater chemical stability for ferrihydrite particles to which P and Si is sorbed.

The respective behavior of various labile Fe phases is discussed at length in the revised manuscript in the context of the new extraction data (Section 4.6). We currently favor the hypothesis that ferrihydrite is indeed dissolved in the SMTZ and that any retained labile Fe (III) is therefore present at Fe (III)-OM.

I look forward to enjoying the revised version of this manuscript.

Kind regards, Peter Kraal Utrecht University, Department of Earth Sciences-Geochemistry
Please also note the supplement to this comment:
https://www.biogeosciences-discuss.net/bg-2017-181/bg-2017-181-RC1-supplement.pdf

Responses to Line by Line supplementary comments from P. Kraal (Referee #1)

P3 Line 6: And, conversely, OM has been shown to stabilize ferrous Fe (Toner et al, Nat Geosci 2, 2009)

We will add the reference to the revised manuscript.

In fact we have not added this reference. We do not focus in detail on the mechanisms of the Fe-OM associations later in the manuscript so the reference is superfluous to the Introduction.

P3 Line 13: Michel et al, Science 316, 2007; Hiemstra et al, GCA 105, 2013: $Fe_{10}O_{14}OH_2.nH_2O$

We will clarify that there are several formulas for ferrihydrite (and indeed several models for its structure) in the literature. The simplified formula we use is taken from Raiswell, Elements 2011.

The Hiemstra reference is added (Introduction paragraph 2).

P3 Line 25: Fh binding sites are overwhelmingly Fe-O groups, not Fe-OH

We will clarify this statement with references to developments in understanding of the structure and sorption characteristics of ferrihydrite. Relevant to the referee's comment, the original OH-rich model for ferrihydrite presented by Drits et al. (Clay Minerals, 28, 1993) has indeed been superseded by more recent works implying a dominance of Fe-O bonds in the structure and thus in sorption sites on the mineral surface, as outlined in Hiemstra, GCA 105, 2013.

The Hiemstra reference is added (Introduction paragraph 2).

P3 Line 29: net

The text will be modified accordingly.

The text has been modified (Section 1).

P5 Line 28: I can imagine that the precision and accuracy of standards may differ from data obtained from solids on filters. Were complete filters combusted, or parts? Were there any replicates for filter analyses?

This issue is addressed in detail in our response to the referee's main comments.

The revised text takes this comment into consideration.

P6 Line 9: Here I have the same question as above, about the relationship between results from standards and results from (pieces of) filters.

This issue is addressed in detail in our response to the referee's main comments.

The revised text takes this comment into consideration.

P6 line 10: I do not follow: if total Fe on filter is measured, and the filtered volume is known, why is TSS needed to convert from umol Fe on filter to umol Fe/L water?

The referee is correct that TSS is not needed to perform this calculation. In our spreadsheets we had used TSS first to estimate the concentration of $Fe_{part.}$ as µmol/g suspended solid material, and subsequently converted this value back to $Fe_{part.}$ in µmol/L. We now checked the direct conversion as

described by the referee and the results are consistent with those initially calculated. We will reword this section.

The revised text is reworded as stated above.

P8 Line 15: And, in light of the possible role of FeS, maybe spell out that it's a low estimate for sulfide-associated Fe.

This issue is addressed in detail in our response to the referee's main comments.

The calculations concerning FeS and pyrite are now modified (equations 3-7).

P8 Line 21: No info on standards.

This issue is addressed in detail in our response to the referee's main comments.

A selection of relevant reference spectra is presented in Figure 7.

P10 Line 4: Based on measurements of gravimetric water loss?

The assumed constant value of 90% is of course a simplification of the true porosity profile, but sufficient for the qualitative discussion of diagenetic processes presented in the original paper. For completeness, we will adjust the CH_4 concentration data using a best-fit line through the porosity data derived from gravimetric water loss, which are indeed available.

The revised manuscript includes more detailed calculations and discussion of diagenetic processes and their rates, hence the generation of gravimetric water loss data – and the subsequent conversion to porosity – are properly described, and the results are used in the calculations (Sections 3.4, 3.12, 3.13).

P12 Line 8: Are the stacked 100% plots necessary?

It is difficult to convey clearly all the information in this large dataset (multiple operational fractions + multiple stations, Fe + organic matter dynamics) in a single figure. We decided to include the stacked 100% plots to improve our chances of succeeding in this. For example in the case of the plot of the organic matter fractions, the absolute concentrations show clearly that there are lower values in the stations close to the sill, while the stacked 100% plot shows that the relative concentrations of terrestrial and phytoplankton material are unaffected by the presence of the sill (i.e. the samples plot approximately where expected in the offshore trend).

The revised manuscript retains the stacked 100% plots for the reasons given.

P12 Line 8: Well, station B stands out but for the rest I do not see much of a (general) trend.

We will adjust the text accordingly.

The text has been adjusted (Section 4.5).

P12 Line 14: The "marked" difference does not become apparent, because the phases normally associated with the stages are not mentioned here. For clarity, I would refer to the operational

fractions above (L12, 13) as it is the first mention of the "stages" in the results section (instead of later on in L25 and 27), mention the corresponding stages and then keep referring to the stages.

This issue is addressed in detail in our response to the referee's main comments.

The interpretation of the extraction data has been substantially revised (Table 3, Sections 4.6, 4.7).

P12 Line 19: Any way to substantiate this? Yu et al used XAS, here it's Mossbauer without any Fe-OM reference phase?

This issue is addressed in detail in our response to the referee's main comments.

The interpretation of the Mössbauer data has been substantially revised (Sections, 4.7, Figure 7).

P12 Line 25: Consider the order of section 4.5 and the place of this paragraph; would it not fit better before the Mossbauer results?

We will consider this advice when restructuring the manuscript.

The order has been restructured according to the distinction between labile and refractory phases (Sections 4.6, 4.7).

P13 Line 15: Why H2S in the text, when HS- (the major species at circumneutral pH) is used in the formula?

We will correct this inconsistency.

We now use exclusively H_2S as given in the formulations of Reed et al. L&O 56, 2011.

P13 Line 18: And why H2S here, while HS- in Eq 5?

We will correct this inconsistency.

We now use exclusively H_2S as given in the formulations of Reed et al. L&O 56, 2011.

P13 Line 20: What does "efficiently" mean in this context? Rapid reaction?

Yes, we will clarify this.

The text related to the diagenetic reactions has been modified substantially (Section 4.8).

P13 Line 21: vertical extent

We will adjust the text.

The text related to the diagenetic reactions has been modified substantially (Section 4.8).

P14 Line 6: Why is there no direct evidence for OM flocculation for this study? Fig 3b presents data, but does not show DOM/POM trends along the gradient.

This is because the original experimental design was focused on Fe and POM did not include measurements of DOM in 2 dimensions June 2015. The DOM data were added later to help explain the distribution of N/C_{POM} and $\delta^{13}C_{POM}$.

The above response answers the Referee's question.

P14 Line 10: I find it hard to understand this remark and its context, some more detail would be beneficial. What kind of variations in end-member values?

We will expand this section briefly. The statement refers to the fact that the freshwater DOM endmember characteristics (and magnitude) are temporally variable, for example in response to the seasonal cycle or discharge events. In estuaries with a long freshwater residence time this variability may be transmitted downstream slowly, meaning that an instantaneous sampling of an entire transect for DOM characteristics may reveal not only the steady-state mixing dynamics, but also the signal of the changing freshwater endmember. Hence interpretations of conservative vs. non-conservative mixing need to be made with care. These concepts are discussed at length in Asmala et al., Frontiers in Marine Science 12, 2016.

In fact we have not expanded on this issue due to the fact that the manuscript is now more focused towards Fe behavior independent of DOM and does not require extensive discussion of this issue. We refer the Referee to the above response and citation for further relevant information.

P14 Line 15: I wonder about effects of changes in pH and DO, that may affect the kinetics of Fe oxidation and precipitation. Are there jumps in these values when going from the river into the estuary?

This issue is addressed in detail in our response to the referee's main comments.

In the revised manuscript we emphasize the partial decoupling of Fe from DOM during flocculation (see revised Title, Abstract, Introduction paragraph 4, Section 5.2), emphasizing some of the factors listed by the Referee.

P15 Line 5: Crucial. Unsure about the reasoning; Can it simply be the "natural" distribution between DOM and POM for plant material?

This issue is addressed in detail in our response to the referee's main comments.

We refer the Referee to our original response above.

P16 Line 13: This is the smoking gun; but is it syngenetic or diagenetic? And, there is no direct evidence for Fe-OM from the data, there is just a pool of "undocumented Fe" that is assumed to be organic-bound Fe based on XAS data from Yu et al. I assume that siderite was in the library? Dithionite-citrate may have potential for siderite dissolution? More info on the standards explored is necessary to validate the claim that the Fe was undocumented and thus likely associated with OM.

This issue is addressed in detail in our response to the referee's main comments.

The interpretation of both extraction and Mössbauer data are substantially revised (Sections 4.5, 4.6, 4.7, Figures 5, 6, 7). The undocumented Fe (II) phase at Station A is now thought to be wüstite and in fact a pollution signal from the nearby blast furnace (Fig. 1).

P16 Line 18: This is pretty speculative (based on Yu); any evidence for the fact that it occurs in the water column? Following sentences infer the role of diagenesis, the Fe(III)-OM is purely hypothetical?

This issue is addressed in detail in our response to the referee's main comments.

The interpretation of both extraction and Mössbauer data are substantially revised (Sections 4.5, 4.6, 4.7, Figures 5, 6, 7). The undocumented Fe (II) phase at Station A is now thought to be wüstite and in fact a pollution signal from the blast furnace.

P16 Line 33: OK, so siderite was a standard (which is a Fe(II) mineral)

Yes. Siderite was one of the reference spectra. This issue is addressed in detail in our response to the referee's main comments.

A selection of relevant reference spectra is given in Figure 7.

P16 Line 33: Even fresh ferrihydrite dissolved very slowly at the pH of Na acetate (4.5), are there lit examples of Fh dissolving under those conditions?

This issue is addressed in detail in our response to the referee's main comments.

We have adjusted our interpretation of the extraction behavior of ferrihydrite (Section 4.6, Table 3).

P17 Line 5: This is interesting, in that redox suttling causes maximum Fh (the most labile and easily reduced Fe(III) phase) accumulation in the surface sediment, where H2S already seems to accumulate (Fig. 7). Perhaps some more words (beyond "seasonally oxygen depleted) can be spent on the equlibrium of a state with apparently co-occurring abundant Fh and H2S accumulation?

This issue is addressed in detail in our response to the referee's main comments.

The revised text includes a discussion of this issue (Section 4.6).

P18 Line 13: Is there not potential for a role of sediment DOC/POC as Fe(II) sink, i.e. diagenetic OM-Fe(II) formation?

Diagenetic formation of OM-Fe complexes is indeed suggested in the papers of Lalonde et al. (2012) and Shields et al. (2016). i.e. according to their model, the association between Fe and OM occurs after sedimentation. Due to the close association of Fe and OM in the water column of boreal estuaries, we have focused on the idea that Fe and OM are transferred together to the sediments. However we cannot discount the possibility that diagenesis affects the nature of the association and we will acknowledge this in the revised text.

We do not focus on the mechanism of the Fe-OM association in sediments in the revised version. Indeed with the data available it is not possible to state whether the associations implied by the 1M

HCl extraction data are pre- or post-depositional and this is stated in Section 5.5. We worked with the hypothesis that at least a fraction of flocculated Fe is deposited as Fe (III)-OM and that subsequent transformations of this material occur in the sediment.

P19 Line 3: The mechanism could be explained more explicitly: how does the recovery drive increased Fe and DOM transport?

We will expand this section briefly. The mechanism is related to the ionic strength of freshwaters and consequent residence time of DOM in drainage systems.

We have added the phrase “and elevated ionic strength” in Section 5.6).

P20 line 25: (

We will correct the typo.

Done.

2.Responses to online discussion Referee #2

The following document contains both the responses given during the Open Discussion of "Flocculation of dissolved organic matter controls the distribution of iron in boreal estuarine sediments" and a description of the subsequent revisions leading to the submission of "Impacts of flocculation on the distribution and diagenesis of iron in boreal estuarine sediments".

[Referee comments in bold]

[Responses in italics]

[Indication of subsequent revisions in regular text]

This is a paper on the removal mechanisms of Fe to sediments in the riverine-estuarine transition of a long riverine estuary on the Eastern Baltic Sea and the effect of this removal for the corresponding iron diagenesis in the underlying sediment. The key message of this paper, if I understand this right, is that riverine Fe is removed by flocculation in the riverine-estuarine transition of the Eastern Baltic Sea. These results are similar to the Fe story presented in Yu et al (2015) Chemical Geology in another Finnish estuary. The flocculation occurs as an organic Fe complex.

These results are based on the interpretation of Mössbauer spectra, which revealed an unknown Fe phase that was neither well-crystallized silicate, magnetite, nor ferrihydrite. The inference is therefore not direct, but indirect, and that is a major shortcoming.

In the underlying sediments of the outer estuary and the Baltic Sea, Fe accumulation occurs as different phases than in the riverine part, where more crystalline Fe hydroxides occurred than in the distal part where organic Fe dominates.

In principal I believe some of the story, e.g., the organic-Fe transport and rapid removal in the estuary. But I failed to see how the results translate into different diagenetic Fe processes in the sediment.

In particular, I felt that the story on the anaerobic oxidation of methane by iron was underdeveloped. While this is an impressively large data set from many stations, much of the potential novelty hinges upon the interpretation of the Mössbauer data. The combination of Mössbauer/extraction data call for a major reinterpretation of the operational Fe extractions, in particular of a re-assessment of the dithionite extraction as an organic Fe phase. This has large ramifications for many published papers and the authors need to be very careful in their assessment and interpretations.

We thank the referee for the careful consideration of our manuscript. Below, we respond to each of the question posed by the referee.

I would like the authors to address and comment on a number of questions I have:

Why do you not present Mössbauer spectra of riverine material, dissolved and particulate? This would be most interesting to see.

We agree with the referee that such data would be extremely interesting. However the present study was not designed to include Mössbauer analysis of riverine dissolved and particulate material. This would require far greater volumes of water to be filtered (and with various grades of filters) than that required for the determination of total Fe_{diss}. and Fe_{part}. Indeed, this would constitute a separate study in itself. However in response to the comments of both referees we are currently analyzing additional sediment samples by Mössbauer. These include a sample from the river bed of the Mustionjoki, upstream from Station A, which may shed some light on the composition to material transported in the river.

The revised manuscript includes a Mössbauer spectrum from a river bed sediment sample taken at Station 'a' (Figs. 1, 7 and Supplementary Figure 2).

Why do you claim that hydroxylamine-extracted Fe occurs as Fe2+, when hydroxylamine is a strong reducing agent? No information on prior oxidation state is possible using this extraction method.

It is true that hydroxylamine-HCl is a reducing agent and in fact we did not claim in the original text that hydroxylamine-HCl extracts Fe^{2+}. We assume the referee is referring to our claim that dithionite (another reducing agent) extracts Fe^{2+} from OM-Fe(II) complexes. In response to the comments of both referees we have addressed the issue of solubility of various Fe phases in our original extraction scheme extensively. Please refer to Figures R2–R5 and associated text in this file.
The Fe (II) and Fe (III) components of the labile Fe fraction are now deconvolved on the basis of the additional extractions (Fig. 6, Section 4.6).

Why do you not even consider or discuss the extraction of FexSy phases with dithionite? This is well known. Not all Fe may be organically associated to the same extent throughout the transect and not necessarily as Fe2+, because dithionite is also a reducing agent.

The exact nature of the dithionite-soluble phase(s) remain difficult to determine conclusively, and we require the additional Mössbauer data to advance this discussion. The additional extractions suggest that unsulfidized Fe (II), including the potential OM-Fe (II) complexes, is in fact dissolved in Stages 1+2 of the Poulton and Canfield method, rather than Stages 3+4 (dithionite + oxalate) as suggested in the original manuscript. With respect to the possible dissolution of FexSy phases in dithionite, pyrite is not considered to be dithionite-soluble (see for example Berner, Amer. J. Sci. 268, 1970; Canfield, GCA 53, 1989; Raiswell et al., Chem. Geol., 111, 1994) while greigite is not expected to be a major phase in the sediments at this location. The role of FeS has been established by the additional extractions: this is expected to be dissolved in Stages 1+2 (Fig. R3).

The revised manuscript presents a version of Fig. R3 (as Fig. 6a) and also presents the interpretation given in the above statements (Section 4.6). Additionally, we now suggest that the major dithionite/oxalate-soluble phases observed at Station A are wüstite and magnetite, derived from industrial inputs and identified on the basis of the Mössbauer spectra (Sections 4.7 and 5.4).

In your table or on the Mössbauer spectra you should show the patterns for FexSy or FeS2 phases to convince the reader that the composite spectrum is not influenced by these phases.

This is a fair criticism and similar to comments from Referee #1. We will present all relevant reference spectra in the revised version.

We now present reference spectra from a range of potential sedimentary Fe phases alongside the sample spectra (Fig. 7). We discuss the potential interference of pyrite with superparamagnetic Fe (III), among other limitations of the Mössbauer approach for detecting minor Fe phases (Sections 3.10 and 4.7).

The Mössbauer spectroscopy standardization and reference spectra are not explained. It is not clear why your conclusion is that the phase must be an organic Fe2+ phase. If it is ferrihydrite associated with organic matter, what kind of association is this?

This is a fair criticism and similar to comments from Referee #1. We will present all relevant reference spectra in the revised version. The allocation of Fe(II) vs. Fe (III) to unknown phases in Mössbauer spectra is made according to the position of the spectrum in x-y space of quadrupole splitting vs. isomer shift, as outlined in Murad and Cashion, Springer 2004. This detail will be included in the revised version.

We now present reference spectra from a range of potential sedimentary Fe phases alongside the sample spectra (Fig. 7). The principles regarding the interpretation of Mössbauer spectra are given substantially more weight (Section 3.10).

Is there a possibility that the unknown spectrum is an amorphous Fe-silica phase?

We have no basis to suspect this at the present time.
We now suggest that the previously unknown Fe phase is wüstite (Fig. 7, Section 4.7). As reported by Manning et al., Can. Mineral. 18, 291–299, 1980, amorphous ferric silicate phases display spectra consistent with superparamagnetic Fe (III).

Why is it that there are hardly any changes in Fe speciation at Station D, although the S content changes so significantly and therefore likely the concentrations of FeS and FeS2?

We apologize to the referee, but we made a significant mistake in the plotting of Figure 6 (and associated text) which is relevant to this question and likely influenced the referee's understanding of the data. The scale of the sedimentary Fe content reads 0–4 %, while it should read 0–40 %. Hence the true figure should look like this:

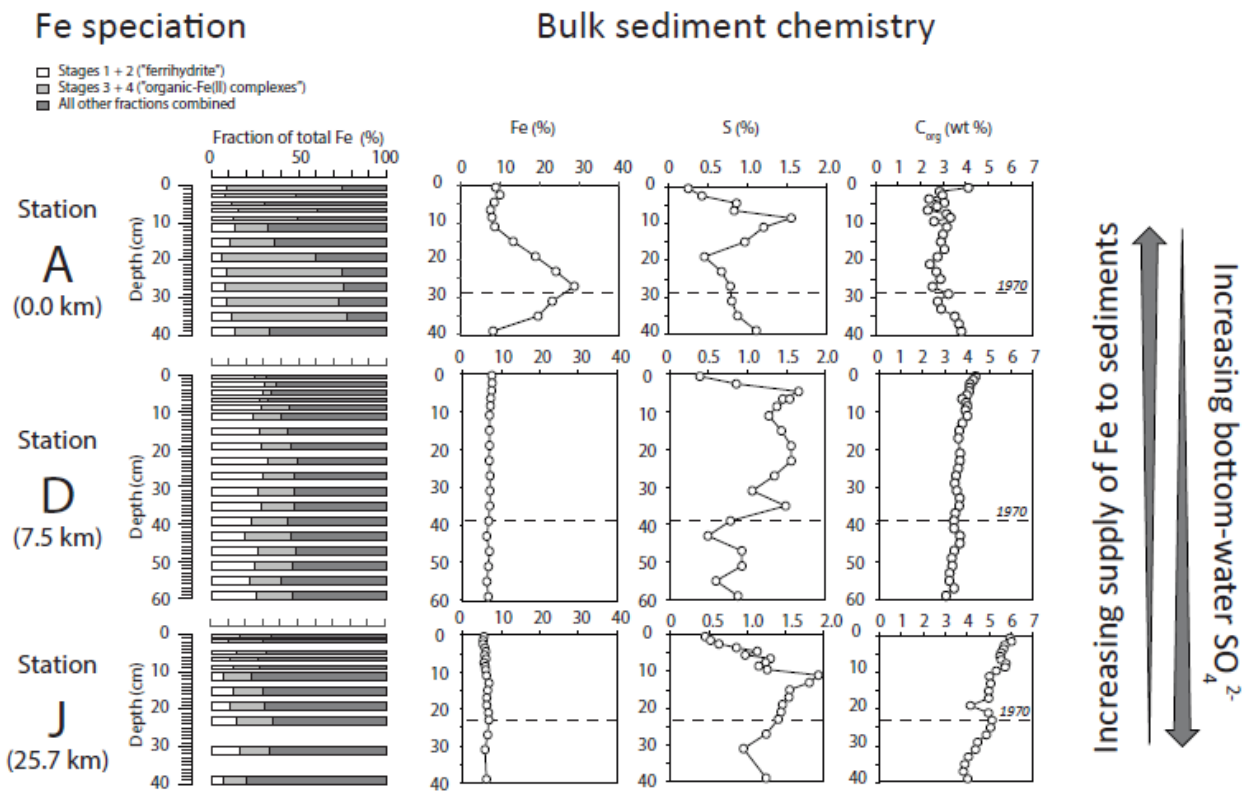

Fig. R6. Corrigendum to Figure 6 in the original manuscript. Note the scales on the axes of weight % Fe in the sediments (0–40%).

Note that all other plots of sedimentary Fe content in μmol/g units are correct, as are the Fe/Al weight ratios given in Fig. 8.

Clearly, the Fe content of the sediments at all stations is far higher than the S content, also on a molar basis, and this is the reason that the downcore changes in S content are not reflected in changing Fe speciation. This is best illustrated in Fig. R2 of this document, where "sulfide-Fe" (calculated as described in the manuscript assuming all S as pyrite) is shown to be only a minor component. This conclusion does not change when the calculation is performed taking into account the AVS (FeS) component now calculated in the additional extractions. For clarity we will add both molar and weight % scales to the figures in the revised version.

We apologize again for this error. The data are now correct and the contribution of S-bound phases to total Fe is made clear in Figs. 5 and 6.

What is the major Fe carrier down the river, i.e., what is the speciation of Fe in river and estuarine water? How much is associated with the organic fraction – how much is present as ferrihydrite – what is the exact molecular association?

For the reasons outlined earlier, we did not carry out speciation work on the suspended particulate (or operationally "dissolved") Fe. We emphasize again the relevance of the study of Neubauer et al., ES&T 47, 2013, which discusses the speciation of Fe in boreal rivers.

The revised manuscript emphasizes that a significant proportion of total water-borne Fe is likely present as discrete colloidal ferrihydrite, which influences the partial decoupling from terrestrial OM during flocculation and sedimentation (Section 5.3). However we simply do not have the data to quantify the relative amounts of Fe-OM and ferrihydrite in the present study.

Figure 5 figure caption and left figure panel don't agree. The caption reads Fe2+/FeT, the other Fe3+/FeT ratio.

We thank the referee for this observation and will correct the text and figure.

The presentation of the Mössbauer data has been modified substantially (Fig. 7, Supplementary figure 2, Table 4).

Figure 6: The down-core operational Fe profiles don't exactly make sense in light of the pronounced changes in S content with depth at Station A. At least, the 100% scaling makes it difficult to associate the species changes with the S concentration changes. I recommend to show the Fe species as concentrations, e.g., as summed bars totaling to the actual Fe concentration. That would help at least for comparing the data of Station A. The Fe species do not correspond at all to the sulfur concentrations. How is this possible, if FeS/FeS2 forms? My conclusion would be that the dithionite-extracted species seem to be associated at least partly with some FeS/FeS2. This needs to be accounted for.

Again, we apologize to the referee for the mistake in Figure 6 which is relevant to this comment (see earlier response). We will take onboard the suggestion to plot the Fe speciation data as concentrations. A version of Fig. R2 will be included in the revised manuscript.

In the revised manuscript, the data are now correct and the contribution of S-bound phases to total Fe is made clear in Figs. 5 and 6. The 100% summation of Fe phases is removed from the downcore plots (Fig. 5 in the revised version) to make visual comparisons with the S profile easier.

p.14 l.25: I think the authors mean 'isotopically depleted'

No. The deeper water samples are indeed more isotopically enriched (less negative values than surface water samples).

This text has remained unchanged for the reason given.

p.16, l.16-17 Fe-Si amorphous phases; FeS mackinawite-like material?: Why Fe2+, could also have been Fe3+?

We will present all relevant reference spectra in the revised version. The allocation of Fe(II) vs. Fe (III) to unknown phases in Mössbauer spectra is made according to the position of the spectrum in x-y space of quadrupole splitting vs. isomer shift, as outlined in Murad and Cashion, Springer 2004. This detail will be included in the revised version.

See earlier comment. There is now more detail on Mössbauer principles in Section 3.10 and reference spectra are presented in Fig. 7 and Supplementary Figure 2.

p.17, l.1-5 hydroxylamine hydrochloride is a strong reducing agent suggesting that the Fe could have been reduced by the extraction.

It is true that hydroxylamine-HCl is a reducing agent and is specifically used to target poorly crystalline Fe oxides in this scheme. We do not claim in this passage of text that hydroxylamine-HCl extracts Fe^{2+}.

The revised manuscript presents a comprehensive new interpretation of the labile Fe phases (Section 4.6).

I would also like to see a transect plot of DOM and POM.

We do have a transect plot of POC from the same samples used to generate the corresponding plots for N/C and $\delta^{13}C$. *(Fig. R7). This can be included as a supplement if needed but does not contribute significant extra information. The distribution strongly resembles N/C, suggesting that phytoplankton dominates the POC pool at the time of sampling in June 2015.*

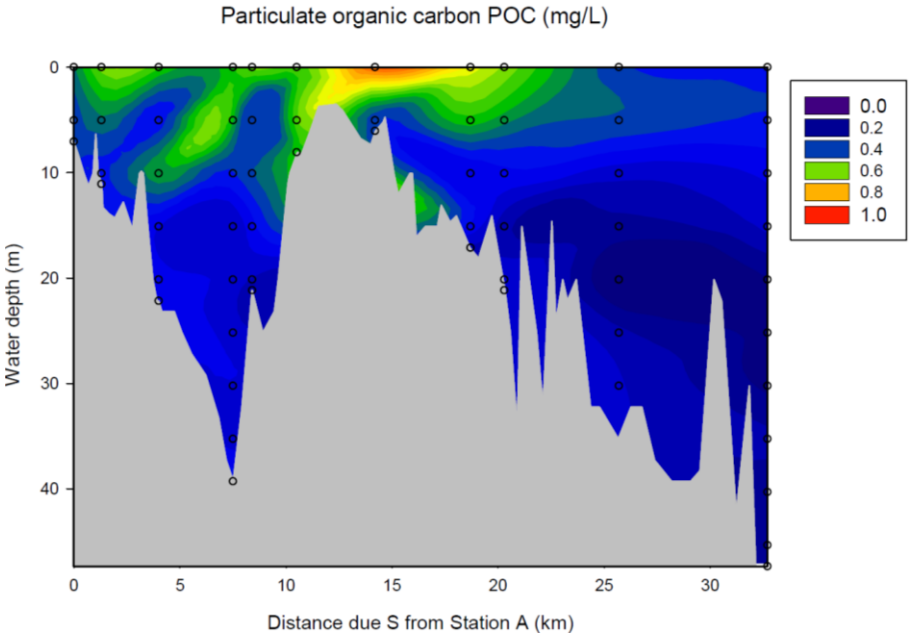

Fig. R7. POC along the transect in June 2015 (mg/L)

Unfortunately we do not have a corresponding plot for DOC (or DOM) as this sampling was not included in the original experimental setup (which was focused on Fe and POM).

This plot is visible in the online discussion, but since it is not referred to in the revised manuscript we do not intend to upload it as a supplement unless requested to do so by the Referee or Editor.

p.18. Are the salinity differences significant enough to impact the Fe-S system? I don't think so.

We disagree. The changes in sulfate penetration depth from Station A–D–J (Fig. 7) indicate a significant impact of bottom water salinity on the diagenetic zonation of the sediments. As highlighted

in the discussion of this Figure, the depth of the SMTZ, and the intensity of the associated H_2S peak, contrast strongly between the sites. As mentioned also by Referee #1, the distribution of H_2S in the pore waters (between stations and the downcore profile at each station) should then have a strong impact on the stability of Fe phases. We will devote more lines to this in the revised version.

The revised manuscript includes a substantially expanded description and quantitative evaluation of the diagenetic processes (Sections 3.13, 4.8, 5.5).

p.18 l.24 what do you mean by background rates: How are these background rates? Aren't these the major reactions? What about sulfate reduction rates and coupled oxidation of sulfide by ferrihydrite?

We will rephrase the sentence to remove the term "background".

Undoubtedly, both sulfate reduction coupled to organic matter oxidation, and oxidation of sulfide by ferrihydrite – along with many other diagenetic reactions – are also occurring at these sites. We will expand the discussion to give a broader overview of the various diagenetic processes, including first order estimates of process rates derived from pore water profiles. However it was not (and is still not) our intention to perform a detailed diagenetic modeling study, rather to highlight the diagenetic zones that are clearly visible in the pore water profiles, in order to qualitatively discuss the differences that are observed along the transect (and the link to Fe inputs from flocculation).

The revised manuscript includes a substantially expanded description and quantitative evaluation of the diagenetic processes (Sections 3.13, 4.8, 5.5).

The anaerobic oxidation of methane by iron is often invoked these days, but to argue for this process there has to be good direct evidence. I am sure the authors are aware that AOM also can be coupled indirectly to reduction of iron oxyhydroxides through sulfide oxidation, but cannot be distinguished easily without performing specific experiments. Concentration profiles alone are not enough. The authors should refrain from inferring that AOM by iron is a major process controlling deep iron diagenesis when they have not addressed sulfide oxidation processes. They do not even present DIC data to support their assertion. In addition, should this process occur, it is easy to assess the quantitative significance by assessing the methane flux and the required removal of Fe to account for methane oxidation.

We are indeed aware of the alternative indirect pathways by which reduction of Fe oxyhydroxides may be coupled to methane oxidation. The most relevant is of course the so-called cryptic sulfur cycle as described in Holmkvist et al., GCA 75 (2011), in which downward-diffusing H_2S from the SMTZ is oxidized by Fe oxyhydroxides, leading to the formation of native sulfur and subsequent disproportionation to SO_4^{2-} and H_2S (the SO_4^{2-} then going on to oxidize CH_4). We do not dispute the validity of the mechanism presented by those authors and indeed coupled sulfur cycling and methane oxidation have been confirmed by further studies (e.g. Milucka et al., Nature 491, 2012).

However, as discussed at length in the review process for Slomp et al. Plos ONE 8, 2013 and Egger et al., ES&T 49 (2015) for sediments from the Bothnian Sea, in the low-salinity systems of the northern Baltic the SMTZ is sufficiently shallow that H_2S diffusing downwards from the SMTZ is exhausted well above the base of a typical GEMAX core. This is confirmed in the profiles in Figure 6, where H_2S is undetectable below approx. 20 cm at Stations D and J. It is therefore problematic to invoke the cryptic sulfur cycle as the cause of high pore water Fe^{2+} at depth, because the downward diffusion of H_2S is the ultimate driver of this process. Although H_2S is regenerated during sulfur

disproportionation within the cryptic sulfur cycle, only three moles are produced for every four moles of H_2S that initially react with Fe oxyhydroxides. So cryptic sulfur cycling is in fact a net consumer of H_2S and cannot sustain H_2S-driven Fe oxyhydroxide reduction well below the downward-penetrating H_2S front. This concept is nicely illustrated in the study of Egger et al., Biogeosciences 13, 2016 for Black Sea sediments (see their Figure 8, where pore water Fe^{2+} production due to cryptic sulfur cycling is shown to be restricted to a narrow depth interval just below to the downward-penetrating H_2S front). Hence we are confident that the large increase in pore water Fe^{2+} observed in the deeper parts of the cores in our study are not driven by cryptic sulfur cycling.

To clarify, in the original manuscript we also give two possible mechanisms for the production of pore water Fe^{2+} (Eq. 7 and 8), thereby acknowledging that both dissimilatory reduction of Fe oxyhydroxides, and Fe-AOM, may be active in the deep sediments. Hence coupled to the above discussion re. cryptic sulfur cycling, we disagree with the assertion that too much weight is given to the likelihood of Fe-AOM.

In related work we are performing experiments to determine the rates of AOM in these sediments, but these results are beyond the scope of the current paper.

The revised manuscript includes a substantially expanded description and quantitative evaluation of the diagenetic processes (Sections 3.13, 4.8, 5.5).

Along these lines, generally there is also too little discussion on sulfide oxidation coupled to iron reduction in the surface sediments. These organic-rich sediments likely have very low oxygen penetration depths of a few mm. Based on many other studies in estuarine systems, it is likely that anaerobic degradation processes such as sulfate reduction commence in the first centimeter. This makes it possible that FeS phases already occur in the topmost cm, and that not only iron reduction, but co-existing iron and sulfate reduction take place in the topmost cm.

The referee is correct that oxygen penetration is in the order of mm, and that both sulfate reduction and Fe reduction likely co-occur in the uppermost cm. This is implied by the immediate decline in pore water sulfate below the sediment-water interface at all sites, and the basic principle that Fe oxide reduction is more than twice as energy efficient as sulfate reduction per mole carbon oxidized (Stumm and Morgan, Wiley, 1981) and therefore should activate at a shallower depth horizon. In reality the diagenetic zones in these sediments overlap extensively, which in the surface sediments is also related to bioturbation and bioirrigation processes including by the invasive polychaete Marenzellaria (e.g. Norkko et al., Glob. Ch. Biol. 18, 2011). The referee is also correct that FeS may be present in the surface cm, either formed in situ by the co-occurrence of sulfate reduction and Fe reduction, or transported vertically from deeper horizons by the "smoothing" action of bioturbation. All of these concepts will be included in an expanded discussion of the diagenetic processes in the revised version of the manuscript.

The revised manuscript includes a substantially expanded description and quantitative evaluation of the diagenetic processes (Sections 3.13, 4.8, 5.5).

Finally, although the authors do very well in describing the bathymetry of this estuarine system, they fail to associate the bathymetric features with the current transport/ hydrography and the resulting particle transport and accumulation. For example, Station D likely must be influenced by saline water transport upstream, which is the only explanation to explain the higher bottom salinities. Therefore, inshore/upstream transport of organic material and of Fe has to be considered for the deep depressions.

It is true that saline inflows across the sill are responsible for the relatively high salinity deep water of the inner estuary. Inflows typically occur in winter as established in early literature on this system (e.g. Virta, Nordic. Hydrol. 8, 1977) and Niemi (Meri, 4, 1977). We will include an expanded introduction to the hydrodynamics in Section 2 (Study location). We are also aware of the likely lateral transport of Fe and OM (indeed Page 17, Lines 4–14 of the original manuscript specifically address this issue). We will rephrase this section to emphasize that lateral transport into the bathymetric depression of Station D may occur in both and upstream and downstream direction. Figure 4 will also be modified to highlight the position of the bathymetric depression and the sill in the data series of OM and Fe.

The revised manuscript includes the expanded background information about the hydrography and saline inflows (Section 2), and acknowledges that currents may play a role in transporting Fe from the sill towards Station D (Section 5.3).

In addition, Station D, being the deepest station of the inner estuary, is clearly a particle trap of fine-grained material, also of organic material. As such, the focusing and accumulation of material here may override the estuarine mixing signal the authors have as their overriding study target. Stations C or E may be more informative in this context. Do the authors note the same signals at stations C, D, and E?

As outlined in the previous response we are aware of the potential effects of lateral transport and focusing at Station D and will emphasize these more clearly in the revised version. In terms of the relative effects of the focusing and estuarine mixing on the observed signals, and the comparison of Stations C, D, and E: It could indeed be argued that Stations C and D display slightly elevated concentrations of "phytoplankton-derived" OM relative to the offshore trend (see Fig. 4b, lower left panel). We will give more weight to this in the revised version. The missing Fe data from Station C makes the equivalent assessment more difficult in the case of Fe.

See previous response. The revised manuscript acknowledges that both Fe and organic matter are likely transported downslope towards Station D, and discusses the decoupling of Fe from terrestrial OM that occurs during this process (Section 5.3).

3. Marked up revised manuscript

~~Flocculation of dissolved organic matter controls~~Impacts of flocculation on the ~~distribution~~ distribution and diagenesis of iron in boreal estuarine sediments

Tom Jilbert[1,2], Eero Asmala[~~3~~1,2,3], Christian Schröder[4], Rosa Tiihonen[1,2], Jukka-Pekka Myllykangas[1,2], Joonas J. Virtasalo[5], Aarno Kotilainen[5], Pasi Peltola[6], Päivi Ekholm[7], and Susanna Hietanen[1,2]

[1]Department of Environmental Sciences, Faculty of Biological and Environmental Sciences, University of Helsinki, P.O. Box 65, 00014 University of Helsinki, Finland
[2]Tvärminne Zoological ~~Station~~Station, University of Helsinki, J.A. Palménintie 260, 10900 Hanko, Finland
[3]Department of Bioscience -Applied Marine Ecology and Modelling, Aarhus University, Frederiksborgvej 399, 4000 Roskilde, Denmark
[4]Biological and Environmental Sciences, Faculty of Natural Sciences, University of Stirling, Stirling FK9 4LA, Scotland, United Kingdom
[5]Marine Geology, Geological Survey of Finland (GTK), P.O. Box 96, 02151 Espoo, Finland
[6]Boliden Rönnskär, 932 81 Skelleftehamn, Sweden

[7]Department of Food and Environmental Sciences, P.O. Box 66, 00014 University of Helsinki, Finland
Correspondence to: Tom Jilbert (tom.jilbert@helsinki.fi)

Abstract. Iron (Fe) plays a key role in sedimentary diagenetic processes in coastal systems, participating in various redox reactions and influencing the burial of organic carbon. Large amounts of Fe enter the marine environment from boreal river catchments associated with dissolved organic matter (DOM) and as colloidal Fe oxyhydroxides, principally ferrihydrite. However, the fate of this Fe pool in estuarine sediments has not been extensively studied. Here we show that flocculation ~~of DOM~~processes along a salinity gradient~~s~~ in an estuary of the northern Baltic Sea efficiently transfer~~s~~ Fe and OM from the dissolved phase into particulate material that accumulates in the sediments. Flocculation of Fe and OM is partially decoupled, likely due to the presence of discrete colloidal ferrihydrite in the freshwater Fe pool which responds differently from DOM to estuarine mixing. Further decoupling of Fe from OM occurs during sedimentation. While we~~Consequently, we~~ observe a clear decline with distance offshore in ~~both the Fe content of the sediments and~~the proportion of terrestrial material in the sedimentary particulate organic matter (POM) pool~~pool.~~, the distribution of flocculated Fe in sediments is modulated by focusing effects. ~~Mössbauer spectroscopy and sequential extractions suggest that~~ Labile Fe phases are most abundant at a deep site in the inner basin of the estuary, consistent with input from flocculation and subsequent focusing. The majority of the labile Fe pool is present as Fe (II), including both acid-volatile sulfur (AVS)-bound Fe and unsulfidized phases. The ubiquitous presence of unsulfidized Fe (II) throughout the sediment column suggests Fe (II)-OM complexes derived from reduction of flocculated Fe (III)-OM, while other Fe (II) phases are likely derived from the reduction of flocculated ferrihydrite. Depth-integrated rates of Fe (II) accumulation (AVS-Fe + unsulfidized Fe (II) + pyrite) for the period 1970–2015 are greater in the inner basin of the estuary with respect to a site further offshore, confirming higher rates of Fe reduction in near-shore areas. Mössbauer ^{57}Fe spectroscopy shows that refractory Fe is composed largely of superparamagnetic Fe (III), high-spin Fe (II) in silicates, and, at one station, also~~large amounts of Fe in sediments of the upper estuarine zone are associated with organic matter as unsulfidized Fe (II) complexes, or present in the form of ferrihydrite, implying a direct transfer of flocculated material to the sediments.~~ oxide minerals derived from past industrial activities. Our results highlight that the cycling of Fe in boreal estuarine environments is complex, and that the partial decoupling of Fe from OM during flocculation and sedimentation is key to understanding the role of Fe in sedimentary diagenetic processes in coastal areas. ~~Accordingly, the contribution of these components to the total sedimentary Fe declines with distance offshore while other Fe phases become proportionally more important. Sediment core records show that the observed lateral distribution of Fe minerals has remained similar over recent decades, despite variable Fe inputs from anthropogenic sources and eutrophication of the coastal zone. Pore water data suggest that the vertical zonation of diagenetic processes in the sediments is influenced by both the availability of Fe and by bottom water salinity, which controls the availability of sulfate (SO_4^{2-}).~~

Copyright statement

The authors certify the following:

- All co-authors have approved publication of the manuscript and authorized the corresponding author to enter into copyright agreements for publication in *Biogeosciences*
- The work described has not been published before
- The work described is not under consideration for publication elsewhere
- The work does not contain any previously copyrighted material

1 Introduction

Iron (Fe) is present in marine and freshwater sediments in a wide range of phases. Reactive Fe minerals, such as oxides, sulfides, phosphates and carbonates, are involved in diagenetic reactions in sediments and consequently influence the cycling of carbon and nutrients (e.g., Berner, 1970; Slomp et al., 1996a,b; Lovley et al., 2004; Jilbert and Slomp, 2013; Kraal et al., 2015; Robertson et al., 2016). Iron has also recently been shown to stabilize organic carbon in sediments, promoting carbon burial (Lalonde et al., 2012; Shields et al., 2016). Hence, the lateral and vertical distribution of Fe in sediments is important for broader biogeochemical cycles. Critical to understanding the distribution of sedimentary Fe is a knowledge of the processes converting Fe between its various forms, and how they vary spatially in aquatic systems.

In boreal terrestrial environments, Fe is released during the chemical weathering of Fe-bearing minerals in soils. These include silicates in the fine fraction of till (~~Lahermo et al., 1996~~Lahermo et al., 1996), and, especially in areas overlain with late- or post-glacial lacustrine and brackish water sediments, previously deposited reactive Fe minerals (Virtasalo and Kotilainen, 2008). During weathering under oxic conditions in the absence of organic ligands, Fe (II) is quickly oxidized to Fe (III), which in turn precipitates as oxides (Schwertmann and Taylor, 1977). Typically, the first-formed oxide mineral is amorphous, ~~highly reactive~~ labile ferrihydrite. The structure of ferrihydrite is still debated, but a recent study suggested the relatively FeO-rich (and Fe-OH poor) formula of $Fe_{10}O_{14}OH_2.nH_2O$ to be most accurate (Hiemstra, 2013). ~~$(Fe^{3+}_{4-5}(OH,O)_{12})$, which~~Ferrihydrite may subsequently mature into crystalline, refractory ~~crystalline~~ oxides such as ~~goethite and~~ goethite and hematite (Raiswell, 2011). Although such maturation is rapid in tropical and temperate systems, under the cold, low pH conditions of boreal aquatic environments its half-life may be several years (Schwertmann et al., 2004). However, goethite may also form directly during the oxidation of Fe (II) in sedimentary environments (e.g. van der Zee et al., 2003).

Formatted: Subscript
Formatted: Subscript
Formatted: Subscript
Formatted: Subscript

Weathering of Fe in boreal systems also frequently occurs under anoxic conditions, in the presence of dissolved organic compounds such as humic and fulvic acids (Krachler et al., 2016), for example in peatland environments. These compounds are effective chelators of dissolved Fe, and form complexes with Fe (II) in anoxic soil solution (Sundman et al., 2014). Such complexes are typically nanoparticulate–colloidal in size and hence pass through 0.2–0.45 µm pore-size filters, to operationally classify as dissolved material. The stability of Fe (II)-organic complexes (Fe (II)-OM) in river systems depends on the concentration of chelating organic compounds and the time available for oxidation (Ingri and Conrad, 2015). Typically, dissolved Fe in upstream areas of boreal catchments ~~is dominated by~~consists of both Fe (III)-organic complexes (Fe (III)-OM) and ferrihydrite~~, while increasing pH conditions further downstream may convert the Fe in these complexes to ferrihydrite~~ (Neubauer et al., 2013). Ferrihydrite itself is nanoparticulate (Raiswell, 2011), and its high surface area ~~and density of hydroxyl groups~~ favors continued association with DOM colloids via sorption (Dzombak et al., 1990; Eusterhues et al., 2008). However,

the fraction of riverine Fe present as discrete ferrihydrite particles has been shown to increase with rising pH, as is typically observed with increasing stream order towards the coastal zone (Neubauer et al., 2013).

In estuarine environments, elevated electrolyte strength along salinity gradients induces the flocculation of DOM (Sholkovitz et al. 1978) and ~~associated~~ Fe (Boyle et al., 1977) from river waters. This phenomenon is usually explained by the cation-induced ~~coagulation~~ aggregation of colloidal humic substances, which carry a net negative surface charge (Eckert and Sholkovitz 1976~~).~~). Any Fe associated directly with DOM is therefore expected to aggregate passively during this process. Flocculation of DOM is typically selective for humic substances of high molecular weight and larger colloidal particle size (Uher et al., 2001; Asmala et al., 2014). Consequently, the 'truly dissolved' DOM-associated Fe which passes through the flocculation zone of estuaries (e.g., Dai and Martin, 1995) is associated with DOM of lower molecular weight and smaller colloidal particle size (e.g., < 3 nm), most likely in the form of fulvic acids (Stolpe and Hassellöv, 2007). This component may be more substantial than previously thought and hence play a role in providing Fe as a micronutrient to the oceans (Kritzberg et al., 2014; Krachler et al., 2016). However, the majority of ~~the majority of dissolved Fe in river water is associated with higher molecular weight DOM, hence most~~ riverine dissolved Fe is retained ~~by flocculation~~ in estuaries (Raiswell, 2011~~).~~), implying an important role for flocculation in the removal of dissolved Fe. Importantly, the flocculation behavior of Fe in boreal estuaries appears to differ from that of bulk DOM (Asmala et al., 2014), which may be partly related to factors influencing the discrete ferrihydrite-bound Fe component rather than Fe directly associated to DOM. These factors include pH gradients and the concentration of suspended clay material (Forsgren et al., 1996)

Together with the deposition of riverine particulate Fe close to river mouths (Poulton and Raiswell, 2002, Li et al., 2016), flocculation may thus be expected to act as an important mechanism of Fe sedimentation in the coastal zone. The role of flocculation ~~in Fe sedimentation~~ may be particularly enhanced in boreal estuarine systems due to the high~~, where high~~ DOM and dissolved Fe concentrations in this region~~fluxes maintain a relatively large component of riverine Fe in the dissolved phase~~ (Kritzberg et al., 2014). However, few studies have attempted to investigate the connection between flocculation and the Fe distribution in boreal estuarine sediments. This is a significant gap in existing knowledge, since an increasing number of studies have demonstrated the importance of reactive Fe minerals in sedimentary diagenesis in boreal coastal areas, including their roles in the anaerobic oxidation of methane (AOM) (Slomp et al., 2013; Egger et al., 2015a) and in phosphorus retention in sediments (Reed et al., 2011; Norkko et al., 2012; Egger et al., 2015b). Furthermore, Fe has recently been suggested to play an important role in carbon burial (Lalonde et al., 2012; Shields et al., 2016) and nitrogen cycling (Robertson et al., 2016) in marine sediments.

Understanding the distribution of Fe minerals in boreal sedimentary environments will improve our knowledge of the broader role of Fe in sediment biogeochemistry. Here we present a combined study of water column, sediment and pore water chemistry

in a non-tidal estuarine system in the northern Baltic Sea, to investigate the impact of ~~DOM~~ flocculation on the distribution of Fe in boreal coastal sediments and the subsequent diagenetic transformations during burial. In the estuarine water column, we study the distribution of dissolved and particulate Fe and organic matter, to assess the transfer of these components from the dissolved to particulate phase along the salinity gradient. Using sediment core data from selected locations, we show how processes in the water column control the lateral distribution of labile and refractory Fe, and~~Fe and~~ organic matter, in estuarine sediments. ~~. Furthermore, we investigate the degree to which these processes have remained stable during recent changes in nutrient inputs to the coastal zone of the Baltic, and industrial activity in the vicinity of our study sites.~~ Finally, we demonstrate how the lateral distribution of labile Fe, together with salinity ~~and redox~~ gradients, influences the vertical diagenetic zonation of the sediments along the estuarine transect and net rates of Fe transformations in the sediment column.~~:~~

2 Study location

The Finnish coastline of the western Gulf of Finland and Archipelago Sea (northern Baltic Sea) is characterized by a mosaic of islands and small bays, intersected by a network of channel-like, non-tidal estuaries (Fig. 1a). The undulating mosaic represents the bedrock surface known as the pre-Cambrian peneplain (Winterhalter et al., 1981), while the channels correspond to fault lines in the bedrock (Hausen, 1948; Virtasalo et al., 2005). The entire area was covered by the Fennoscandian continental ice-sheet during the last glacial (Weichselian) maximum. The ice-margin retreat from the area ca. 12 ka ago was followed by the successive deposition of till, outwash, glaciolacustrine rhythmite, patchily-distributed debrites, postglacial lacustrine clay and brackish-water mud drift (Virtasalo et al., 2007). These deposits provide the source material for mobile Fe in the drainage basins of southern Finland, and each deposit has a distinct Fe mineralogy (Virtasalo and Kotilainen, 2008).

The principal study area is the estuary of the Mustionjoki river and its adjacent archipelago (Fig. 1a). This river and its estuary appear under several alternative Finnish-, Swedish- and English- language names in cartographic material and the scientific literature, including Karjaanjoki (e.g., Asmala et al., 2014), Pohjanpitäjänlahti (e.g., Virta, 1977), Pojoviken (e.g., Niemi, 1977) and Pojo Bay. The First Salpausselkä ice-marginal formation intersects the estuary close to the town of Ekenäs (Fig. 1a). The First Salpausselkä forms a shallow sill of < 10m water depth, separating the inner basin of the estuary (maximum water depth 39 m) from the slope of the archipelago towards the open Gulf of Finland (Fig. 1b). A pronounced estuarine circulation is observed, with continuous freshwater outflow at the surface and intermittent brackish water inflows at depth. Inflows typically occur in winter, when discharge from the river is at a minimum (Virta, 1977). Subsequent stagnation of the deep water masses leads to oxygen depletion, with hypoxic conditions (oxygen concentrations < 2mg L^{-1}) observed during the late summer and autumn months of some years (Niemi, 1977).

Formatted: Superscript

3 Materials and methods

3.1 Hydrographic profiling

Over 2 days of sampling onboard R/V Saduria and R/V J.A. Palmén in June 2015, water column temperature, salinity and dissolved oxygen profiles were collected at ~~station~~Stations A–K in the estuary of the Mustionjoki river and adjacent archipelago, using multiparameter water quality sondes (YSI™ CTD with optical oxygen sensor and Valeport MiniCTD). The 11 vertical profiles for each parameter were interpolated into cross-sectional contour plots using the Sigmaplot™ software package (Fig. 1b). ~~Station~~Station A is situated at the mouth of the Mustionjoki river, while ~~station~~Station K is situated 33 km due S of the river mouth (~40 km absolute distance along transect) in the open Gulf of Finland. The precise locations of the ~~station~~stations were selected on the basis of suitability for sediment sampling; all are situated in ~~10–100 m scale~~ bathymetric depressions of 10–100 m-lateral scale, where soft sediments are expected to accumulate.

3.2 Sampling and analysis of suspended particulate organic matter

During the sampling campaign in June 2015, discrete water samples were collected at 5 m depth intervals at ~~station~~Stations A–K in the estuary of the Mustionjoki river and adjacent archipelago, using a 5 L Limnos™ water sampler. Water samples were transferred onboard to acid-washed polyethylene bottles, stored at 4°C and filtered within 48 hours of sampling at Tvärminne Zoological ~~Station~~Station, Hanko, Finland. One 500 ml aliquot of each sample was filtered through pre-weighed, pre-combusted (450°C for 4 h) Whatman® GF/F filters (nominal pore size 0.7 µm). ~~GF/F filters were freeze-dried and re-weighed to estimate total suspended solids (TSS).~~ Total carbon (C_{tot}) and total nitrogen (N_{tot}) on the filters, and the stable isotopic ratio of carbon relative to the Vienna Pee Dee Belemnite ($\delta^{13}C$), were estimated by thermal combustion elemental analysis-mass spectrometry (TCEA-MS) at Tvärminne Zoological ~~Station~~Station. Precision and accuracy of all parameters as checked by in-house and reference standards was < 2.5% relative standard deviation (RSD). Replicate analysis yielded results that were identical within measurement error (see Figure R1 in the Response to Referee supplement in the associated Discussion paper). Particulate inorganic carbon and nitrogen are assumed insignificant in this setting, hence C_{tot} and N_{tot} are assumed equal to organic carbon and nitrogen, respectively (C_{org} and N_{org}).

3.3 Sampling and analysis of particulate and dissolved Fe

During the sampling campaign in June 2015, two additional 250 ml aliquots of water from each sample were filtered through parallel Whatman® Nuclepore track-etched polycarbonate membrane filters (pore size 0.4 µm). Filtrate was collected in 15 ml centrifuge tubes and acidified to 1M HNO_3 for analysis of dissolved Fe and other elements by ICP-MS at University of Helsinki Department of Geosciences and Geography. Filters were freeze-dried and acid-digested in Teflon™ vessels (digestion in 2.5 mL HF + 2.5 mL $HClO_4$/HNO_3 at volumetric ratio 3:2, reflux at 90°C for 12 h, followed by evaporation of acids until gel texture and re-dissolution in 20 mL 1M Suprapur® HNO_3). Analysis of particulate Fe (among other elements) in the resulting

digests was performed by ICP-OES at University of Helsinki Department of Food and Environmental Sciences (precision and accuracy < 5% RSD as determined by in-house and reference standards). All ~~Values~~ values ~~were converted to~~are reported as µmol L^{-1} ~~using TSS estimates from the corresponding GF/F filter~~.

3.4 Sediment sampling and preparation

In September 2014 onboard R/V Saduria, sediments were collected from ~~station~~Stations A–K on the Mustionjoki estuary transect using a GEMAX™ short gravity corer (internal diameter 9 cm, core length 30–60 cm). Four to five sediment slices of 2 cm thickness, evenly spaced with depth over the full length of the core, were obtained from each ~~station~~station (e.g., ~~station~~Station K: 0–2 cm; 8.5–10.5 cm, 17–19 cm, 25.5–27.5 cm, 34–36 cm). During sampling campaigns in 2015, GEMAX™ cores were taken from ~~station~~Stations A, D (June) and J (April, June) and sliced completely at 1 cm resolution (0–10 cm depth) and 2 cm resolution (10 cm depth–core base). An additional sample from the surface sediments of the Mustionjoki river, taken close to Station "a" (lower case) in Fig. 1a, was obtained with a grab sampler in September 2015. In all campaigns, whole sediment slices were transferred immediately to plastic bags, dipped in water to seal the bag, and deposited in a gas-tight jar that was flushed with nitrogen within 1 h of sampling and stored dark at 4°C until further processing. Due to the large volume of tightly-packed sediment in each jar, visible oxidation effects during sampling and storage were minimal.

Subsamples of wet sediment slices were ~~obtained~~ taken from the jars under nitrogen atmosphere, frozen, freeze-dried and homogenized, and stored in N_2-filled gas-tight jars until further processing. Parallel wet samples were stored frozen at -20°C. Water content (% water by weight) and porosity (% water by volume) were estimated from weight loss during freeze drying, assuming a solid-phase density of 2.65 g cm^{-3} (Schulz and Zabel, 2006). The content of salt material in the dried sediment matter was estimated from water content and the measured bottom water salinity at each site.

Formatted: Superscript

3.5 Analysis of sedimentary organic matter

Selected sediment samples were prepared for analysis of sedimentary organic matter. Sub-samples of dried, powdered sediments were weighed into aluminium capsules. Total sedimentary carbon (C_{tot}) and nitrogen (N_{tot}), and the stable isotopic ratio of carbon reported relative to Vienna Pee Dee Belemnite ($\delta^{13}C$), were estimated by thermal combustion elemental analysis-mass spectrometry (TCEA-MS) at Tvärminne Zoological ~~Station~~Station and University of California, Davis, USA. Precision and accuracy of all parameters as checked by in-house and reference standards was < 2.5% RSD. Sedimentary inorganic carbon and nitrogen are assumed insignificant in this setting, hence C_{tot} and N_{tot} are assumed equal to organic carbon and nitrogen, respectively (C_{org} and N_{org}).

3.6 Quantification of organic matter sources

A simple two-component mixing model was applied for a first-order quantification of the relative contributions of terrestrial plant-derived organic material ($\%OC_{terr}$), vs. riverine–estuarine phytoplankton ($\%OC_{phyt}$), to total organic matter in both water column and sediment samples. The calculation uses only the molar N/C ratio of organic matter, and end-member values, N/C_{EM}, based on the study of Goñi et al. (2003):

$$\%OC_{phyt} = \frac{\left(N/C_{sample} - N/C_{EM-terr}\right)}{\left(N/C_{EM-phyt} - N/C_{EM-terr}\right)} \times 100 \quad (1)$$

$$\%OC_{terr} = 100 - \%OC_{phyt} \quad (2)$$

where $N/C_{EM\text{-}terr} = 0.04$, and $N/C_{EM\text{-}phyt} = 0.13$. The calculation assumes that plant matter and phytoplankton are the only sources of organic material present in the samples, that their N/C values are spatially and temporally fixed at the end-member values, and that these values do not alter significantly during sedimentation and burial of organic matter. Fields in N/C vs. $\delta^{13}C$ space, also taken from Goñi et al. (2003) and corresponding to riverine–estuarine phytoplankton, marine phytoplankton, and terrestrial C3 plants respectively, were used in the interpretation of the data.

3.7 Analysis of sedimentary Fe, S and Pb by ICP-OES

Selected sediment samples were prepared for ICP-OES analysis. Sub-samples of dried, powdered sediments were weighed into Teflon digestion vessels and digested in an acid cocktail (digestion in 2.5mL HF + 2.5 mL $HClO_4/HNO_3$ at volumetric ratio 3:2, reflux at 90°C for 12 h, followed by evaporation of acids until gel texture and re-dissolution in 20 mL 1M Suprapur^R HNO_3). ICP-OES analysis for total Fe, sulfur (S) and lead (Pb), among other elements, was performed at University of Helsinki Department of Food and Environmental Sciences (precision and accuracy < 5% as determined by in-house and reference standards). Total Fe and S from ICP-OES analysis were used in combination with other extraction data to estimate pyrite and residual silicate-bound Fe ("Subsample 3" in Table 2).

3.8 Estimate of sedimentation rates using sedimentary Pb profiles

Sedimentation rates for ~~station~~Stations A, D and J were estimated on the basis of total Pb (Pb_{tot}) profiles measured on the three GEMAX^{TM} cores from 2015. Each core profile showed a distinct peak in Pb_{tot} (Supplementary ~~Figure~~ Fig. 1) which was assigned to the year 1970 (Renberg et al., 2001; Zillen et al., 2012). A first order estimate of sedimentation rate was calculated assuming constant ~~mass accumulation~~sedimentation over the period 1970–2015.

3.9 Sequential extraction and analysis of sedimentary Fe phases

~~Selected sediment samples were subjected to the~~ A set of complementary extraction procedures was performed on sediment samples to assist in the identification of labile and refractory Fe phases (Table 2). The distinction between labile and refractory in this study is made on the basis of the extractions employed, and does not directly translate to reactive vs. non-reactive Fe. For example, refractory phases include crystalline oxides and pyrite, which classify as reactive Fe by common definitions. Initially, for the surface sediment samples from 2014 (0–2 cm), and full downcore profiles (minimum 10 samples) from Stations A, D and J from 2015, the sequential extraction procedure for Fe described by Poulton and Canfield (2005) was carried out (Table 2, "Subsample 1"). Here, Stages 1 and 2 of this protocol are considered to extract labile Fe, while the remaining components are considered refractory. Sub-samples of dried, powdered sediments were weighed into extraction vessels and a series of reagents was applied sequentially ~~(Table 2)~~. After each addition, samples were placed in an orbital shaker for the duration of the extraction, then centrifuged at 3000 rpm for 5 minutes before decanting the supernatant. To limit the risk of oxidation affecting the Fe speciation during the extraction, ~~stages~~ Stages 1–4 of the extraction procedure were performed under nitrogen atmosphere, and reagents were purged with nitrogen for 30 mins prior to addition to the samples. All supernatants were analyzed for Fe (among other elements) by Microwave Plasma-Atomic Emission Spectroscopy (MP-AES) at University of Helsinki Department of Geosciences and Geography. Replicate extraction of parallel samples yielded RSD values of < 15% for all stages of the procedure.

Subsequently, 5 additional samples from each of the 2015 cores (Stations A, D, and J) were subjected to a 1 hour room-temperature 1M HCl extraction as described in Burton et al. (2011) and Yu et al. (2015), to further investigate the labile Fe phases (Table 2, "Subsample 2"). These samples were taken from wet sediments, frozen shortly after sampling and dried under nitrogen prior to the extraction. Two parallel weighed subsamples were treated with, respectively, 1M HCl and 1 M HCl + 1M hydroxylamine-HCl for 1 hr. All reagents were purged with nitrogen for 30 mins prior to addition to the samples, and the addition of reagents was performed under nitrogen before transfer to an orbital shaker. Both extractions are expected to dissolve all labile Fe (II) and Fe (III) phases. After extraction, the 1M HCl extract may contain both Fe (II) and Fe (III), whereas in the combined extract, the reducing agent hydroxylamine-HCl maintains all dissolved Fe in the divalent state. Fe (II) in each extract was determined spectrophotometrically by the 1,10 phenanthroline method (APHA, 1998), allowing 1M-HCl soluble Fe (II) and 1M HCl-soluble Fe (III) to be deconvolved as follows:

$$1M\ HCl\ soluble\ Fe\ (III) = Total\ 1M\ HCl\ soluble\ Fe - 1M\ HCl\ soluble\ Fe\ (II)\ \text{(all units µmol g}^{-1}\text{)} \quad (3)$$

A trap was added to the 1M HCl extraction vessel to collect evolved hydrogen sulfide (H_2S) released during the dissolution of acid-volatile sulfur (AVS). The trap consisted of an open test tube inside the closed extraction vessel as described in Burton et

Formatted: Subscript

al. (2008). The test tube was filled with a solution of 0.2 M zinc acetate in 1M NaOH and the extraction vessel was placed on the shaker in vertical orientation. Evolved H_2S from the sample was visibly trapped as a ZnS precipitate in the alkaline solution. The concentration of AVS in the samples was determined by iodometric titration of the ZnS precipitate after redissolution by acidification (Burton et al., 2008). Assuming AVS to be dominantly present as iron monosulfide (FeS), the concentrations of sulfidized and unsulfidized 1M HCl-soluble Fe (II) were estimated thus:

$$Sulfidized\ 1M\ HCl\ soluble\ Fe\ (II) = AVS\ Fe \text{ (all units µmol g}^{-1}\text{)} \quad (4)$$

$$Unsulfidized\ 1M\ HCl\ soluble\ Fe\ (II) = Total\ 1M\ HCl\ soluble\ Fe\ (II) - AVS\ Fe \text{ (all units µmol g}^{-1}\text{)} \quad (5)$$

where AVS-Fe is Fe bound to AVS. Furthermore, assuming zero-valent sulfur to be a negligible component of total S in sediments from this region (see Yu et al., 2015), the fraction of pyrite (FeS_2)-bound Fe was estimated from ICP-OES-derived total S, and AVS, as follows:

$$Pyrite\ Fe = \frac{Total\ S - AVS}{2} \text{ (all units µmol g}^{-1}\text{)} \quad (6)$$

where AVS = AVS-Fe due to the 1:1 stoichiometry of FeS. For depth intervals of the 2015 cores where no AVS-Fe data was available, the division of total S into AVS and pyrite was estimated from mean ratios of these components for each core. For the surface sediments form 2014, all S-bound Fe was assumed to be pyrite as per equation 3 of the associated Discussion paper. Total S data were corrected prior to equation (6) for the contribution of crystallized sulfate salts during sample drying. The contribution of sulfate to the total salt content of dried sediment matter was determined for each sediment depth by reference to the corresponding pore water sulfate profile. Crystallized salt contributes approximately 25% of total S in the surface sediments at Station J, where salinity, sulfate concentration and water content are all at maximum values. The contribution declines significantly with depth and at lower salinity sites (e.g., 1.3% of total S in the surface sediments at Station A). ~~The Poulton and Canfield (2005) protocol does not include an explicit stage for the extraction of Fe from sulfide minerals. For the purposes of this study, we assumed the dominant sulfide mineral present in the samples to be pyrite (FeS_2), which is insoluble in stages 1–5 of the protocol (Poulton and Canfield, 2005). Hence, we estimated the contribution of sulfide-bound Fe to total Fe according to:~~

~~$$Sulfide\ Fe = 0.5 \times Total\ S \text{ (all units µmol g}^{-1}\text{)} \quad (3)$$~~

~~This is a conscious approximation, since sediments from this region are known to also contain iron monosulfide (FeS) (e.g., Egger et al., 2015a, Yu et al., 2015); however the approximation has no bearing on the main conclusions of the study.~~

Formatted: Subscript

Formatted: Subscript

The sum of the 5 stages of the Poulton and Canfield (2005) sequential extraction procedure, plus the estimated contribution of ~~sulfide~~pyrite-bound Fe, were subtracted ~~form~~ from total Fe as determined by ICP-OES, to estimate residual (non-soluble) Fe, assumed to be present in unreactive silicate minerals:

$$Residual\ Fe = Total\ Fe - \sum Stages\ 1\ to\ 5 - \sout{Sulfide}Pyrite\ Fe \text{ (all units µmol g}^{-1}\text{)} \quad (4\sout{7})$$

3.10 Mössbauer spectroscopy of sedimentary Fe phases

Additional information about Fe phases present in the sediments was gathered from room temperature (RT) ^{57}Fe Mössbauer spectroscopy (e.g., Murad and Cashion, 2004; Gütlich and Schröder, 2012). A total of seven dried, powdered samples were analyzed at the University of Stirling, U.K. For each sample, 50–100 mg of dried material was placed in acrylic glass tubs with a circular cross section of ~1 cm². Mössbauer spectra were collected using a miniaturized Mössbauer spectrometer (MIMOS II, Klingelhöfer et al. 2003) set up in backscattering geometry, or a standard transmission Mössbauer spectrometer (Wissel, Germany). Both instruments used a ^{57}Co in Rh matrix radiation source in constant acceleration mode. Two samples (Station A, 0–1 cm and Station D, 0–1 cm) were analyzed in backscattering mode. Peaks in backscatter spectra display as emission maxima (Supplementary Fig. 2). The remaining five samples (river bed sediment from Station 'a', Station A (26–28 cm), Station D (26–28 cm), Station J (0–1 cm) and Station J (30–32 cm)) were analyzed in transmission mode. Troughs in transmission spectra correspond to absorption maxima (Supplementary Fig. 2). All spectra were calibrated against alpha-iron at room temperature. Backscatter Mössbauer spectra were evaluated using an in-house routine (Mbfit) with Lorentzian line profiles, based on the least-squares minimization routine MINUIT (James 2004). Transmission Mössbauer spectra were evaluated using Recoil software (University of Ottawa, Canada) and the Voigt-based fitting routine (Rancourt and Ping, 1991).

Mössbauer spectroscopy allows estimation of the relative contribution of Fe (II) and Fe (III) phases to a bulk sample, due to the distinctly different isomer shift of Fe (II) vs. Fe (III) compounds (see Fig. 7). Allocation of the subspectral components to known (groups of) Fe (II) and Fe (III) phases was performed by comparison of the hyperfine parameters – isomer shift (δ) in mms^{-1}, quadrupole splitting (ΔEQ) in mms^{-1}, and internal magnetic field (B_{hf}) in T – of each subspectrum with those of library reference spectra (e.g., Stevens et al., 2002) for a range of Fe-bearing compounds. The subspectral components were assigned either to distinct Fe minerals (in the case of unambiguous hyperfine parameters), or to generic groups of minerals characterized by similar isomer shift, quadrupole splitting and internal magnetic field characteristics (e.g., "superparamagnetic (SP) Fe (III)", "silicate-Fe (II)"). Assuming equal recoil-free fractions of total absorbed energy – no f-factor correction was applied – the concentration of each component was estimated directly from its contribution to the area of the Mössbauer absorption/emission

spectrum, and bulk Fe (II): Fe (III) ratios for each sample were estimated directly from the total contribution of Fe (II) and Fe (III) components.

Diamagnetic and paramagnetic mineral phases generally display as a doublet (two related peaks) in Mössbauer spectra whereas magnetically ordered phases display as a sextet (six related peaks). It should be noted that size of the crystal domain influences magnetic ordering in some minerals. This is particularly important in the case of goethite, a crystalline oxide which at room temperature displays superparamagnetic behavior (hence a doublet spectrum) for particle sizes < 12 nm, but magnetically ordered behavior (sextet spectrum) for particle sizes > 12 nm (van der Zee et al., 2003). Furthermore, spectral interferences between some components limit the sensitivity of RT Mössbauer spectroscopy for minor components of total sedimentary Fe. For example, the doublet for pyrite (FeS_2) shows a strong overlap with that of superparamagnetic Fe (III). To aid the reader, we present a selection of relevant Mössbauer reference spectra alongside the sample data of this study (Fig. 7 and Supplementary Fig. 2). ~~Surface sediment samples (0–1 cm) from stations A and D sampled in June 2015 were prepared for Mössbauer spectroscopy. Sub-samples of dried, powdered sediments (station A: 52 ±9 mg; station D: 97 ±9 mg) were placed in acrylic glass tubs with a circular cross section of ~1 cm². Mössbauer spectra were collected using a miniaturized Mössbauer spectrometer MIMOS II (Klingelhöfer et al. 2003) with a ^{57}Co in Rh matrix radiation source in constant acceleration mode. The source had an activity of ~1.4 GBq and the instrument was set up in backscattering geometry. Measurements were performed at room temperature. Spectra were calibrated against alpha-iron at room temperature and fitted with an in-house routine (Mbfit) using Lorentzian line profiles. Mbfit is based on the least-squares minimization routine MINUIT (James 2004). Quantification of iron-bearing phases and iron oxidation states is based on relative subspectral areas. No f-factor correction was applied.~~

3.11 Pore water sampling

Prior to sediment slicing during the June 2015 campaign, pore water was sampled through pre-drilled holes (⌀ 4 mm) in the GEMAX™ coring tubes, using Rhizons™ mounted on a purpose-built plastic rack. Two parallel series of samples (vertical resolution 2 cm) were obtained for each core; one for analysis by ICP-OES, the other for analysis of dissolved hydrogen sulfide (H_2S). Samples were collected in polyethylene syringes connected directly to the Rhizons™, which were held open by a wooden spacer to create a vacuum. The syringes of the H_2S series were pre-filled with 1 ml 10% zinc acetate solution to trap sulfide as ZnS. All samples were transferred from the syringes to 15 ml centrifuge tubes in the laboratory within 2 h of sampling. From the first series, a sub-sample for ICP-OES analysis was taken immediately and acidified to 1 M HNO_3. A parallel GEMAX™ core, pre-drilled with holes of ⌀ 15 mm, was used for sampling for dissolved methane (CH_4). 10 ml wet sediment was collected through each hole using a cut-off syringe and transferred to a 65 ml glass vial filled with saturated NaCl solution (Egger et al., 2015a). Vials were capped with a rubber stopper, and a headspace of 10 ml N_2 (quality 5.0) was injected using a gas-tight glass syringe. Methane in pore waters was assumed to be quantitatively salted out into the headspace

during equilibration (O'Sullivan and Smith, 1970). Samples were stored upside-down until analysis such that headspace gas was not in contact with the rubber stopper.

3.12 Pore water analysis

Acidified pore water sub-samples from the first series of Rhizons™ were analyzed for total Fe and S, among other elements, by ICP-OES at University of Helsinki Department of Food and Environmental Sciences. Iron is assumed to be present in pore waters as Fe^{2+}, while S is assumed to represent SO_4^{2-} only, due to the loss of H_2S during sample acidification (Jilbert and Slomp, 2013). H_2S concentrations in pore water samples from the second series of Rhizons™ were determined by spectrophotometry (670 nm) after direct addition of an acidic solution of $FeCl_3$ and n,n-dimethyl-p-phenylenediamine (Cline, 1969; Reese et al., 2011) to the sample vials. This procedure dissolves the ZnS precipitate and immediately complexes S as methylene blue for spectrophotometric analysis. H_2S concentrations were calibrated against a series of standard solutions of $Na_2S \cdot 3H_2O$, fixed in Zn acetate in the same manner as the samples. The exact concentration of S in the $Na_2S \cdot 3H_2O$ stock solution was determined by iodometric titration (Burton et al., 2008).

For analysis of dissolved CH_4, 1 ml headspace gas was sampled from the 65 ml vials using a gas-tight glass syringe. An equivalent volume of salt solution was allowed to flow into the vial through a parallel syringe to equalize pressure in the headspace. Gas samples were then injected into 12 mL gas-tight glass Exetainer™ vials (LabCo model 839W). An additional 20 mL N_2 gas was injected into the Exetainers to generate overpressure prior to analysis. CH_4 concentrations were analyzed using an Agilent Technologies 7890B gas chromatograph (GC) at University of Helsinki Department of Environmental Sciences, equipped with flame ionization detector (FID) at 250°C, oven temperature 60°C, 2.4 m Hayesep Q column with 1/8" connection, 80/100 mesh range, 1.0 mL sample loop and helium carrier gas at flow rate 21 mL min^{-1}. Raw peak area data were converted to mole fraction (ppm) using a 4-point linear calibration of standard gas mixtures (certified concentrations ± 2%) and blanks, analyzed prior to each sample series. Single standards were analyzed after every 10 samples to monitor within-series drift, which was observed to be negligible. Concentrations in the pore water of the original 10 ml wet sediment sample were back-calculated ~~assuming a constant porosity of 90%~~using a best-fit line through the porosity profile from the parallel core for solid-phase sampling.~~.~~

3.13 Calculation of diagenetic process rates

Formatted: Font: Bold

To investigate instantaneous relative rates of anaerobic diagenetic processes, the portion of the sediment column corresponding to 1970–2015 for each of the Stations A, D, and J was used to define a 1-dimensional model domain. For the analysis of pore water profiles, a simplified version of the 1-dimensional mass conservation equation of Boudreau (1997) and Berg et al. (1998) was used:

$$\frac{d}{dx}\left(\varphi D_s \frac{dC}{dx}\right) + R = 0 \quad (8)$$

in which x = depth, φ = porosity, D_s = molecular diffusivity of a given species, corrected for tortuosity, salinity and temperature, C = concentration of the species in the pore water or bottom water, and R = the net rate of production of the species due to diagenetic reactions, expressed per unit volume of sediment. This simplified form of the mass conservation equation assumes steady state conditions, and neglects pore water advective processes, biodiffusion and bioirrigation. The equation states that the net rate of production or consumption of a dissolved species in the pore waters at a given depth can be calculated from the change in gradient of the concentration (i.e. the second derivative of the concentration, C) at the same depth, provided the diffusivity and porosity are known.

The above equation was used to estimate net rates of production and consumption of pore water iron (Fe^{2+}), sulfate (SO_4^{2-}) and methane (CH_4) within discrete depth intervals of the sediment column from the measured pore water profiles of these species. Calculations were performed using the PROFILE software (Berg et al., 1998), which selects the optimum number of discrete depth intervals of production and consumption based on a least squares fitting routine.

To study the longer-term relative rates of Fe reduction and sulfate reduction at the same stations, we estimated depth-integrated accumulation rates of reduced solid-phase Fe and S in the sediments within the interval 1970–2015. Assuming solid-phase reactive Fe to accumulate at the sediment water interface as Fe (III) only, we estimated the mean rate of production of reactive Fe (II) from 1970–2015 within the sediment column as:

$$\sum Fe\ (II) = Unsulfidized\ 1M\ HCl\ soluble\ Fe\ (II) + AVS\ Fe\ + Pyrite\ Fe \quad \text{(all units µmol cm}^{-2}\ \text{yr}^{-1}\text{)} \quad (9)$$

A similar exercise was done for sulfur. Assuming all sedimentary sulfur to be derived from the reduction of seawater sulfate, we estimated the mean rate of production of reduced sulfur from 1970–2015 within the sediment column as:

$$\sum S = AVS + Pyrite\ S \quad \text{(all units µmol cm}^{-2}\ \text{yr}^{-1}\text{)} \quad (10)$$

Note that pore water Fe^{2+} and H_2S are considered negligible contributors to ΣS and ΣFe (II).

Because the individual data series have variable depth resolution, prior to the above calculations, weighted mean mass concentrations of each sediment parameter for the interval 1970–2015 were estimated for each core. Volume concentrations were then estimated from weighted mean mass concentrations as follows:

$$C_v = C_m \times 2.65 \times (1 - \varphi) \quad (11)$$

Formatted: Subscript

Formatted: Subscript

Formatted: Superscript

Formatted: Subscript

Formatted: Superscript

Formatted: Superscript

Formatted: Superscript

Formatted: Subscript

where C_v is weighted mean volume concentration in µmol cm^{-3}, C_m is weighted mean mass concentration in µmolg^{-1}, and 2.65 is the density of solid matter in sediments in g cm^{-3}.

Formatted: Subscript

Formatted: Subscript

3.13 Additional supporting data

N/C and $\delta^{13}C$ of DOM was measured from surface-water samples from six locations along the Mustionjoki estuary transect (~~station~~Stations *a–f*, Fig. 1a) during three sampling campaigns (April, August and October) in the year 2011, as reported in Asmala et al. (2014) and Asmala et al. (2016). Sampling locations are given in Table 1.

Surface sediment (0–1 cm) total Fe and Al data was generated for six locations in the estuary of the Paimionjoki river and its adjacent archipelago (~~station~~Stations L–Q, Fig. 1a). Samples were obtained in August and September 2001 during a 94-~~station~~Station survey of Archipelago Sea sediments, as reported in the studies of Virtasalo et al. (2005) and Peltola et al. (2011). For comparability with the present study, new subsamples of this material were digested and analyzed as ~~outlined above~~described in Section 3.7. The locations and water depths of ~~station~~Stations L–Q are given in Table 1.

4 Results

4.1 Hydrography of the transect

At the time of the primary sampling campaign in June 2015, the water column in the estuary of the Mustinojoki river and the adjacent archipelago was strongly stratified. ~~Strong v~~Vertical temperature stratification was evident throughout the transect (Fig. 1b, top), while ~~strong~~ salinity stratification was also present in the inner basin of the estuary (Fig. 1b, middle). The freshwater input from the Mustionjoki river was sufficient to generate a surface-water lens of salinity 0–2 extending across the entire inner basin north of the First Salpausselkä, which forms the sill at Ekenäs. The halocline shallowed towards the sill, and the salinity isolines between ~~station~~Stations C and G were strongly inclined. Deep waters upstream of the sill showed depleted concentrations of dissolved oxygen relative to surface-water values (7–8 mg L^{-1} vs. 10–11 mg L^{-1}).

4.2 Dissolved and particulate Fe in the water column

Dissolved Fe concentrations in the surface water at the mouth of the Mustionjoki river in June 2015 (~~station~~Station A, salinity 1.0) were 1.3 µmol L^{-1} (Fig. 2a). Concentrations decreased offshore to values around 0.02 µmol L^{-1} ~~µmol/L~~ in the open waters of the Gulf of Finland (~~station~~Station K). The isolines of [Fe_{diss}] in the estuarine water column were inclined similarly to those of salinity (Fig. 1b), with a relatively deep surface layer of Fe-rich waters at the river mouth shallowing towards the sill at Ekenäs. However, surface water salinity and [Fe_{diss}] along the transect show a strongly non-linear relationship, ~~suggesting~~

indicating non-conservative mixing between river and offshore water with respect to [Fe_{diss}], due to removal of Fe_{diss} from solution (Fig. 2b).

Particulate Fe in the water column of the estuary in June 2015 showed a contrasting distribution to that of [Fe_{diss}] (Fig. 2a). Although maximum [Fe_{part}] was also observed at the river mouth (3.9 µmol L^{-1} in surface waters at ~~station~~Station A), values decreased rapidly within a short distance offshore (~~station~~Station B surface water = 1.4 µmol L^{-1}; ~~station~~Station B, 5 m depth = 0.6 µmol L^{-1}). Further away from the river mouth, [Fe_{part}] showed higher values in a zone extending from 15 m depth at ~~station~~Station C to the surface waters at ~~station~~Station G (Fig. 2a), approximately coinciding with the halocline of salinity = 2–4 (Fig. 1b). In the archipelago region of the transect (~~station~~Stations G–J), [Fe_{part}] declined gradually offshore.

4.3 Particulate organic matter in the water column

Particulate organic carbon (POC) and nitrogen (PON) concentrations in the water column of the estuary in June 2015 ranged from 5–75 µmol L^{-1} and 0.5–7 µmol L^{-1}, respectively, and were consistently highest in surface waters (~~not shown~~see Figure R7 in the Response to Referee supplement of the associated Discussion paper). Moreover, surface waters throughout the transect were characterized by a relative enrichment of N (N/C = 0.14–0.17, Fig. 3a). In contrast, deeper waters had lower concentrations of particulate organic matter and a relative depletion of N (N/C = 0.08–0.13). The region close to the river mouth displayed the most pronounced N/C enrichments anywhere on the transect.

The distribution of $\delta^{13}C_{POC}$ showed a general similarity to that of N/C. Relatively depleted values were observed in surface waters (-29‰ – -31‰), with the most depleted values observed close to the river mouth, while deep water values were relatively enriched (-26‰ – -28‰) (Fig. 3a, bottom). One anomalous sample of relatively enriched values (approx. -26‰) was observed in the surface waters at site G, close to the sill at Ekenäs. When N/C and $\delta^{13}C_{POC}$ values are plotted in x-y space, surface water samples for most ~~station~~stations, regardless of salinity, plot close to the riverine end of the riverine–estuarine phytoplankton continuum. At each site, samples from deeper in the water column trend away from this region of the diagram towards the field corresponding to terrestrial C3 plants (Fig. 3b).

4.4 Sedimentary organic matter along the transect

Mean total organic carbon (C_{org}) contents of the upper 30–50 cm of sediments sampled in September 2014 were highest in the archipelago (Stations H–K, 4%–5%), followed by the estuary (~~close to 4% dry weight at station~~Stations A–~~D~~E, 4%) and lowest at the sill ~~in the inner Mustionjoki estuary (Fig. 4b).(Station~~Stations ~~E~~F–G, 2–3%, Fig. 4b). ~~in the vicinity of the sill at Ekenäs showed lower values (e.g. station F = 2.2%), while stations in the archipelago and offshore region (H–G) showed the highest values anywhere on the transect (4%–5%).~~ The four samples from site A, at the mouth of the Mustionjoki river, all showed molar N/C ratios of 0.05–0.09 and $\delta^{13}C_{org}$ of -26‰ – -29‰, hence plot close to the terrestrial C3 plants field in N/C vs. $\delta^{13}C_{org}$ space (Fig. 4a). With increasing distance along the transect, from the estuary through the sill to the archipelago,

mean N/C increases and $\delta^{13}C_{org}$ becomes more enriched, ~~values of sediments fro~~hence m successive ~~station~~stations ~~trend towards~~plot progressively closer to the riverine–estuarine phytoplankton continuum. Samples from ~~station~~Station K showed molar N/C ratios of 0.12–0.14 and $\delta^{13}C_{org}$ of -23‰ – -24‰, close to the estuarine end of the continuum. ~~Variation of values between different depth intervals within each sediment core was substantially less (N/C < 0.04, $\delta^{13}C_{org}$ < 2‰) than between the mean values of station A and station K.~~

Correspondingly, ~~The~~ the computed contribution~~s of terrestrial plant derived and~~ of phytoplankton-derived organic matter to sedimentary C_{org} ~~vary~~ increases systematically along the transect. As a first-order estimate ~~Based~~ based on the assumed end-member values, >70% of sedimentary C_{org} at ~~station~~Station A is derived from terrestrial plant material, whereas sedimentary C_{org} at ~~station~~Station K is entirely phytoplankton-derived. ~~The rate of change in~~Station C and D stand out from the offshore trend with slightly elevated contributions of ~~%$OC_{terr.}$ and~~ %$OC_{phyt.}$ relative to %$OC_{terr.}$ ~~between successive stations is greatest from stations A–C, close to the mouth of the Mustionjoki river~~.

4.5 Total ~~Sedimentary~~ sedimentary Fe along the transect

Surface-sediment total Fe concentrations in 2014 were ~~highest~~ highest in the estuary ~~at s(tation~~Stations A–~~D~~ E, 1000–1700 µmol g^{-1}), followed by the archipelago (Stations H–K, 800–1000 µmol g^{-1}), and lowest at the sill (Stations F–G, 500–700 µmol g^{-1}, Fig. 4b). A~~in the inner estuary, with a~~ maximum value of >1600 µmol g^{-1} was recorded in the surface sediments ~~value of >1600 µmol g^{-1}~~ at ~~station~~Station B ~~(Fig. 4b). A general trend of decreasing Fe concentrations offshore from station B was observed, to values of approx. 800 µmol g^{-1} at station K. Anomalously low values were observed at station F, coincident with the observed minimum in C_{org} content at this location~~. The downcore profiles from Stations A, D and J from 2015 show that total sedimentary Fe has been consistently higher at the stations in the estuary (A and D) relative to the archipelago (J) throughout the studied interval (in each case at least 50 years based on the position of the 1970 depth horizon). Extreme enrichments of Fe are observed at Station A, the site closest to the river mouth, peaking in the interval above the 1970 depth horizon and declining towards the present. Iron enrichments in the uppermost part of the estuary also appear to be highly spatially variable, as evidenced by the difference between the surface sediment value at Station A during the 2014 campaign (1043 µmol g^{-1}, Fig. 4b) and the 2015 campaign (1557 µmol g^{-1}, Fig. 5), measured in cores taken within 10 m of each other.

4.6 Sedimentary Fe speciation 1: labile Fe

Formatted: Heading 2, Space Before: 0 pt, After: 0 pt

Multiple phases of Fe are present in the sediments along the transect. Based on a combination of evidence from the extraction protocols and Mössbauer spectroscopy, we propose a general scheme for the interpretation of the combined data (Table 3). Flocculated Fe is assumed to accumulate as labile Fe in the form of ferrihydrite and Fe (III)-OM, both of which are subject to diagenetic transformations after sedimentation.

Labile Fe phases (Stage 1- and Stage 2- soluble Fe in the Poulton and Canfield (2005) extraction) are present in the surface sediments at all sites (Fig. 4b), and at all depths in the downcore profiles from Stations A, D, and J (Fig. 5). The near 1:1 match between the combined Stage 1+2 fraction and total 1 M HCl-soluble Fe from the Burton et al. (2008; 2011) extraction suggests that the two approaches are consistent in extracting 100% of the labile Fe pool (Fig. 6b). However, Na acetate- (Stage 1)-soluble Fe dominates over hydroxylamine-HCl- (Stage 2)- soluble-Fe in all samples (Fig, 4b, 5). Candidate phases for Na acetate- soluble Fe are Fe (II) carbonates such as siderite and ankerite, as targeted by the extraction protocol, but also labile organic complexes, whose behavior in this extraction scheme is not well defined, and AVS (FeS), which is thought to partially dissolve during Stage 1 (Egger et al., 2015a). Meanwhile, candidate phases for hydroxylamine-HCl-soluble Fe are poorly crystalline Fe oxides such as ferrihydrite and lepidocrocite, any remaining labile organic complexes and FeS from Stage 1, and Fe (II) phosphates such as vivianite (Dijkstra et al., 2014) (Table 3).

By determining the fractions of 1M HCl-soluble sulfidized and unsulfidized Fe (II), and Fe (III), in the parallel extraction, we can further deconvolve the likely composition of the labile Fe pool. The persistent presence of unsulfidized Fe (II), accounting for an average of 53% of labile Fe in the 15 measured samples (Fig. 6a), suggests important contributions of either Fe (II)-OM, Fe (II) carbonates, and/or Fe (II) phosphates. We suggest that Fe (II)-OM contributes significantly to this pool of unsulfidized Fe (II), for two principal reasons. First, Fe (II)-OM has been observed as an important component of total Fe in sediments from a nearby boreal estuary on the basis of X-Ray Absorption Spectroscopy (Yu et al., 2015). Second, Fe (II) carbonates and phosphates if present are expected to form only in the deeper part of the sediment column, where pore water Fe, dissolved inorganic carbon and phosphate concentrations are sufficient to exceed saturation with respect to these minerals (e.g., Egger et al., 2015b for vivianite). In contrast, we find unsulfidized Fe (II) throughout the sediment column at all three stations (Fig. 6a), including within the sulfate-methane transition zone (SMTZ), where the presence of pore water H_2S keeps pore water Fe concentrations close to zero and hence should prevent carbonate and phosphate formation.

The 1M HCl extractions also confirm the presence of labile Fe (III) in most samples (Fig. 6a), including at depths corresponding to the SMTZ. Although ferrihydrite is almost certain to be present at the sediment surface, its persistence in the SMTZ, where pore water H_2S concentrations exceed 100 µmol L_4^{-1} (Station D) and 200 µmol L^{-1} (Station J), seems improbable. The half-life of the sulfidization of ferrihydrite is measured in hours (Raiswell and Canfield, 2012), whereas the residence time of a sediment layer in the H_2S zone during burial at the calculated sedimentation rates in this study is in the order of years. Hence we suggest that the labile Fe (III) present in the sediments is indicative of H_2S-resistant Fe (III)-OM derived from the flocculated material.

The Mössbauer data yield further information concerning the labile Fe pool. Although the bulk spectra are dominated by the major refractory Fe phases (Section 4.7), the presence or absence of minor Fe components can be inferred, especially when these are characterized by distinct hyperfine parameters and hence do not display significant spectral interference with the major components. On this basis, we find no direct evidence for the presence of siderite or other Fe (II) carbonates, whose

Formatted: Subscript

Formatted: Subscript

Formatted: Superscript

Formatted: Subscript

Mössbauer spectra are all characterized by a distinct doublet with narrower quadrupole splitting than observed for Fe (II) in silicate minerals (Fig. 7 and Morris et al., 2010). Furthermore, the bulk spectra do not show evidence for either Fe (II) oxalate or vivianite – two possible analogs for Fe (II)-OM and Fe (II) phosphates in the sediments (Fig. 7). To reconcile this information with the results of the extractions, we interpret the absence of these phases to indicate that Fe (II)-OM and Fe (II) phosphates in our samples must be present in forms other than Fe (II) oxalate and vivianite, and which are characterized by Mössbauer doublet spectra that interfere with silicate Fe (II) and hence cannot be independently resolved. Indeed, Mattievich and Danon (1977) showed that Fe (II) phosphates of varying degrees of hydration display a wide range of hyperfine parameters including various overlaps with silicate Fe (II) as detected in our samples (δ = 1.08–1.19 mms^{-1}, ΔEQ = 2.48–2.65 mms^{-1}, Table 4, Section 4.7). The range of hyperfine parameters for different Fe (II)-OM phases is not well established in the existing literature, but our results suggest that Fe (II) oxalate alone may not be a suitable analog for bulk sedimentary Fe (II)-OM.

4.7 Sedimentary Fe speciation 2: refractory Fe

Refractory Fe compounds (by our definition, all Fe remaining after Stages 1+2 of the Poulton and Canfield (2005) extraction) constitute the majority of Fe in all samples (Fig. 4b, 5). These components are expected to derive principally from suspended minerogenic matter accumulated in the estuarine sediments, although some refractory phases – such as pyrite – may derive from the diagenesis of flocculated labile Fe (Table 3). Mössbauer spectra from five of the 7 analyzed samples (all samples except those from Station A) can be deconvolved into two doublets accounting for >95% of total Fe (Fig. 7 and Supplementary Fig. 2). The first represents superparamagnetic Fe (III) (δ = 0.25–0.40 mms^{-1}, ΔEQ = 0.70–0.86 mms^{-1}, Table 4), and accounts for 49–62% of the modeled spectra in these samples (Table 4). Superparamagnetic Fe (III) in RT ^{57}Fe Mössbauer analysis of sediments has been reported to represent various phases, including ferrihydrite, goethite of particle size < 12 nm (van der Zee et al., 2003) and amorphous ferric aluminosilicates (Manning and Ash, 1978; Manning et al., 1980). As outlined in Section 4.6, a major contribution of ferrihydrite deeper in the sediments seems unlikely, which leaves nanocrystalline goethite and amorphous ferric silicates as prime candidates for the dominant superparamagnetic Fe (III) phases. According to Canfield (1989), goethite is soluble in citrate-dithionite solution (Stage 3 of the Poulton and Canfield (2005) extraction), while amorphous ferric silicates, if present, should be extracted by either citrate-dithionite or ammonium oxalate (Stage 4). However, the contribution of 49–62% superparamagnetic Fe (III) exceeds the sum of Stage 3+4 -soluble Fe in the corresponding extraction (typically 20–30%, Fig. 5). Several explanations are possible for this offset. First, the spectral overlap with diamagnetic pyrite may elevate the estimated contribution of superparamagnetic Fe (III) (Fig 7). Second, assuming Fe (III) oxalate as a reasonable analog for Fe (III)-OM (Barber et al., 2017), this component of labile Fe may also contribute a fraction of total superparamagnetic Fe (III) (Fig. 7). Finally, it is possible that a fraction of goethite and/or amorphous ferric aluminosilicates in our samples may resist dissolution in Stages 3+4 and instead dissolve in Stage 5 (boiling 12 M HCl), thereby giving an underestimate for Stage 3+4 -soluble Fe.

Formatted: Heading 2, Space Before: 0 pt, After: 0 pt

Formatted: Superscript

Formatted: Superscript

Formatted: Superscript

Formatted: Font: Not Italic

The second major doublet in these five samples is high-spin Fe (II) in silicate minerals, identified by its comparatively high isomer shift and quadrupole splitting values (δ = 1.08–1.19 mms^{-1}, ΔEQ = 2.48–2.65 mms^{-1}, Table 4). Iron (II) (alumino)silicates in Baltic Sea sediments include micas such as biotite, as well as secondary clay minerals such as chlorite and illite (Frančišković-Bilinski et al., 2003). Due to strong overlaps in the Mössbauer parameters of these phases, it is difficult to deconvolve high-spin Fe (II) further, and for this reason we report these phases together simply as "silicate Fe (II)". This component typically accounts for 38–49% of the bulk spectrum in these five samples (Table 4), and may include contributions of overlapping labile Fe (II) phases as discussed in Section 4.6.

At Station A, total Fe contents are strongly elevated and the majority of the additional Fe is soluble in Stages 3+4 of the Poulton and Canfield (2005) extraction (Fig. 5). According to the interpretations already given, these fractions should include nanocrystalline goethite and amorphous ferric aluminosilicates, both of which would yield superparamagnetic Fe (III) in the Mössbauer spectra. However, both Mössbauer spectra from Station A (0–1 cm and 26–28 cm) also show evidence for two additional Fe phases, which together account for >50% of total Fe in these samples (Fig. 7) and therefore likely dominate Stage 3+4-soluble Fe at this site. Of these, the major phase is represented by a doublet located between those of superparamagnetic Fe (III) and silicate Fe (II), with isomer shift and quadrupole splitting parameters indicative of an Fe (II) compound (δ = 0.78–0.94 mms^{-1}, ΔEQ = 0.76–0.83 mms^{-1}, Table 4). In the associated Discussion paper we attributed this phase to Fe (II)-OM. However we now favor the hypothesis that this is in fact wüstite (FeO) (Fig. 7). Wüstite is an Fe (II) oxide with a distinct set of hyperfine parameters corresponding to a doublet between those of superparamagnetic Fe (III) and silicate Fe (II), which closely matches the dominant additional phase present in our samples (Fig. 7). The second additional phase in Station A samples is unequivocally magnetite, as evidenced by the broad sextet spectrum indicative of magnetic splitting of the absorption peaks (Supplementary Fig. 2) and thus non-zero internal magnetic field parameters at room temperature (Table 4). The magnetite spectrum can be further deconvolved into $Fe^{2.5+}$ and Fe^{3+} components, each characterized by a distinct set of hyperfine parameters. Hematite is also observed in the sample from 26–28 cm.

~~The Fe speciation of the surface sediments at stations A and B was dominated by Stages 3 and 4 of the sequential extraction protocol, while Stages 1 and 2 of the protocol were most dominant at station D (Fig. 4b).~~

~~57Fe Mössbauer spectroscopy data from surface sediment samples from stations A and D (0–1 cm, June 2015) show markedly contrasting results (Fig. 5; Table 3). The station A spectrum contains an important contribution of an Fe (II) phase which could not be identified from our existing library of minerogenic Fe (II) spectra. The presence of this phase in the sample modulates the relative heights of the major peaks in the spectrum, and generates a distinct shoulder at 1–2 mms-1 (Fig. 5). We interpret this phase to represent complexes of non-sulfidized Fe (II) with organic matter (henceforth organic-Fe (II) complexes), which were recently shown to be a major component of sedimentary Fe in a nearby boreal estuary (Yu et al., 2015). The station A spectrum also contains superparamagnetic Fe (III) (interpreted as nanoparticulate ferrihydrite), silicate-bound Fe (II) and a small contribution of magnetite. In contrast, the sample from station D was dominated by superparamagnetic Fe (III) and silicate-bound Fe (II). No Fe carbonate phases (e.g.~~

Formatted: Superscript
Formatted: Superscript
Formatted: English (United Kingdom)
Formatted: Heading 2, Space Before: 0 pt, After: 0 pt
Formatted: English (United Kingdom), Not Superscript/ Subscript
Formatted: English (United Kingdom)
Formatted: English (United Kingdom), Not Superscript/ Subscript
Formatted: English (United Kingdom)

~~siderite, ankerite), and no further crystalline oxides (e.g., goethite, hematite or akaganéite) were detected in either sample.~~

~~The sequential Fe extraction results for the corresponding samples showed station A to be dominated by Fe soluble in Stages 3 and 4 of the protocol (sodium dithionite and ammonium oxalate soluble Fe, respectively), which together accounted for >50% of all Fe in the sample (Fig. 5). In contrast, Stages 3 and 4 yielded approximately 20% of all Fe in the samples from station D. Conversely, the contribution of Stages 1 and 2 (sodium acetate soluble Fe and hydroxylamine HCl soluble Fe, respectively) to total Fe at station D was greater than for station A.~~

4.~~6~~ 8 ~~Vertical profiles of sedimentary Fe, Corg and S~~Diagenetic zonation of the sediments

Active remineralization of organic matter (OM) at Stations A, D and J is evidenced by declining C_{org} contents from the surface downwards at each site (Fig. 5). Since oxygen penetration in muddy coastal sediments of the northern Baltic Sea typically does not exceed 4 mm (e.g. Hietanen and Kuparinen, 2008; Bonaglia et al., 2013), anaerobic processes initiate within the uppermost centimeter and dominate the pore water chemistry of the upper 50 cm of the sediment column (Sawicka and Brüchert, 2017). These processes are expected to influence the vertical distribution of Fe in the sediments, with a strong impact on flocculated labile Fe phases.

The v~~The along-transect changes in Fe content and speciation persist in the vertical profiles of stations A, D and J (Fig. 6). Background total Fe contents decrease in the order A–D–J (1.0%, 0.8%, 0.5%, respectively), while station A shows a persistently high contribution of dithionite- and oxalate-soluble Fe relative to the other stations. Furthermore the 10–40 cm depth layer in the sediments at station A displays a large enrichment of Fe, peaking at 3% close to the 1970 depth horizon.~~

~~The C_{org} profile of station A also differs markedly from those of stations D and J. The station A profile shows generally constant values of ~3% with a small enrichment in the surface sediments, while the station D and J profiles show systematically decreasing C_{org} contents from the surface sediments towards the base of the core. Meanwhile, the S profiles of all three stations show a distinct broad peak in the post-1970 sediments (Fig. 6).~~

~~4.7 Vertical profiles of pore water CH_4, SO_4^{2-}, H_2S and Fe^{2+}~~

~~At sites A, D and J, a broadly similar v~~ertical zonation ~~of the can be observed in the~~ pore water chemical profiles at Stations A, D, and J is broadly similar, indicating ~~a similar~~a common set of anaerobic diagenetic processes at each ~~site~~ site (Fig. 8)~~(Fig. 7)~~. The following formulations are simplified from the reaction network of Reed et al. (2011), in which OM is given the form $(CH_2O)_a(NH_4^+)_b(H_3PO_4)_c$. $Fe(OH)_3$ represents all Fe oxides, including ferrihydrite derived from flocculation. In the upper 5 cm of the sediment column, we observe evidence for anaerobic OM remineralization coupled to reduction of both Fe oxides (indicated by pore water accumulation of Fe^{2+}) and sulfate (SO_4^{2-}) (indicated by a concave decline of pore water SO_4^{2-} with depth) (Fig. 8):

$$OM_{(s)} + 4aFe(OH)_{3(s)} + 12aH^+_{(aq)} \rightarrow aCO_{2(aq)} + bNH^+_{4(aq)} + cH_3PO_{4(aq)} + 4aFe^{2+}_{(aq)} + 13aH_2O_{(l)} \quad (12)$$

Formatted: Not Superscript/ Subscript
Formatted: Not Superscript/ Subscript
Formatted: Line spacing: single
Formatted: Normal, Space Before: 12 pt, After: 12 pt, Line spacing: single
Formatted: Font: Cambria Math
Formatted: Font: Cambria Math, Subscript
Formatted: Font: Cambria Math
Formatted: Font: Cambria Math, Subscript
Formatted: Font: Cambria Math
Formatted: Font: Cambria Math, Subscript
Formatted: Font: Cambria Math, Superscript
Formatted: Font: Cambria Math
Formatted: Font: Cambria Math, Subscript
Formatted: Font: Cambria Math
Formatted: Font: Cambria Math, Subscript
Formatted: Font: Cambria Math
Formatted: Font: Cambria Math, Subscript
Formatted: Font: Cambria Math
Formatted: Font: Cambria Math, Subscript
Formatted: Subscript
Formatted: Superscript
Formatted: Subscript
Formatted: Superscript

$$OM_{(s)} + 0.5aSO_{4(aq)}^{2-} + aH_{(aq)}^{+} \rightarrow aCO_{2(aq)} + bNH_{4(aq)}^{+} + cH_3PO_{4(aq)} + 0.5aH_2S_{(aq)} + aH_2O_{(l)} \quad (13)$$

Below the depth at which sulfate is exhausted, methane (CH_4) accumulates in pore waters, indicative of anaerobic OM remineralization via methanogenesis:

$$OM_{(s)} \rightarrow 0.5aCO_{2(aq)} + bNH_{4(aq)}^{+} + cH_3PO_{4(aq)} + 0.5aCH_{4\,(aq)} \quad (14)$$

These observations are broadly consistent with the classic zonation of primary diagenetic reactions (Claypool and Kaplan, 1974; Froelich et al., 1979), except that the diagenetic zones strongly overlap, which is typical for coastal areas of the Baltic Sea (Sawicka and Brüchert, 2017). The presence of sulfate reduction (reaction 13) in sediments containing Fe oxides therefore leads to the following reaction, which likely also contributes to the accumulation of Fe^{2+} in the pore waters of the upper sediments:

$$2Fe(OH)_{3(s)} + H_2S_{(aq)} + 4CO_{2(aq)} \rightarrow 2Fe_{(aq)}^{2+} + S_{0\,(s)} + 4HCO_{3\,(aq)}^{-} + 2H_2O_{(l)} \quad (15)$$

Hydrogen sulfide (H_2S) and Fe^{2+} then react to form iron monosulfide (FeS):

$$Fe_{(aq)}^{2+} + H_2S_{(aq)} \rightarrow FeS_{(s)} + 2H_{(aq)}^{+} \quad (16)$$

Iron monosulfide (FeS) is subsequently converted to pyrite (FeS_2) by reaction with native sulfur produced in reaction 15:

$$FeS_{(s)} + S_{0(s)} \rightarrow FeS_{2(s)} \quad (17)$$

A shallow sulfate-methane transition zone (SMTZ) is observed at each of the three stations, within which anaerobic oxidation of methane (AOM) coupled to sulfate reduction occurs (e.g., Egger et al., 2015a; Sawicka and Brüchert, 2017):

~~CH_4 produced by methanogenesis in the deeper sediments diffuses upwards and reacts with SO_4^{2-} diffusing downwards from the bottom water at the so-called sulfate-methane transition zone (SMTZ) (e.g., Egger et al., 2015a). The reaction~~

$$CH_{4(aq)} + SO_{4\,(aq)}^{2-} + CO_{2(aq)} \rightarrow H_2S_{(aq)} ~~HS_{(aq)}^{-}~~ + 2HCO_{3\,(aq)}^{-} + H_2O_{(l)}$$

~~(5~~18)

This reaction also produces H_2S, which accumulates in the pore waters at the SMTZ, hence keeping pore water Fe^{2+} concentrations low and favoring the precipitation of sulfide minerals (reactions 16 and 17).~~produces H_2S, which accumulates in a distinct peak in the SMTZ. Pore water Fe^{2+}, produced by the reduction of Fe (oxyhydr)oxides in various diagenetic reactions, accumulates above and below the SMTZ. Within the SMTZ itself, the reaction between Fe^{2+} and H_2S~~

Formatted: Subscript

Formatted: Superscript

~~$Fe^{2+}_{(aq)} + H_2S_{(aq)} \rightarrow FeS_{(s)} + 2H^+_{(aq)}$~~ ~~(6)~~

~~efficiently removes Fe^{2+} from the pore waters, and FeS is subsequently converted to pyrite (FeS_2)~~

At all stations, pore water Fe^{2+} increases below the SMTZ, indicative of excess production of Fe^{2+} over H_2S (Fig. 8). Such deep production of Fe^{2+} may be associated with persistent organoclastic Fe reduction (reaction 12) or with AOM coupled to Fe oxides (Beal et al., 2009; Sivan et al., 2011; Egger et al., 2015a):

$$CH_{4(aq)} + 8Fe(OH)_{3(s)} + 15H^+_{(aq)} \rightarrow HCO^-_{3\,(aq)} + 21H_2O_{(l)} + 8Fe^{2+}_{(aq)} \quad (19)$$

We note that indirect coupling of Fe oxide reduction to methane oxidation may also occur via the "cryptic sulfur cycle" (Holmkvist et al., 2011). Here, native sulfur and other intermediates of sulfide oxidation by Fe oxides (reaction 15), undergo disproportionation to H_2S and SO_4^{2-}. The following example is given for thiosulfate ($S_2O_3^{2-}$):

$$S_2O^{2-}_{3(aq)} + H_2O_{(l)} \rightarrow SO^{2-}_{4(aq)} + H_2S_{(aq)} \quad (20)$$

The H_2S produced in reaction 20 then feeds back into reaction 15, while the SO_4^{2-} feeds back into reaction 18. However, as shown in Egger et al. (2016) in a study from the Black Sea, such cryptic sulfur cycling is restricted to the depth interval close to the downward-diffusing H_2S front from the SMTZ. This can be explained by the fact that only 3 moles of H_2S are produced by reaction 20, for every 4 moles of H_2S that initially participate in reaction 15 (Egger et al., 2016). Hence, cryptic sulfur cycling is a net consumer of H_2S and cannot persist significantly deeper than the downward-diffusing H_2S front from the SMTZ. For this reason we favor the interpretation that pore water Fe^{2+} accumulating below the SMTZ is produced via reactions 12 and 19.

All stations show a broad maximum of solid-phase S in the post-1970 interval of the sediment column (Fig. 5). This feature is distinctive for sediments from the northern Baltic Sea (e.g., Egger et al., 2015a; Rooze et al., 2016) and represents a recent shoaling of the SMTZ to its current position, in response to eutrophication caused by external nutrient inputs to the Baltic (Gustafsson et al., 2012). The extra input of organic material to the sediments has led to enhanced rates of sulfate reduction (reaction 13), decreasing the sulfate penetration depth and intensifying reactions 15–17 at a shallower horizon in the sediments.

The above reaction network principally describes the diagenetic processes which may impact on flocculated ferrihydrite and its subsequent transformation to sulfide-bound Fe (II) phases. We note that under conditions of elevated pore water Fe (II) concentrations such as observed in the deeper sediments at Stations A and D, precipitation of Fe (II) phosphates may also occur (Egger et al., 2015b), although the Mössbauer data suggest that these phases, if present, are distinct from pure vivianite

Formatted: Subscript
Formatted: Subscript
Formatted: Subscript
Formatted: Superscript
Formatted: Subscript
Formatted: Subscript
Formatted: Superscript
Formatted: Subscript
Formatted: Subscript
Formatted: Subscript
Formatted: Subscript
Formatted: Superscript

(Section 4.6). Furthermore, the effect of diagenetic reactions on Fe-OM complexes is not well understood as thus is typically not included in diagenetic models of Baltic Sea sediments. For the purposes of this study we assume that Fe (III)-OM derived from flocculation may be subject to reduction to Fe (II)-OM in the sediment column, as described in Yu et al. (2015), but that these components do not otherwise partake in the diagenetic reactions.

4.9 Instantaneous rates of diagenetic processes and their relative depth in the sediment column

The PROFILE output broadly confirms the above description of the diagenetic zonation. All sites show evidence for sulfate and methane consumption within the SMTZ. Instantaneous rates of sulfate reduction are in the range 0.0001–0.0008 μmol L^{-1} s^{-1}, which is similar to the range presented recently by Sawicka and Brüchert (2017) for a Swedish estuary. At Station A, low salinity restricts the sulfate reduction zone to the uppermost 5 cm of the sediments. Consequently, the SMTZ is shallower at Station A than at the other sites. However, instantaneous rates of sulfate reduction in the upper sediments of Station A are in fact the highest of the three sites. Net production of pore water Fe is observed in the upper 5 cm at all sites, as well as consumption in the SMTZ. Although Station A and D show strongly elevated concentrations of pore water Fe below the SMTZ, the PROFILE output indicates that production rates in this zone are low, suggesting an upwards diffusion of Fe from reactions occurring deeper in the sediments.

4.10 Long-term rates of Fe and sulfate reduction

Depth-integrated burial rates of S for the period 1970–2015 were highest at Station D, followed by Station A and lowest at Station J (Fig. 6c). By definition, the same pattern is observed in the AVS-Fe and pyrite-Fe fractions of the depth-integrated burial rate of reactive Fe (II). However, the additional component of unsulfidized Fe (II) at Stations A and D enhances the contrast with the Station J, such that reactive Fe (II) burial at Station D is more than a factor 2 greater than at Station J (Fig. 6c).

~~However, the profiles from each station differ in terms of the depth, thickness and intensity of the SMTZ. At station A, where bottom water $[SO_4^{2-}]$ is only 1.3 mM, the SMTZ is relatively shallow and narrow. No detectable accumulation of H_2S is observed, while pore water Fe^{2+} shows only a narrow minimum centered on 7 cm depth. At stations D and J, H_2S accumulations in excess of 150 μm L^{-1} are observed in the SMTZ, while Fe concentrations are close to zero between 5 cm and 20 cm depth. Station J, where bottom water $[SO_4^{2-}]$ is 4.8 mM, shows the deepest SMTZ of the three stations as defined by the H_2S peak (centered on 12 cm).~~

Formatted: Heading 2, Space Before: 0 pt, After: 0 pt

Formatted: Superscript

Formatted: Heading 2, Space Before: 0 pt, After: 0 pt

5 Discussion

5.1 Evidence for ~~Evidence for~~flocculation of DOM ~~DOM flocculation in the estuarine water column and its impact on $Fe_{diss.}$~~

Up to 94% of total organic carbon (TOC) in Finnish river catchments is present as dissolved organic carbon (DOC) (Mattsson et al., 2005). Hence, the vast majority of the organic matter input to Finnish estuaries occurs in the dissolved form. Asmala et al. (2013) showed that DOC concentrations in the Mustionjoki estuary decrease from approx. 600 µmol L_A^{-1} at the river mouth to 350 µmol L_A^{-1} in the offshore region. The decline in DOC along the transect is controlled by mixing of river water with sea water of lower DOC content, and by transformations in the estuarine water column, which may cause non-conservative mixing behavior of DOC vs. salinity. Yet, our compositional analysis shows that the DOM pool retains a strongly terrestrial character throughout the system (Fig. 3b). DOM data cluster around the terrestrial C3 plants field in N/C vs. $\delta^{13}C$ space, with only a minor deviation towards higher N/C observed in the offshore samples.

The principal transformation leading to non-conservative loss of DOM in the Mustionjoki estuary is ~~A recent field and experimental study demonstrated that s~~salinity-mediated flocculation – the aggregation of small particles of organic matter into larger ones under conditions of increasing electrolyte strength ~~– is the dominant process responsible for the loss of DOM along salinity gradients in Finnish estuaries~~ (Asmala et al., 2014). Alternative ~~mechanisms~~transformations, such as microbial degradation and photolytic mineralization of DOM in the estuarine environment (Dalzell et al., 2009; Moran et al., 2000~~; Asmala et al., 2013~~) are considered of lesser importance in this system. Flocculation decreases the fraction of organic matter in the water column which passes through regular filters, and ~~hence decreases the fraction that classifies as DOM.~~therefore transfers terrestrial organic material from the DOM to POM pool.

At the time of sampling in June 2015, POM in surface waters throughout the Mustionjoki estuary and adjacent archipelago was dominated by phytoplankton material, as evidenced by the relatively high N content of POM (circles with letters in Fig. 3a). This strong signal of autochthonous material apparently obscures any evidence for POM derived from flocculation of DOM. However, in deeper waters throughout the transect, POM is characterized by lower N contents and more isotopically enriched C. Consequently, deep water POM samples in N/C vs. $\delta^{13}C$ space trend away from the riverine–estuarine phytoplankton continuum and towards the field corresponding to terrestrial C3 plants (Fig. 3b). This suggests that a second fraction of POM contributes to the net N/C and $\delta^{13}C$ values of the deeper samples, and that this fraction may be derived from flocculation of DOM to POM. The dominance of flocculation-derived material in the deeper samples may be due to both the loss of fresh phytoplankton material due to remineralization during settling, and the typically higher salinity of deep waters.

Formatted: Superscript

Formatted: Superscript

5.2 Flocculation of Fe and partial decoupling from DOM

~~Consequently, negative deviation from conservative mixing is observed when a straight line is drawn between freshwater and offshore end-member values in salinity vs. DOM space (Officer, 1976). However, it should be noted that the conservative mixing approach is sensitive to variations in the end-member values, and quantification of the deviation requires knowledge about the magnitude of this variation (Asmala et al., 2016).~~

Due to the close association of Fe with DOM in boreal riverine systems, ~~flocculation~~ transformations of DOM in the Mustionjoki estuary ~~also~~ are expected to strongly influence ~~s~~ Fe cycling. ~~The rapid loss of Fe_{diss} observed offshore from the river mouth along the Mustionjoki transect (Fig. 2a) confirms that flocculation removes Fe from solution in this system. However, The~~ the degree of negative deviation from conservative mixing of Fe_{diss} vs. salinity ~~in Finnish estuaries was shown experimentally to be greater than for DOC (Asmala et al., 2014),~~along the transect (Fig. 2b) is far greater than observed previously in this system for DOC (Asmala et al., 2014), implying some decoupling of Fe from DOM during flocculation. This is consistent with earlier results for the Öre estuary, Sweden (Forsgren, et al., 1996) which showed that the removal of Fe from solution during estuarine mixing experiments is far more efficient than that of DOC ~~suggesting that Fe is preferentially removed relative to bulk DOM. This could indicate a preferred association of Fe with higher molecular weight compounds, which are more sensitive to flocculation (Asmala et al., 2014) or a mechanistic enhancement of flocculation by the presence of Fe (Forsgren et al., 1996)~~.

In the Forsgren et al. (1996) study, enhanced removal of Fe from solution was suggested to be caused by the presence of clay particle surfaces to which Fe oxyhydroxides can sorb during estuarine mixing. While this mechanism is indeed possible in our system, we note that p-artial decoupling of Fe from DOM likely occurs already in river water upstream of the estuary. The typical pH of the Mustionjoki drainage system is in the order 6.0–6.5 (Lahermo et al., 1996). As shown by Neubauer et al. (2013), a significant fraction of Fe in boreal river waters of pH 6.0–6.5 may exist in the form of discrete ferrihydrite particles, rather than OM-Fe complexes. Moreover, the modal size class of these particles increases with pH, such that a further pH rise in the estuarine environment should stimulate flocculation of Fe, independent of salinity effects or the presence of clay particles. The pH gradient of the estuary spans from 6.0–6.5 in the Mustionjoki river to 8.0–8.4 in the open Gulf of Finland (Omstedt et al., 2010). Hence, the strongly non-conservative behavior of Fe_{diss} along the transect may represent the combined influence of salinity (influencing flocculation of DOM-bound Fe) and pH gradients (influencing the flocculation of discrete ferrihydrite particles) as well as the role of clay particles in the subsequent aggregation of particulate material.

Formatted: Heading 2, Space Before: 0 pt, After: 0 pt

Formatted: Subscript

~~**5.2 The signal of flocculation in suspended POM and $Fe_{part.}$**~~

~~At the time of sampling in June 2015, POM in surface waters throughout the Mustionjoki estuary and adjacent archipelago was dominated by phytoplankton material, as evidenced by the relatively high N content of POM (circles with letters in Fig. 3a). This strong signal of autochthonous organic material apparently obscures any evidence for POM derived from flocculation of DOM in surface waters at the time of sampling. However, in deeper waters throughout the transect, POM is characterized by lower N contents and more isotopically enriched C. Consequently, deep water POM samples in N/C vs. $\delta^{13}C$ space trend away from the riverine–estuarine phytoplankton continuum and towards the field corresponding to terrestrial C3 plants (Fig. 3b). This suggests that a second fraction of POM contributes to the net N/C and $\delta^{13}C$ values of the deep water samples, and that this fraction has N/C and $\delta^{13}C$ characteristics similar to plant material. We note that this material is unlikely to be resuspended sediment, since its $\delta^{13}C$ values have a much narrower range than those of sedimentary material throughout the transect (Fig. 4a).~~

~~Notably, DOM data from the Mustionjoki estuary cluster close to the terrestrial C3 plants field in N/C vs. $\delta^{13}C$ space (Fig. 3b). The samples in the figure were taken in three separate seasons (April, August, October 2011) and hence approximate the mean composition of DOM in the estuarine system. Assuming negligible fractionation of N/C and $\delta^{13}C$ during flocculation, these results suggest that flocculation of DOM to POM in the estuarine environment may provide the second fraction of POM detected in the N/C_{POM} and $\delta^{13}C_{POM}$ data. The relative abundance of sinking phytoplankton material and flocculation-derived POM then determines the net N/C and $\delta^{13}C$ values measured at any given location in the estuarine water column. Deep water samples display values closer to the flocculation-derived component, likely due to both rapid remineralization of fresh phytoplankton material during settling, and the typically higher salinity of deep waters, which favors the accumulation of flocculated material.~~

~~The 2015 $Fe_{part.}$ and Fe_{diss} data show clear evidence for the transfer of Fe from the dissolved to the particulate phase as a consequence of flocculation in the Mustionjoki estuary (Fig 2b). When data from all stations and depths are plotted together,~~Particulate Fe (~~-~~$Fe_{part.}$) also shows an overall negative deviation from conservative mixing along the salinity gradient. ~~This~~ The initial strong decline in $Fe_{part.}$ away from the river mouth likely reflects settling of suspended minerogenic matter due to energy dissipation ~~as river water enters~~in the estuarine environment (Syvitski and Murray, 1981~~),~~). This is supported by a~~as indicated by a~~ similar trend in suspended particulate aluminum (Al) (not shown). However, samples in the salinity range 2–4 show a clear positive deviation, suggesting an input of Fe_{part} through flocculation of Fe_{diss}. Accordingly, ~~In contrast, Fe_{diss} shows a simple logarithmic non-conservative mixing trend with $R^2 = 0.92$. The concentration of Fe_{part} in the salinity range 2–4 (~1.0 µmol L^{-1}) is similar to that of Fe_{diss} close to the river mouth, suggestive of quantitative transfer of Fe from the dissolved to particulate phase with increasing salinity. T~~the 2D cross-section of Fe_{part} along the transect confirms ~~that~~ a pronounced zone

of higher values ~~is observed~~ close to the halocline of the inner estuary~~, which encompasses the salinity range 2–4~~ (Fig. 2a). This material has no corresponding Al enrichment, confirming that it is not derived from suspended minerogenic matter and supporting the flocculation hypothesis. Further offshore, Fe_{part} concentrations decline to a background value of ~0.5 µmol L^{-1}, implying partial settling of the flocculated material to the sediments.

5.3 The impact of flocculation on sedimentary OM and Fe ~~in the upper estuary~~

In the following, we assume that the input of flocculated Fe to sediments occurs in the form of ferrihydrite and Fe (III)-OM, in accordance with the observations of Yu et al. (2015) for a nearby estuary. These fractions in sediments are expected to be observed in the labile Fe pool (i.e. soluble in Stages 1+2 of the Poulton and Canfield (2005) extraction, or in 1M HCl). The same is true for the diagenetic products of flocculated Fe, with the exception of pyrite, which classes as a refractory phase in our scheme (Table 3).

The transfer of terrestrially-derived OM and Fe from the dissolved to the particulate phase ~~in the estuarine water column~~ promotes the accumulation of both components in the sediments. Yet, our data suggests a further decoupling of terrestrial OM and Fe during sedimentation. ~~Our data show a c~~A clear trend of ~~lear trend of~~ decreasing terrestrial OM ~~and total Fe~~ content~~s~~ in sediments ~~in sediments along the Mustionjoki transect~~is observed along the transect, ~~(Fig. 4b)~~consistent with enhanced input of flocculated material in the inner estuary (Fig. 4b). In contrast, the distribution of labile Fe in sediments is less clearly controlled by distance offshore, at least within the range of the Mustionjoki transect (Stages 1+2-soluble Fe, Fig. 4b). Rather, elevated labile Fe contents are seen at Station D, the deepest site in the inner estuary, while anomalously low values are observed at Station F, close to the sill at Ekenäs. This suggests that the bathymetry of the estuary has a modulating effect on the distribution of flocculated Fe.

The modulating effect of bathymetry on labile Fe may be related to two factors. The first is redox shuttling, during which Fe is focused downslope in low-oxygen marine environments due to repeated cycles of reduction and oxidation under the influence of gravity (e.g., Raiswell and Anderson, 2005; Lenz et al., 2015). The second is physical reworking by currents, which favors the transport of fine-grained material such as labile Fe away from shallow areas (Virtasalo et al., 2005). In particular, the upstream flow of saline water across the sill (Fig. 1) may favor the transport of labile Fe away from Station F and towards Station D (Fig. 4). We note that although this mechanism also influences sedimentary organic material, it is the phytoplankton-derived component which appears to be most susceptible. Both the absolute concentration of phytoplankton-derived OM, and its contribution to total OM, are elevated at Station D with respect to its position on the transect (Fig. 4b). This implies that the flocculated Fe fraction most affected by reworking to deeper areas should be ferrihydrite, rather than OM-Fe (III), since the latter is expected to behave similarly to bulk terrestrial OM.

To test whether the impact of flocculation on sedimentary Fe contents could be distinguished above focusing effects over a longer offshore transect, we compared Fe/Al ratios of surface sediments from the Mustionjoki transect with those from the nearby Paimionjoki transect (Fig. 1) and values reported in literature for the open shelves of the Baltic Sea (note that stations A and B have been removed from this analysis for reasons described in Section 5.4). Fe/Al correlates positively with labile Fe at the Mustonjoki sites (R^2 = 0.45, n = 8), hence serves as a first-order proxy for the input of flocculated material. The bathymetry of the Paimionjoki transect is less variable, thus the influence of focusing on the distribution of labile Fe is expected to be reduced. Accordingly, Fe/Al along the Paimionjoki transect shows a steady decline from Fe/Al = 0.93 to Fe/Al = 0.73 over >80 km S from the river mouth (Fig. 9). Furthermore, typical Fe/Al values for oxic shelf areas of the northern Baltic Proper – >100 km offshore from likely riverine Fe sources – are only ~0.5–0.6 (e.g., Lenz et al., 2015). Data from the Mustionjoki transect, though variable due to focusing effects, show a similar mean value to stations at the corresponding position on the Paimionjoki transect. Taken together, these results suggest that there is indeed an offshore decline in the input of flocculated Fe to sediments in the Baltic Sea, whose impact can be observed over large distances (>100 km) from the coastline. This conclusion is supported by our suspended Fe_{part} data, which shows a background of ~0.5 µmol L^{-1} Fe_{part} in the water column of Station K in the open Gulf of Finland (Fig. 2). Hence, although flocculation itself likely occurs further upstream at the contact between fresh and brackish water masses, a fraction of the suspended Fe_{part} apparently evades settling in the estuarine environment and is transported offshore before sedimentation.

Considering the boreal coastal zone more broadly, the spatial impact of flocculation on sedimentary Fe chemistry is likely determined by the steepness of the offshore salinity gradient and the magnitude of the riverine Fe input. The Baltic Sea is characterized by a nearly 2000 km-long N–S surface-water salinity gradient of ~2–15, from the Bothnian Bay to the Danish Straits (Leppäranta and Myrberg, 2009). In the lowest-salinity regions in the Bothnian Bay and Bothnian Sea, the potential zone of estuarine flocculation extends further offshore and the trapping of Fe in estuarine sediments may be expected to be less efficient. At the same time, riverine Fe inputs in this region are higher than elsewhere in the Baltic Sea (Asmala et al., 2014), due to the significant release of Fe from peatlands in the catchment areas (Kortelainen et al., 2006) and the potential release of Fe from acid-sulfate soils (Boman et al., 2010). Due to this combination of factors, flocculated Fe_{part} is likely dispersed over a much larger area in the Bothnian Bay and Bothnian Sea with respect to the Baltic Proper, which could explain the consistently high sedimentary Fe contents in the offshore areas of the Bothnian Sea (Slomp et al., 2013). At the other end of the spectrum, in boreal estuaries draining into fully marine systems such as in the Arctic (e.g., Dai and Martin, 1995), steeper salinity gradients likely limit the dispersion of flocculated material to a relatively narrow zone close to the river mouths.

5.4 Impact of industrial Fe pollution

Extreme Fe enrichments of up to >25% Fe by weight are observed in the deeper sediments at Station A, principally due to elevated concentrations of Stages 3+4-soluble Fe (Fig. 5). The ^{57}Fe Mössbauer spectra from both the surface- and deep-sediment samples from this station deviate significantly from all other measured samples, showing the presence of wüstite and

Formatted: Superscript

Formatted: Heading 2, Space Before: 0 pt, After: 0 pt

Formatted: Superscript

magnetite alongside the typical doublets of superparamagnetic Fe (III) and silicate Fe (II) (Fig. 7). Such high concentrations of these minerals are rarely observed in natural aquatic sediments and suggest a significant impact of industrial pollution at this site.

The lack of wüstite and magnetite in the river bed sample at Station 'a' imply that the most likely source of these minerals in Station A sediments is the blast furnace at Åminnefors (Fig. 1a), which is located <1 km from the river mouth and was active from the late 19th century until 1977. Both minerals may form as oxidation films on the surface of metallic Fe (Kim et al., 2000), which likely occurred continuously at the blast furnace immediately following the smelting process. Indeed, inputs of wüstite to sediments in Hamilton Harbor, Ontario, were interpreted to derive from precisely such a source (Manning et al., 1980).

The timing of maximum input of industrial Fe pollution shortly after 1970, and decline thereafter, is consistent with the timeline of activity at the blast furnace. However, the signal of wüstite and magnetite in the surface sediments at Station A, and considering the extraction results, likely also Station B (Fig. 4b), suggests a legacy effect in which this material is both cycled upwards in the sediment column by bioturbation, and gradually spread downstream by bottom transport. At present, there is no evidence for wüstite or magnetite at Station D, implying that the signal is currently restricted to the uppermost kilometers of the estuary. The presence of industrial Fe pollution a Stations A and B complicates the interpretation of offshore trends in Fe/Al, and therefore these stations were removed from Figure 9.

5.5 Impact of flocculation and sediment focusing on sedimentary diagenesis

The diagenetic zonation at Stations A, D and J is broadly similar (Fig. 8). The principal difference that can be discerned from the pore water profiles is that the SMTZ at Station A is shallower in the sediment column and is not defined by a pore water H_2S enrichment such as observed at the other sites. The shallowness of the SMTZ at Station A is related to the low bottom-water sulfate concentration in the upper estuary, which limits the depth to which sulfate can penetrate before it is consumed. This itself may be the cause of the lack of H_2S accumulation, due to the restricted zone in which sulfate reduction occurs and hence the total consumption of produced H_2S by Fe^{2+}_{aq} (reaction 16). However, it is notable that both instantaneous sulfate reduction rates (Fig. 8), and net burial of S during the period 1970–2015 (Fig. 6c) are actually higher at Station A than at Station J, the furthest offshore of the three sites. Hence, bottom-water sulfate is apparently not limiting the net rate of sulfate reduction and subsequent formation of AVS and pyrite in this system. This result would appear to be consistent with the modeling simulations of Rooze et al. (2016), which showed that variations in bottom water sulfate in northern Baltic Sea sediments should not strongly impact on the solid-phase S profiles (Figure 6d in their paper), despite affecting other aspects of sedimentary diagenesis.

Net burial of S during the period 1970–2015 is highest at Station D, suggesting that high sedimentation rates and focusing of phytoplankton-derived OM in the deep basin of the inner estuary promotes higher long-term rates of sulfate reduction than

Formatted: Heading 2, Space Before: 0 pt, After: 0 pt

Formatted: Subscript

Formatted: Subscript

Formatted: Subscript

Formatted: Superscript

observed at either Station A or Station J (Fig. 6c). Furthermore, the presence of unsulfidized Fe (II) in the sediments at both Stations A and D enhances net rates of reactive Fe (II) burial at these sites, over and above the contribution from AVS and pyrite (Fig. 6c). This implies that net rates of Fe reduction (including reduction of both ferrihydrite and Fe (III)-OM) are greater within the estuary than in the offshore region. Again, the highest rate is observed at Station D, consistent with the focusing of labile flocculated Fe to the deep inner basin (Fig. 4b).

The PROFILE output indicates that the high concentrations of pore water Fe^{2+} in the deep sediments at Stations A and D are not produced *in situ* and hence likely represent Fe produced below the model domain (e.g. via reactions 12 and 19) which is currently diffusing vertically towards the SMTZ (Fig. 8). Therefore, it is possible that a fraction of the Fe (II) precipitated in the sediment interval corresponding to 1970–2015 is in fact derived from earlier-deposited labile Fe (III) which is remobilized during deep burial, and therefore that the numbers for recent Fe (II) burial may be overestimated. Still, this observation reinforces our assertion that Fe reduction rates throughout the whole sediment column are higher at the sites in the estuary than further offshore, due to the more intense accumulation of flocculated labile Fe.

While the behavior of flocculated ferrihydrite during sedimentary diagenesis can be well described by the reaction network in Section 4.8, the details of the reductive transformation of Fe (III)-OM to Fe (II)-OM during burial remain unresolved by this study. We have assumed the model of Yu et al. (2015) to apply in our system, in which Fe (III) complexed to carboxylate and phenolate functional groups within humic material in the water column is reduced *in situ* in sediments, retaining its association with these functional groups during burial. However it is also possible that Fe (II) may associate with OM after release from the reduction of ferrihydrite in the absence of H_2S. Moreover, the retention of a portion of Fe (III)-OM during burial, as implied by the 1M HCl extraction data (Fig. 6a) suggests either that not all of the flocculated Fe (III)-OM is reduced in sediments, or that new complexes of Fe (III) and relatively labile OM are formed during remineralization of OM in the sediment column and preserved during burial (Lalonde et al., 2012: Barber et al., 2017).

Interestingly, the higher rates of Fe and sulfate reduction observed at Station A with respect to Station J run contrary to the assumption that the dominance of terrestrial plant-derived OM in the upper estuarine sediments should lower the net degradability of OM in the sediments (Arndt et al., 2013). Flocculated DOM is characterized by high contents of humic substances, derived from complex polymers in vascular plants, such as cellulose, lignin, cutin and cutan (de Leeuw and Largeau, 1993), which are relatively resistant to degradation by the sediment microbial community (e.g. Hedges et al., 2000). In contrast, phytoplankton-derived OM contains high concentrations of degradable compounds such as proteins, nucleic acids and simple carbohydrates, and in the shallow coastal system may be expected to experience relatively little pre-ageing before deposition in the sediments. We suspect that the relatively high rates of diagenetic processes at Station A are related to high mass accumulation rates at this site. Although sedimentation rate is approximately similar to Station J (Fig. 5, 6), porosity of the sediments at Station A is significantly lower, yielding mass accumulation rates a factor 1.7 higher than Station J and therefore similarly increasing the accumulation rate of degradable organic material. ~~. Maximum values are observed at sites~~

Formatted: Superscript

Formatted: Font: Italic

Formatted: Subscript

A and B, within 2 km due S of the river mouth, implying maximum accumulation of flocculated material in this zone. At first glance this result appears surprising, since the flocculation maximum in the June 2015 data is observed in the halocline of salinity 2–4, located further offshore (Figs. 1, 2). However, the mean annual position of the halocline is likely further upstream (i.e. closer to the river mouth) than recorded during our sampling in June, when discharge in the Gulf of Finland catchment is at its annual maximum (Voipio, 1981). Assuming the suspended particulate maximum and associated gravitational settling to follow the lateral migration of the halocline through time (Geyer, 1993; Sanford et al., 2001), the focal point of sedimentation for flocculated material may thus be closer to the river mouth than implied by the June 2015 data. Notably, maximum sedimentary Fe concentrations were observed at station B (Fig. 4b), which likely falls close to the intersection of the halocline with the sediment-water interface during mean flow conditions (see Fig. 1). On the other hand, the maximum contribution of terrestrial material to sedimentary OM is recorded at station A. This discrepancy could indicate that settling of riverine suspended microparticulate POM, along with flocculated DOM, contributes to the total sedimentary OM pool at this site. Indeed, organic detritus, including terrestrial plant material, was readily visible in sediment cores from station A.

The speciation of sedimentary Fe at stations A and B contrasts strongly with that at stations further offshore. Stations A and B are characterized by relatively high contributions of dithionite- and oxalate- soluble Fe (Fig. 4b). According to the protocol of Poulton and Canfield (2005), which was originally developed for river sediments, these fractions should represent crystalline Fe oxides such as goethite, akaganéite and hematite (in the dithionite-soluble component) and magnetite (in the oxalate-soluble component). However, of these phases only magnetite is identified in the 57Fe Mössbauer spectrum of the surface sediment from station A (Fig. 5). Moreover, the same spectrum indicates a large contribution of organic-Fe (II) complexes (Fig. 5, Table 3). The behavior of such material in the Poulton and Canfield (2005) protocol has not been previously described, but the large fraction of dithionite- and oxalate- soluble Fe in these samples, coupled to the lack of mineralogical evidence for crystalline oxides, suggest that Stages 3 and 4 of the sequential extraction may be interpreted as primarily indicating organic-Fe (II) complexes in this environment.

The high contents of dithionite- and oxalate- soluble Fe in the sediments of the upper estuary (Fig. 4) thus suggest direct transfer of flocculated Fe-OM aggregates to the sediments, and confirm the suggested role of OM flocculation as a mechanism for trapping Fe in estuaries (Lisitsyn, 1995). Flocculated material in the oxic estuarine water column is likely present as Fe (III) partitioned between organic-Fe (III) complexes and ferrihydrite (Neubauer et al., 2013). Reduction of organic-Fe (III) complexes after sedimentation may generate the organic-Fe (II) complexes detected in our sedimentary mineralogical data. Specifically, iron (III) complexed to carboxylate and phenolate functional groups within humic material in the water column may be reduced in situ in sediments, retaining its association with these functional groups as demonstrated by X-Ray Absorption Spectroscopy (XAS) (Yu et al., 2015). It is noteworthy that this mechanism for Fe-OM association in sediments differs slightly from that proposed by Lalonde et al. (2012), in which complexes of Fe (III) and relatively labile OM are formed during remineralization of OM in the sediment column and preserved during burial.

Considering the presence of ferrihydrite in flocculated material, flocculation likely also acts as a vector of ferrihydrite to the sediments. Our Mössbauer data detect a large component of superparamagnetic Fe (III), interpreted as nanoparticulate ferrihydrite, in the surface sediments at both stations A and D (Fig. 5, Table 3). Although ferrihydrite is generally thought to be extracted exclusively in Stage 2 of the Poulton and Canfield (2005) protocol (Table 2), the abundance of superparamagnetic Fe (III) in the Mössbauer data, and the absence of carbonate minerals, lead us to conclude that Stages 1 and 2 (Na acetate and hydroxylamine-HCl) both extract ferrihydrite or similar poorly crystalline

Formatted: English (United Kingdom)

Formatted: Heading 2, Space Before: 0 pt, After: 0 pt

Formatted: English (United Kingdom), Not Superscript/ Subscript

Formatted: English (United Kingdom)

Formatted: Font: Not Italic, English (United Kingdom)

Formatted: English (United Kingdom)

~~Fe (oxyhyr)oxides from the sediments in this setting. Accordingly, the net contribution of Stages 1 and 2 to total extracted Fe in surface sediments generally decreases offshore (Fig. 4a), consistent with a declining input from flocculation.~~

~~Notably however, the maximum input of ferrihydrite to sediments occurs at station D, located 7.5 km due S from the river mouth, at the deepest point of the inner estuarine basin. This suggests that focusing of ferrihydrite occurs in the upper estuary, due to redox shuttling effects under seasonally oxygen depleted conditions (e.g., Raiswell and Anderson, 2005; Lenz et al., 2015). Indeed, the Mustionjoki estuary is known to display deep water hypoxia (oxygen concentrations < 2 mg L^{-1}) in the autumn months (Niemi, 1977) and displayed moderate oxygen depletion during our sampling in June 2015 (Fig. 1b). Redox shuttling, and physical reworking of sediments in shallow areas, are known to influence the distribution of both reactive Fe and organic material in the coastal archipelagos of the Baltic Sea, favoring higher concentrations of both components in deeper areas (Virtasalo et al., 2005). Accordingly, the only section of the transect where surface sediment C_{org} and Fe contents are substantially lower than the whole-transect mean values of 3.5% (C_{org}) and 970 µmol g^{-1} (Fe) are stations F and G, located close to the sill of the First Salpausselkä (Fig. 1b).~~

~~5.4 The broader impact of flocculation on sediment biogeochemistry~~

~~The enhanced inputs of Fe-OM complexes and ferrihydrite to the sediments in the upper estuary influence diagenetic processes in the sediments, as indicated by the contrasting sediment and pore water chemistry at stations A, D and J (Figs 6, 7). Most importantly, the dominance of terrestrial plant-derived OM at station A lowers the net degradability of OM in the sediments. Humic substances in the flocculated material are derived from complex polymers in vascular plants, such as cellulose, lignin, cutin and cutan (de Leeuw and Largeau, 1993), which are relatively resistant to degradation by the sediment microbial community (e.g. Hedges et al., 2000). The comparatively constant C_{org} content throughout the upper 40 cm at station A (Fig. 6) is consistent with a low range of k-values for net organic matter degradation at this site (see Arndt et al., 2013). In contrast, stations D and J show decreasing C_{org} contents with depth, implying more efficient net degradation of OM (hence a higher range of k-values) due to the proportionally greater input of phytoplankton material at these sites (Fig. 4). Phytoplankton-derived OM contains high concentrations of degradable compounds such as proteins, nucleic acids and simple carbohydrates, and in the shallow estuarine system may be expected to experience relatively little pre-ageing before deposition in the sediments. The abundance of such fresh material thus likely causes the higher net degradability of OM in the sediments at stations D and J (see Arndt et al., 2013). Comparatively low rates of organic matter remineralization in the upper estuary are also reflected in the concentration of primary metabolites in the pore waters. In the sub-SMTZ sediments, maximum concentrations of both methane (Fig. 5) and ammonium (not shown) are significantly lower at station A with respect to the other stations, indicative of lower rates of production of these compounds during organic matter remineralization (e.g., Berg et al., 1998).~~

~~Beyond the impact on sedimentary OM degradability, flocculation also influences the concentration of Fe in the sediment, with potentially important consequences for diagenetic processes. However, the influence of Fe must be considered in the context of changes in bottom water [SO_4^{2-}], due to the close coupling of Fe and S cycling in sediments (Berner, 1970; Berner and Raiswell, 1984). Due to the salinity gradient of the Mustionjoki transect (Fig. 1b), the three sites A–D–J encompass opposing gradients of total sedimentary Fe content and bottom water [SO_4^{2-}] (Figs. 6, 7). At station A, the relative concentration of Fe with respect to SO_4^{2-} is thus at a maximum. Low bottom-water [SO_4^{2-}] leads to a shallow SMTZ (5–10 cm) and despite the production of H_2S during sulfate-mediated AOM (equation 5), no accumulation of H_2S is observed in the pore waters due to the subsequent reaction with Fe^{2+} (equation 6). Conversely, at stations D and J the relative availability of Fe compared to SO_4^{2-} declines, the SMTZ is located progressively deeper, and H_2S accumulates to progressively higher concentrations in the pore waters (Fig. 7). A similar conclusion was~~

Formatted: English (United Kingdom), Not Superscript/ Subscript
Formatted: English (United Kingdom)
Formatted: English (United Kingdom), Not Superscript/ Subscript
Formatted: English (United Kingdom)
Formatted: English (United Kingdom), Not Superscript/ Subscript
Formatted: English (United Kingdom)
Formatted: English (United Kingdom), Not Superscript/ Subscript
Formatted: English (United Kingdom)
Formatted: Line spacing: single
Formatted: English (United Kingdom)
Formatted: Heading 2, Space Before: 0 pt, After: 0 pt
Formatted: English (United Kingdom), Not Superscript/ Subscript
Formatted: English (United Kingdom)
Formatted: English (United Kingdom), Not Superscript/ Subscript
Formatted: English (United Kingdom)
Formatted: English (United Kingdom), Not Superscript/ Subscript
Formatted: English (United Kingdom)
Formatted: English (United Kingdom), Not Superscript/ Subscript
Formatted: English (United Kingdom)
Formatted: English (United Kingdom), Not Superscript/ Subscript
Formatted: English (United Kingdom)
Formatted ...
Formatted: English (United Kingdom)
Formatted ...
Formatted: English (United Kingdom)
Formatted ...
Formatted: English (United Kingdom)
Formatted ...
Formatted: English (United Kingdom)
Formatted ...
Formatted: English (United Kingdom)
Formatted ...
Formatted: English (United Kingdom)

~~predicted for a hypothetical bottom water [SO_4^{2-}] gradient in a recent modeling study focused on the Bothnian Sea (Rooze et al., 2016).~~

~~The organic Fe (II) complexes which dominate sedimentary Fe at station A likely do not participate significantly in the diagenetic reactions determining the pore water chemistry shown in Figure 7. Assuming these complexes to be formed by in situ reduction of Fe (III) from Fe (III) organic complexes after sedimentation (Yu et al., 2015), Fe is retained in the particulate organic phase and not released into the pore waters. Instead, the Fe^{2+} observed in the pore water profiles is likely produced during the reduction of Fe (oxyhydr)oxides, including ferrihydrite, either during dissimilatory reduction coupled to organic matter oxidation (e.g., Canfield et al., 2005):~~

~~$$CH_2O_{(s)} + 4Fe(OH)_{3(s)} + 7CO_{2(aq)} \rightarrow 8HCO_{3(aq)}^- + 3H_2O_{(l)} + 4Fe_{(aq)}^{2+} \quad (7)$$~~

~~or, as recently suggested by various studies (Sivan et al., 2011; Slomp et al., 2013; Egger et al., 2015a), during Fe-mediated anaerobic oxidation of methane (Fe-AOM):~~

~~$$CH_{4(aq)} + 8Fe(OH)_{3(s)} + 15H_{(aq)}^+ \rightarrow HCO_{3(aq)}^- + 21H_2O_{(l)} + 8Fe_{(aq)}^{2+}$$~~

~~The higher accumulations of Fe^{2+} in the pore waters of the sub-SMTZ depth interval at stations A and D with respect to station J (Fig. 7) thus indicate higher background rates of Fe (oxyhydr)oxide reduction, consistent with higher net inputs of ferrihydrite to the sediments in the upper estuary (Fig. 4b).~~

5.~~5~~ ~~76~~ Temporal stability of flocculation impacts on sedimentation

The coastal zone of the Baltic Sea has been impacted severely by anthropogenic activities during the last century. First of all, enhanced nutrient inputs have altered coastal ecosystems and triggered hypoxia in many areas (Conley et al., 2011). Also land use changes such as ditching and forest clearance have influenced the inputs of particulate material to the coastal zone (Yu et al., 2015). ~~Moreover, the~~The transport of riverine Fe and DOM into the Baltic has increased in recent decades as a consequence of brownification (Kritzberg et al., ~~2014~~2012), related primarily to the recovery of boreal freshwater systems from industrial acidification and elevated ionic strength in the mid-20th century (Monteith et al., 2007). Finally, the coastal zone is impacted by variable direct inputs of industrial Fe pollution such as those observed in this study. ~~These~~ Each of these changes may be expected to influence both the sediment composition and diagenetic processes in the sediments at our study sites through time.

The ~~The~~ most pronounced effect of recent coastal eutrophication on sediment chemistry has been to increase the flux ~~of autochthonous~~of phytoplankton-derived organic matter to the sediments. As outlined in Section 4.8~~Due to the consumption of electron acceptors in organic matter remineralization~~, this increased carbon loading has led to a vertical migration of the redox zones of the sediments. Recent shoaling of the ~~, including the~~ SMTZ at Stations A, D and J is indicated by~~(Slomp et al., 2013; Egger et al., 2015a). Evidence for an upwards shift of the SMTZ can be seen~~ peaks in ~~the~~ total sulfur (S) ~~contents of the sediments at stations A, D and J (Fig. 6), each of which show a distinct peak~~ in the post-1970 sediments~~, close to the current position of the SMTZ~~ (Fig. 5~~.~~), consistent~~This is consistent~~ with the time-dependent modeling simulations of Rooze at al. (2016), in which rates of ~~FeS~~ AVS and ~~FeS_2~~ pyrite precipitation in the SMTZ were shown to increase in response to carbon loading in the late 20th century.

Formatted ...
Formatted ...
Formatted ...
Formatted ...
Formatted ...
Formatted: Line spacing: single
Formatted: English (United Kingdom)
Formatted: Font: Not Italic

However, A distinct interval of elevated sedimentary Fe contents can be seen at station A, centered on the early 1970s (Fig. 6). Total Fe contents in this layer are up to 3 times higher than at the present day (3% vs. 1%), indicating a dramatically increased input of Fe. No corresponding peak is observed in C_{org}, suggesting that the Fe profile cannot be explained by a simple increase in DOM input to the estuary at this time, leading to enhanced rates of flocculation and sedimentation. Nevertheless, the Fe in this interval is predominantly in the form of organic-Fe (II) complexes (Fig. 6), indicating flocculation as the likely mechanism for sedimentation of Fe. This implies that the Fe/C ratio of the riverine DOM was elevated at this time due to a secular increase in the input of Fe to the river water from an anthropogenic source, possibly the nearby blast furnace at Åminnefors (Fig. 1a), which was active from the late 19th century until 1977.

Ddespite the these various potential anthropogenic impacts, the role of flocculation in determining sedimentary Fe chemistry along the Mustionjoki transect appears to have rhas remained largely unchanged throughout the last centurythe studied interval. Labile Fe contents at Station D are quite constant throughout the core profile, implying that this site has served as a trap for flocculated material since at least the mid-20th century (Fig. 5). Similarly, labile Fe concentrations at Station D have been consistently lower during the same interval. Only at Station A is there evidence for slightly enhanced inputs in the past, coincident with the strong industrial pollution input in the 1970s. Evidence of enhanced Fe input centered on the early 1970s is restricted to station A. In contrast, stations D and J record relatively constant Fe contents throughout the sediment column (Fig. 6), implying relatively static net Fe inputs. This suggests that any recent changes in riverine Fe inputs due to brownification (Sarkkola et al., 2013; Kritzberg and Ekström, 2012) have not strongly influenced sedimentary Fe in this system. Moreover, the offshore decline in sedimentary Fe contents observed in the modern surface sediments (Fig. 4b) is reproduced in the systematic decrease in Fe contents from station A–D–J observed at all depths in the sediment column (Fig. 6). Hence, on the scale of the entire transect, it can be concluded that the role of flocculation in determining the Fe distribution in these estuarine sediments has not been significantly influenced by human activities over the last century.

Formatted: Superscript

5.6 The spatial extent of the flocculation signal in sediment Fe chemistry

Our data confirm that estuarine sediments may trap large amounts of the Fe transported to the boreal coastal zone via rivers. When the additional surface sediment data from the Paimionjoki transect are plotted together with those from the Mustionjoki transect, sedimentary Fe/Al ratios show an apparent logarithmic decline with distance offshore. Fe/Al provides a simple indication of the reactive Fe content of sediments (Lyons and Severmann, 2006), and in this case describes the net enrichments of both organic-Fe (II) complexes and ferrihydrite, introduced to sediments as a consequence of flocculation. The absence of extreme Fe enrichments in the Paimionjoki transect is likely due to the absence of stations close to the river mouth, where organic-Fe (II) complexes are expected to accumulate, and the lack of a pronounced bathymetric sill, which limits the redox shuttling effects on ferrihydrite observed in the Mustionjoki estuary. However, Fe/Al along the Paimionjoki transect alone

~~shows a steady decline from Fe/Al = 0.93 to Fe/Al = 0.73 over >80 km S from the river mouth (Fig. 8). Furthermore, typical Fe/Al values for oxic shelf areas of the northern Baltic Proper – several hundred km offshore – are ~0.5–0.6 (e.g., Lenz et al., 2015), implying an ongoing decline in Fe/Al offshore from station Q, our most distal sampling point. Taken together, these results suggest that the spatial signal of flocculation in sedimentary Fe chemistry in the brackish Baltic Sea is detectable over a large distance (>100 km) from the coastline. This conclusion is supported by our suspended Fe_{part} data, which shows a background of ~0.5 µmol L^{-1} Fe_{part} in the water column of station K in the open Gulf of Finland (Fig. 2). Hence, although flocculation itself likely occurs further upstream at the contact between fresh and brackish water masses, a fraction of the suspended Fe_{part} apparently evades settling in the estuarine environment and is transported offshore before sedimentation.~~

~~Considering the boreal coastal zone more broadly, the spatial impact of flocculation on sedimentary Fe chemistry is likely determined by the steepness of the offshore salinity gradient and the magnitude of the riverine Fe input. The Baltic Sea is characterized by a nearly 2000 km-long N–S surface-water salinity gradient of ~2–15, from the Bothnian Bay to the Danish Straits (Leppäranta and Myrberg, 2009). In the lowest-salinity regions in the Bothnian Bay and Bothnian Sea, the potential zone of estuarine flocculation extends further offshore and the trapping of Fe in estuarine sediments may be expected to be less efficient. At the same time, riverine Fe inputs in this region are higher than elsewhere in the Baltic Sea (Asmala et al., 2014), due to the significant release of Fe from peatlands in the catchment areas (Kortelainen et al., 2006) and the potential release of Fe from acid sulfate soils Boman et al., 2010). Due to this combination of factors, flocculated $Fe_{part.}$ is likely dispersed over a much larger area in the Bothnian Bay and Bothnian Sea with respect to the Baltic Proper, which could explain the consistently high sedimentary Fe contents in the offshore areas of the Bothnian Sea (Slomp et al., 2013). At the other end of the spectrum, in boreal estuaries draining into fully marine systems such as in the Arctic (e.g., Dai and Martin, 1995), steeper salinity gradients likely limit the dispersion of flocculated material to a relatively narrow zone close to the river mouths.~~

6 Conclusions

In boreal estuaries, ~~salinity-mediated~~ flocculation of DOM and ~~associated~~ Fe strongly influences the chemistry of the sediments and the diagenetic reactions involving Fe. We can draw the following main conclusions from the study:

- Flocculation of DOM and Fe are partially decoupled, likely due to the presence of discrete ferrihydrite colloids in the freshwater input which show a secular response to estuarine mixing from Fe associated with DOM
- Flocculation of Fe is reflected in strongly non-conservative mixing of $Fe_{diss.}$ along the estuarine salinity gradient. $Fe_{diss.}$ is preferentially removed from solution with increasing salinity, and potentially pH.
- The POM generated by flocculation of DOM can be detected in suspended particulate matter using $\delta^{13}C$ and N/C of DOM as end-member reference values. Due to the presence of phytoplankton material in surface waters at the time of sampling, flocculated OM is primarily detected in deeper waters.

- The ~~true~~ zone of Fe flocculation in the estuarine water column can be identified using parallel measurements of Fe_{diss} and Fe_{part}.~~,~~ ~~and~~ This occurs at low salinities, close to the primary contact between fresh and saline water masses. In the Mustionjoki estuary, this zone corresponds to the halocline of the stratified inner basin~~, which is laterally mobile during the seasonal cycle~~.
- Flocculation causes accumulation of labile Fe in the form of ferrihydrite and Fe (III)-OM in near-shore areas. ~~The impacts of flocculation on sediment chemistry are most pronounced in the upper estuarine zone, where the halocline intersects the sediment-water interface. However, flocculated material accumulates in progressively lower concentrations up to tens or hundreds of kilometers offshore.~~ The spatial scale of the flocculation signal in offshore sediment chemistry is likely dependent on the steepness of the salinity gradient, with greater dispersal in low-salinity systems. Redox shuttling and physical reworking modulate the influence of flocculation on sedimentary Fe chemistry, by focusing flocculated labile Fe into bathymetric depressions.
- ~~Flocculation transfers POM of terrestrial origin, likely humic materials, from the water column to the sediments~~In contrast to Fe, ~~T~~the contribution of ~~this~~ flocculated terrestrial OM ~~material~~ to total sedimentary OM ~~declines~~ shows a clear offshore decline less impacted by focusing effects, as indicated by $\delta^{13}C$ and N/C of sedimentary OM.
- ~~Flocculation transfers Fe to the sediments in two principal forms: organic-Fe (III) complexes and ferrihydrite. In sediments, Fe in organic-Fe (III) complexes is reduced *in situ*, producing organic-Fe (II) complexes which are preserved during burial. In contrast, ferrihydrite takes part in sedimentary diagenetic reactions, influencing the pore water and sediment chemistry~~During diagenesis, flocculated ferrihydrite and Fe (III)-OM are reduced in the sediment column, leading to the accumulation of AVS, pyrite and unsulfidized Fe (II), including Fe (II)-OM.~~.~~
- ~~Organic-Fe (II) complexes in sediments are strongly concentrated close to river mouths. Ferrihydrite in sediments is also more concentrated in upper estuarine regions, but due to redox shuttling effects may be redistributed from the original site of sedimentation.~~
- ~~The impact of flocculation on sediment chemistry is modulated by the gradient of bottom water sulfate concentrations along the estuarine salinity gradient. Opposing gradients of Fe and sulfate availability for diagenetic reactions are observed with increasing distance offshore. These impact on the vertical zonation of sediment biogeochemistry, most markedly in determining the depth of the SMTZ and the accumulation of hydrogen sulfide and Fe^{2+} in pore waters.~~Net rates of Fe reduction in sediments are higher in the inner estuary with respect to offshore areas, consistent with enhanced inputs of flocculated labile Fe.
- ~~Although Fe and DOM inputs to boreal estuaries have been shown to be increasing over recent decades due to brownification, Fe inputs to sediments in our principal study transect remained largely constant over the same interval. However, coastal eutrophication has had a strong impact on sediment chemistry through increased carbon inputs, leading to a shoaling of the SMTZ and increased rates of the associated sedimentary reactions~~Industrial activities in coastal areas can lead to significant signals of Fe pollution in near-shore sediments.~~.~~

Data availability

All data from Figures 1–~~8~~ 9 of the manuscript and Supplementary Figures 1 and 2 will be made available in Pangaea upon publication of the article.

Supplement link

Supplementary Figures 1 and 2 ~~is~~ are uploaded in parallel with the manuscript and ~~is~~ are available from the Biogeosciences website.

Author contributions

TJ devised the study, carried out field and laboratory work, interpreted the data, produced the figures and wrote the paper. EA interpreted the data and assisted with writing the paper. CS carried out the Mössbauer analysis, interpreted the data and assisted with writing the paper. RT carried out fieldwork and sequential Fe extractions, interpreted the data, produced figures and wrote the MSc thesis which formed the basis for the paper. J-PM carried out fieldwork, analyzed methane samples and assisted with writing the paper. JV, AK and PP provided sample material, interpreted the data and assisted with writing the paper. PE assisted with ICP-OES analysis. SH managed the project which principally funded the study, carried out fieldwork, interpreted the data and assisted with writing the paper.

Competing interest statement

The authors declare no competing interest.

Acknowledgements

We acknowledge support in field campaigns from Tvärminne Zoological ~~Station~~Station, Göran Lundberg, Veijo Kinnunen, Ari Ruuskanen, Mikael Kraft, Petra Tallberg, Anni Jylhä-Vuorio and Kaarina Lukkari. Analytical and laboratory assistance was provided by Juhani Virkanen, Antti Nevalainen, Jaana Koistinen and Asko Simojoki. The comments of Peter Kraal and one anonymous reviewer substantially improved the study. This research was funded by Academy of Finland projects 139267, 272964 and 267112, Maa ja Vesitekniikan Tuki projects 31749 and 32861, and by the BONUS COCOA project (grant agreement 2112932-1), funded jointly by the EU and Danish Research Council. C.S. acknowledges a Travel and

Formatted: Font: Bold

Formatted: List Paragraph, Bulleted + Level: 1 + Aligned at: 0,63 cm + Indent at: 1,27 cm

Formatted: Heading 1, Space Before: 0 pt, After: 0 pt

Formatted: Heading 1, Space Before: 0 pt, After: 0 pt

Formatted: Heading 1, Space Before: 0 pt, After: 0 pt

Formatted: Heading 1, Space Before: 0 pt, After: 0 pt

Formatted: Heading 1, Space Before: 0 pt, After: 0 pt

Instrumentation Award from the STFC-funded Geological Repositories Network and funding from the Carnegie Trust for the Universities of Scotland (Trust Reference No: 50357).

References

APHA: Standard methods for the examination of water and wastewater. 20th ed. American Public Health Association–American Water Works Association, Baltimore, USA, 1998.

Arndt, S., Jorgensen, B. B., LaRowe, D. E., Middelburg, J. J., Pancost, R. D. and Regnier, P.: Quantifying the degradation of organic matter in marine sediments: A review and synthesis, Earth-Sci. Rev., 123, 53-86, 10.1016/j.earscirev.2013.02.008, 2013.

Asmala, E., Autio, R., Kaartokallio, H., Pitkanen, L., Stedmon, C. A. and Thomas, D. N.: Bioavailability of riverine dissolved organic matter in three Baltic Sea estuaries and the effect of catchment land use, Biogeosciences, 10, 6969–6986, 10.5194/bg–10–6969–2013, 2013.

Asmala, E., Bowers, D. G., Autio, R., Kaartokallio, H. and Thomas, D. N.: Qualitative changes of riverine dissolved organic matter at low salinities due to flocculation, J. Geophys. Res. –Biogeosci., 119, 1919–1933, 10.1002/2014JG002722, 2014.

Asmala, E., Kaartokallio, H., Carstensen, J. and Thomas, D. N.: Variation in riverine inputs affect dissolved organic matter characteristics throughout the estuarine gradient, Front. Mar. Sci., 2, 125, 2016.

Barber, A., Brandes, J., Leri, A., Lalonde, K., Balind, K., Wirick, S., Wang, J. and Gélinas, Y.: Preservation of organic matter in marine sediments by inner-sphere interactions with reactive iron, Sci. Rep., 7, 366, 10.1038/s41598-017-00494-0, 2017.

Beal, E. J., House, C. H. and Orphan, V. J.: Manganese and iron dependent marine methane oxidation, Science, 325, 184−187, 10.1126/science.1169984, 2009.

Belley, F., Ferre, E. C., Martin-Hernandez, F., Jackson, M. J., Dyar, M. D., and Catlos, E.: The magnetic properties of natural and synthetic $(Fe_x,Mg_{1-x})_2SiO_4$ olivines, Earth. Planet. Sci. Letts., 284, 516–526, 10.1016/j.epsl.2009.05.016, 2009.

Berg, P., Risgaard–Petersen, N. and Rysgaard, S.: Interpretation of measured concentration profiles in sediment pore water, Limnol. Oceanogr., 43, 1500–1510, 10.4319/lo.1998.43.7.1500, 1998.

Berner, R.: Sedimentary pyrite formation, Am. J. Sci., 268, 1–23, 1970.

~~Berner, R. and Raiswell, R.: C/S method for distinguishing fresh-water from marine sedimentary rocks, Geology, 12, 365–368, 10.1130/0091–7613(1984)12<365:CMFDFF>2.0.CO;2, 1984.~~

Boman, A., Frojdo, S., Backlund, K. and Astrom, M. E.: Impact of isostatic land uplift and artificial drainage on oxidation of brackish-water sediments rich in metastable iron sulfide, Geochim. Cosmochim. Acta, 74, 1268–1281, 10.1016/j.gca.2009.11.026, 2010.

Bonaglia, S., Bartoli, M., Gunnarsson, J. S., Rahm, L., Raymond, C., Svensson, O., Yekta, S. and Brüchert, V.: Effect of reoxygenation and Marenzelleria spp. bioturbation on Baltic Sea sediment metabolism, Mar. Ecol.-Prog. Ser., 482, 43–55, 10.3354/meps10232, 2013.

Boudreau, B.P: Diagenetic models and their implementation: Modelling transport and reactions in aquatic sediments. Springer-Verlag, Berlin-Heidelberg, Germany, 1997.

Boyle, E., Edmond, J. and Sholkovitz, E.: Mechanism of iron removal in estuaries, Geochim. Cosmochim. Acta, 41, 1313–1324, 10.1016/0016–7037(77)90075–8, 1977.

Burton, E. D., Sullivan, L. A., Bush, R. T., Johnston, S. G. and Keene, A. F.: A simple and inexpensive chromium-reducible sulfur method for acid–sulfate soils, Appl. Geochem., 23, 2759–2766, 10.1016/j.apgeochem.2008.07.007, 2008.

Burton, E. D., Bush, R. T., Johnston, S. G., Sullivan, L. A. and Keene, A. F.: Sulfur biogeochemical cycling and novel Fe–S mineralization pathways in a tidally re-flooded wetland, Geochim. Cosmochim. Acta, 75, 3434–3451, 10.1016/j.gca.2011.03.020, 2011.

Canfield, D. E.: Reactive iron in marine sediments, Geochim. Cosmochim. Acta, 53, 619–632, 10.1016/0016-7037(89)90005-7, 1989.

Claypool, G. E., and Kaplan, I. R.: The origin and distribution of methane in marine sediments, in: Natural gases in marine sediments, Kaplan, I. R. (Ed.), Plenum Press, New York, U.S.A., 99–139, 1974.

~~Canfield, D. E., Kristensen, E., and Thamdrup, B.: Aquatic Geomicrobiology, Elsevier, Amsterdam, the Netherlands, 2005.~~

Cline, J.: Spectrophotometric determination of hydrogen sulfide in natural waters, Limnol. Oceanogr., 14, 454–&, 1969.

Conley, D. J., Carstensen, J., Aigars, J., Axe, P., Bonsdorff, E., Eremina, T., Haahti, B., Humborg, C., Jonsson, P., Kotta, J., Lannegren, C., Larsson, U., Maximov, A., Medina, M. R., Lysiak–Pastuszak, E., Remeikaite–Nikiene, N., Walve, J., Wilhelms, S. and Zillen, L.: Hypoxia is increasing in the coastal zone of the Baltic Sea, Environ. Sci. Technol., 45, 6777–6783, 10.1021/es201212r, 2011.

Dai, M. and Martin, J.: First data on trace-metal level and behavior in 2 major Arctic river-estuarine systems (Ob and Yenisey) and in the adjacent Kara Sea, Russia, Earth Planet. Sci. Lett., 131, 127–141, 10.1016/0012–821X(95)00021–4, 1995.

Dalzell, B. J., Minor, E. C. and Mopper, K. M.: Photodegradation of estuarine dissolved organic matter: a multi-method assessment of DOM transformation, Org. Geochem., 40, 243–257, 10.1016/j.orggeochem.2008.10.003, 2009.

D'Antonio, M. C., Wladimirsky, W., Palacios, D., Coggiola, L., Gonzáles-Baró, A. C., Baran, E. J. and Mercader, R. C.: Spectroscopic investigations of iron (II) and iron (III) oxalates, J. Braz. Chem. Soc., 20, 445-450, 10.1590/S0103-50532009000300006, 2009.

de Leeuw, J.W., and Largeau, C.: A review of macromolecular organic compounds that comprise living organisms and their role in kerogen, coal and petroleum formation, in: Organic Geochemistry, Principles and Applications, Engel, M. H. and Macko, S.A. (Eds), Plenum Press, New York, U.S.A., 23–72, 1993.

Dijkstra, N., Kraal., P., Kuypers, M. M. M., Schnetger, B., and Slomp, C.P.: Are iron-phosphate minerals a sink for phosphorus in anoxic Black Sea Sediments? PLoS ONE 9(7): e101139, 10.1371/journal.pone.0101139, 2014.

Dyar, M. D., Jawin, E., Breves, E. A., Marchand, G. J., Nelms, M., Lane, M. D., Mertzman, S. A., Bish, D. L., and Bishop, J. L.: Mössbauer parameters of iron in phosphate minerals: Implications for interpretation of Martian data, Amer. Mineral., 99, 5–6, 914–942, 10.2138/am.2014.4701, 2014.

Dyar, M. D., Jawin, E., Breves, E. A., Marchand, G. J., Nelms, M., Lane, M. D., Mertzman, S. A., Bish, D. L., and Bishop, J. L.: Mössbauer parameters of iron in phosphate minerals: Implications for interpretation of Martian data, Amer. Mineral., 99, 5–6, 914–942, 10.2138/am.2014.4701, 2014.

Dzombak, D., and Morel, F. M. M.: Surface complexation modeling: Hydrous ferric oxide, Wiley, New York, U.S.A., 1990.

Eckert, J. and Sholkovitz, E.: Flocculation of iron, aluminum and humates from river water by electrolytes, Geochim. Cosmochim. Acta, 40, 847–848, 10.1016/0016–7037(76)90036–3, 1976.

Egger, M., Rasigraf, O., Sapart, C. J., Jilbert, T., Jetten, M. S. M., Rockmann, T., van der Veen, C., Banda, N., Kartal, B., Ettwig, K. F. and Slomp, C. P.: Iron-mediated anaerobic oxidation of methane in brackish coastal sediments, Environ. Sci. Technol., 49, 277–283, 10.1021/es503663z, 2015a.

Egger, M., Jilbert, T., Behrends, T., Rivard, C. and Slomp, C. P.: Vivianite is a major sink for phosphorus in methanogenic coastal surface sediments, Geochim. Cosmochim. Acta, 169, 217–235, 10.1016/j.gca.2015.09.012, 2015b.

Egger, M., Kraal, P., Jilbert, T., Sulu–Gambari, F., Sapart, C. J., Rockmann, T. and Slomp, C. P.: Anaerobic oxidation of methane alters sediment records of sulfur, iron and phosphorus in the Black Sea, Biogeosciences, 13, 5333–5355, 10.5194/bg–13–5333–2016, 2016.

~~Egger, M., Rasigraf, O., Sapart, C. J., Jilbert, T., Jetten, M. S. M., Rockmann, T., van der Veen, C., Banda, N., Kartal, B., Ettwig, K. F. and Slomp, C. P.: Iron-mediated anaerobic oxidation of methane in brackish coastal sediments, Environ. Sci. Technol., 49, 277–283, 10.1021/es503663z, 2015.~~

Eusterhues, K., Wagner, F. E., Haeusler, W., Hanzlik, M., Knicker, H., Totsche, K. U., Koegel–Knabner, I. and Schwertmann, U.: Characterization of ferrihydrite-soil organic matter coprecipitates by X-ray Diffraction and Mössbauer spectroscopy, Environ. Sci. Technol., 42, 7891–7897, 10.1021/es800881w, 2008.

Forsgren, G., Jansson, M. and Nilsson, P.: Aggregation and sedimentation of iron, phosphorus and organic carbon in experimental mixtures of freshwater and estuarine water, Estuar. Coast. Shelf Sci., 43, 259–268, 10.1006/ecss.1996.0068, 1996.

Froelich, P. N., Klinkhammer, G. P., Bender, M. L., Luedtke, N. A., Heath, G. R., Cullen, D., Dauphin, P., Hammond, D., Hartman, B. and Maynard, V.: Early oxidation of organic matter in pelagic sediments of the eastern equatorial Atlantic: Suboxic diagenesis, Geochim. Cosmochim. Acta, 43, 1075–1090, 10.1016/0016-7037(79)90095-4, 1979.

Frančišković-Bilinski

, S., Bilinski, H., Tibljas, D. and Hanžel, D.: Estuarine sediments from the boreal region – an indication of weathering, Croat. Chem. Acta 76, 167–176, 2003.

Formatted: English (United States)

Formatted: English (United States)

~~Geyer, W.: The importance of suppression of turbulence by stratification on the estuarine turbidity maximum, Estuaries, 16, 113–125, 10.2307/1352769, 1993.~~

Goñi, M., Teixeira, M. and Perkey, D.: Sources and distribution of organic matter in a river-dominated estuary (Winyah Bay, SC, USA), Estuar. Coast. Shelf Sci., 57, 1023–1048, 10.1016/S0272–7714(03)00008–8, 2003.

Gustafsson, B. G., Schenk, F., Blenckner, T., Eilola, K., Meier, H. E. M., Müller-Karulis, B., Neumann, T., Ruoho-Airola, T., Savchuk, O. P., and Zorita, E.: Reconstructing the development of Baltic Sea eutrophication 1850–2006, Ambio, 41, 534–548, 10.1007/s13280-012-0318-x, 2012.

Gütlich, P., and Schröder, C.: Mössbauer Spectroscopy, in: Methods in Physical Chemistry, Schäfer, R. and Schmidt, P. C. (Eds), Wiley-VCH, Weinheim, Germany, pp. 351–389, 10.1002/9783527636839.ch11, 2012.

Hausen, H.: Ytgestaltningen i Åbolands–Ålands skärgård och dess orsaker, in: Skärgårdsboken, Nordenskiöld-samfundet i Finland, Helsinki, Finland, 30–73, 1948 (in Swedish).

Hedges, J., Mayorga, E., Tsamakis, E., McClain, M., Aufdenkampe, A., Quay, P., Richey, J., Benner, R., Opsahl, S., Black, B., Pimentel, T., Quintanilla, J. and Maurice, L.: Organic matter in Bolivian tributaries of the Amazon River: A comparison to the lower mainstream, Limnol. Oceanogr., 45, 1449–1466, 2000.

Hiemstra, T.: Surface and mineral structure of ferrihydrite, Geochim. Cosmochim. Acta, 105, 316–325, 10.1016/j.gca.2012.12.002, 2013.

Hietanen, S. and Kuparinen, J.: Seasonal and short-term variation in denitrification and anammox at a coastal station on the Gulf of Finland, Baltic Sea, Hydrobiologia, 596, 67–77, 0.1007/s10750-007-9058-5, 2008.

Holmkvist, L., Ferdelman, T. G. and Jørgensen, B. B.: A cryptic sulfur cycle driven by iron in the methane zone of marine sediment (Aarhus Bay, Denmark), Geochim. Cosmochim. Acta, 75, 3581−3599, 10.1016/j.gca.2011.03.033, 2011.

Ingri, J., and Conrad, S.: Distinct iron isotope signatures in suspended matter in the northern Baltic Sea; implications for cycling of organic carbon and phosphorus, EGU General Assembly, Vienna, Austria, 12–17 April 2015, EGU2015–11738, 2015.

James, F.: MINUIT Tutorial – Function Minimization, in: Proceedings of the 1972 CERN computing and data processing school, Pertisau, Austria, 10–24 September, 1972, CERN, Switzerland, 72–21, http://seal.web.cern.ch/seal/documents/minuit/mntutorial.pdf, 2004.

Jilbert, T. and Slomp, C. P.: Iron and manganese shuttles control the formation of authigenic phosphorus minerals in the euxinic basins of the Baltic Sea, Geochim. Cosmochim. Acta, 107, 155–169, 10.1016/j.gca.2013.01.005, 2013.

Kim, H.-J. Park, J.-H. and Vescovo, E.: Oxidation of the Fe(110) surface: An Fe_3O_4(111)/Fe(110) bilayer, Phys. Rev. B., 61, 2000.

Klingelhöfer, G., Morris, R. V., Bernhardt, B., Rodionov, D., de Souza Jr., P. A., Squyres, S. W., Foh, J., Kankeleit, E., Bonnes, U., Gellert, R., Schröder, C., Linkin, S., Evlanov, E., Zubkov, B., and Prilutski, O.: Athena MIMOS II Mössbauer spectrometer investigation. J. Geophys. Res., 108, E12, 8067, http://dx.doi.org/10.1029/2003JE002138, 2003.

Formatted: English (United States)

Formatted: Default Paragraph Font, Font: 12 pt

Formatted: English (United States)

Formatted: Subscript

Formatted: Subscript

Kortelainen, P., Mattsson, T., Finer, L., Ahtiainen, M., Saukkonen, S. and Sallantaus, T.: Controls on the export of C, N, P and Fe from undisturbed boreal catchments, Finland, Aquat. Sci., 68, 453–468, 10.1007/s00027–006–0833–6, 2006.

Kraal, P., Burton, E. D., Rose, A. L., Kocar, B. D., Lockhart, R. S., Grice, K., Bush, R. T., Tan, E. and Webb, S. M.: Sedimentary iron-phosphorus cycling under contrasting redox conditions in a eutrophic estuary, Chem. Geol., 392, 19–31, 10.1016/j.chemgeo.2014.11.006, 2015.

Krachler, R., Krachler, R. F., Wallner, G., Steier, P., El Abiead, Y., Wiesinger, H., Jirsa, F. and Keppler, B. K.: Sphagnum–dominated bog systems are highly effective yet variable sources of bio-available iron to marine waters, Sci. Total Environ., 556, 53–62, 10.1016/j.scitotenv.2016.03.012, 2016.

Kritzberg, E. S. and Ekstrom, S. M.: Increasing iron concentrations in surface waters – a factor behind brownification?, Biogeosciences, 9, 1465–1478, 10.5194/bg–9–1465–2012, 2012.

Kritzberg, E. S., Villanueva, A. B., Jung, M. and Reader, H. E.: Importance of boreal rivers in providing iron to marine waters, PLoS One, 9, e107500, 10.1371/journal.pone.0107500, 2014.

Lahermo, P., Väänänen, P., Tarvainen, T. and Salminen, R.: Geochemical Atlas of Finland Part 3: Environmental Geochemistry – stream waters and sediments, Geological Survey of Finland, Espoo, Finland, 1996.

Lalonde, K., Mucci, A., Ouellet, A. and Gélinas, Y.: Preservation of organic matter in sediments promoted by iron, Nature, 483, 198–200, 10.1038/nature10855, 2012.

Lenz, C., Jilbert, T., Conley, D. J. and Slomp, C. P.: Hypoxia-driven variations in iron and manganese shuttling in the Baltic Sea over the past 8 kyr, Geochem. Geophys. Geosyst., 16, 3754–3766, 10.1002/2015GC005960, 2015.

Leppäranta, M., and Myrberg, K.: Physical Oceanography of the Baltic Sea, Springer-Praxis, Heidelberg, Germany, 2009.

Li, C., Yang, S., Lian, E., Wang, Q., Fan, D. and Huang, X.: Chemical speciation of iron in sediments from the Changjiang Estuary and East China Sea: Iron cycle and paleoenvironmental implications, Quatern. Int., 452, 116–128, http://dx.doi.org/10.1016/j.quaint.2016.07.014, ~~in press.~~2017.

~~Lisitsyn, A. P.: The marginal filter of the ocean, Oceanology 34, 671–68, 1995.~~

Lovley, D., Holmes, D. and Nevin, K.: Dissimilatory Fe(III) and Mn(IV) reduction, Advances in Microbial Physiology, 49, 219–286, 10.1016/S0065–2911(04)49005–5, 2004.

Manning, P. G. and & Ash, L.A.: Mössbauer spectral studies of Lake Erie sediments, Can. Mineral. 16, 577–580, 1978.

Manning, P. G., Jones, W. and Birchall, T.: Mössbauer spectral studies of iron-enriched sediments from Hamilton Harbor, Ontario, Can. Mineral. 18, 291–299, 1980.

Mattsson, T., Kortelainen, P. and Räike, A.: Export of DOM from boreal catchments: Impacts of land use cover and climate, Biogeochemistry, 76, 10.1007/s10533-005-6897-x, 373–394.

~~Lyons, T. W. and Severmann, S.: A critical look at iron paleoredox proxies: New insights from modern euxinic marine basins, Geochim. Cosmochim. Acta, 70, 5698–5722, 10.1016/j.gca.2006.08.021, 2006.~~

Monteith, D. T., Stoddard, J. L., Evans, C. D., de Wit, H. A., Forsius, M., Hogasen, T., Wilander, A., Skjelkvale, B. L., Jeffries, D. S., Vuorenmaa, J., Keller, B., Kopacek, J. and Vesely, J.: Dissolved organic carbon trends resulting from changes in atmospheric deposition chemistry, Nature, 450, 537-U9, 10.1038/nature06316, 2007.

Moran, M., Sheldon, W. and Zepp, R.: Carbon loss and optical property changes during long–term photochemical and biological degradation of estuarine dissolved organic matter, Limnol. Oceanogr., 45, 1254–1264, 2000.

Morris, R. V., Ruff, S. W., Gellert, R., Ming, D. W., Arvidson, R. E., Clark, B. C., Golden, D. C., Siebach, K., Klingelhöfer, G., Schröder, C., Fleischer, I., Yen, A., and Squyres, S. W.: Identification of carbonate-rich outcrops on Mars by the Spirit Rover, Science, 329, 421–-424, 10.1126/science.1189667, 2010.

Murad, E. and Cashion, J.: Mössbauer spectroscopy of environmental materials and their industrial utilization, Springer, New York, U.S.A., 10.1007/978-1-4419-9040, 2004.

Neubauer, E., Kohler, S. J., von der Kammer, F., Laudon, H. and Hofmann, T.: Effect of pH and stream order on iron and arsenic speciation in boreal catchments, Environ. Sci. Technol., 47, 7120–7128, 10.1021/es401193j, 2013.

Niemi, Å.: Hydrography and oxygen fluctuations in Pojoviken, southern coast of Finland, 1972–1975. Meri 4, 23–35, 1977.

Norkko, J., Reed, D. C., Timmermann, K., Norkko, A., Gustafsson, B. G., Bonsdorff, E., Slomp, C. P., Carstensen, J. and Conley, D. J.: A welcome can of worms? Hypoxia mitigation by an invasive species, Global Change Biol., 18, 422–434, 10.1111/j.1365–2486.2011.02513.x, 2012.

Omstedt, A., Edman, M., Anderson, L. and Laudon, H.: Factors influencing the acid–base (pH) balance in the Baltic Sea: a sensitivity analysis, Tellus B, 62, 280–295, 10.1111/j.1600-0889.2010.00463.x, 2010.

~~Officer, C. B.: Physical oceanography of estuaries, Wiley, New York, U.S.A., 1976.~~

O'Sullivan, T. D., and Smith, N.O.: The solubility and partial molar volume of nitrogen and methane in water and in aqueous sodium chloride from 50 to 125'C and 100 to 600 atm, J. Phys. Chem., 74, 1460–1466, 1970.

Peltola, P., Virtasalo, J. J., Oberg, T. and Astrom, M.: Geochemistry of surface sediments in the Archipelago Sea, SW Finland: a multiparameter and multivariate study, Environ. Earth Sci., 62, 725–734, 10.1007/s12665–010–0561–z, 2011.

Poulton, S. and Canfield, D.: Development of a sequential extraction procedure for iron: implications for iron partitioning in continentally derived particulates, Chem. Geol., 214, 209–221, 10.1016/j.chemgeo.2004.09.003, 2005.

Poulton, S. and Raiswell, R.: The low-temperature geochemical cycle of iron: From continental fluxes to marine sediment deposition, Am. J. Sci., 302, 774–805, 10.2475/ajs.302.9.774, 2002.

Raiswell, R.: Iron transport from the continents to the open ocean: The aging–rejuvenation cycle, Elements, 7, 101–106, 10.2113/gselements.7.2.101, 2011.

Raiswell, R. and Anderson, T.: Reactive iron enrichment in sediments deposited beneath euxinic bottom waters: constraints on supply by shelf recycling, Geol. Soc. Spec. Publ., 248, 179–194, 10.1144/GSL.SP.2005.248.01.10, 2005.

Raiswell, R. and Canfield, D. E.: The iron biogeochemical cycle past and present, Geochem. Perspect. 1, 10.7185/geochempersp.1.1, 2012.

Rancourt, D. G. and Ping, J. Y.: Voigt-based methods for arbitrary-shape static hyperfine parameter distributions in Mössbauer spectroscopy, Nucl. Instrum. Meth. Phys. Res. B58, 85–97, 1991.

~~Raiswell, R.: Iron transport from the continents to the open ocean: The aging–rejuvenation cycle, Elements, 7, 101–106, 10.2113/gselements.7.2.101, 2011.~~

Reed, D. C., Slomp, C. P. and Gustafsson, B. G.: Sedimentary phosphorus dynamics and the evolution of bottom–water hypoxia: A coupled benthic-pelagic model of a coastal system, Limnol. Oceanogr., 56, 1075–1092, 10.4319/lo.2011.56.3.1075, 2011.

Reese, B. K., Finneran, D. W., Mills, H. J., Zhu, M. and Morse, J. W.: Examination and refinement of the determination of aqueous hydrogen sulfide by the methylene blue method, Aquat. Geochem., 17, 567–582, 10.1007/s10498–011–9128–1, 2011.

Renberg, I., Bindler, R. and Brannvall, M. L.: Using the historical atmospheric lead–deposition record as a chronological marker in sediment deposits in Europe, Holocene, 11, 511–516, 2001.

Robertson, E. K., Roberts, K. L., Burdorf, L. D. W., Cook, P., and Thamdrup, B.: Dissimilatory nitrate reduction to ammonium coupled to Fe (II) oxidation in sediments of a periodically hypoxic estuary. Limnol. Oceanogr. 61, 365–381, 2016.

Rooze, J., Egger, M., Tsandev, I. and Slomp, C. P.: Iron-dependent anaerobic oxidation of methane in coastal surface sediments: Potential controls and impact, Limnol. Oceanogr., 61, S267–S282, 10.1002/lno.10275, 2016.

Sawicka, J. E. and Brüchert, V.: Annual variability and regulation of methane and sulfate fluxes in Baltic Sea estuarine sediments, Biogeosciences, 14, 325–339, 0.5194/bg-14-325-2017, 2017.

Schulz, H. and Zabel, M. (Eds.): Marine geochemistry, Springer-Verlag, Berlin-Heidelberg, Germany, 2009. 10.1007/3-540-32144-6.

~~Sanford, L., Suttles, S. and Halka, J.: Reconsidering the physics of the Chesapeake Bay estuarine turbidity maximum, Estuaries, 24, 655–669, 10.2307/1352874, 2001.~~

~~Sarkkola, S., Nieminen, M., Koivusalo, H., Lauren, A., Kortelainen, P., Mattsson, T., Palviainen, M., Piirainen, S., Starr, M. and Finer, L.: Iron concentrations are increasing in surface waters from forested headwater catchments in eastern Finland, Sci. Total Environ., 463, 683–689, 10.1016/j.scitotenv.2013.06.072, 2013.~~

Schwertmann, U. and Taylor, R.M., Iron oxides, in: Minerals in Soil Environments, Dixon, J. B., Weed, S. B., Kittrick, J. A., Milford, M. H. and White, J. L. (Eds), Soil Science Society of America, Madison, Wisconsin, U.S.A., 145–180, 1977.

Schwertmann, U., Stanjek, H. and Becher, H.: Long–term in vitro transformation of 2-line ferrihydrite to goethite/hematite at 4, 10, 15 and 25 degrees C, Clay Miner., 39, 433–438, 10.1180/0009855043940145, 2004.

Shields, M. R., Bianchi, T. S., Gelinas, Y., Allison, M. A. and Twilley, R. R.: Enhanced terrestrial carbon preservation promoted by reactive iron in deltaic sediments, Geophys. Res. Lett., 43, 1149–1157, 10.1002/2015GL067388, 2016.

Sholkovitz, E., Boyle, E. and Price, N.: Removal of dissolved humic acids and iron during estuarine mixing, Earth Planet. Sci. Lett., 40, 130–136, 10.1016/0012–821X(78)90082–1, 1978.

Sivan, O., Adler, M., Pearson, A., Gelman, F., Bar–Or, I., John, S. G. and Eckert, W.: Geochemical evidence for iron–mediated anaerobic oxidation of methane, Limnol. Oceanogr., 56, 1536–1544, 10.4319/lo.2011.56.4.1536, 2011.

Slomp, C. P., Mort, H. P., Jilbert, T., Reed, D. C., Gustafsson, B. G. and Wolthers, M.: Coupled dynamics of iron and phosphorus in sediments of an oligotrophic coastal basin and the impact of anaerobic oxidation of methane, PLoS ONE, 8, e62386, 10.1371/journal.pone.0062386, 2013.

Slomp, C. P., Epping, E. H. G., Helder, W. and Van Raaphorst, W.: A key role for iron-bound phosphorus in authigenic apatite formation in North Atlantic continental platform sediments, J. Mar. Res., 54, 1179–1205, 1996.

Slomp, C., Van der Gaast, S. and Van Raaphorst, W.: Phosphorus binding by poorly crystalline iron oxides in North Sea sediments, Mar. Chem., 52, 55–73, 10.1016/0304–4203(95)00078–X, 1996.

Stevens, J. G., Khasanov, A. M., Niller, J. W., Pollak, H., and Li, Z.: Mössbauer Mineral Handbook, Mössbauer Effect Data Center, 2002.

Stolpe, B. and Hassellov, M.: Changes in size distribution of fresh water nanoscale colloidal matter and associated elements on mixing with seawater, Geochim. Cosmochim. Acta, 71, 3292–3301, 10.1016/j.gca.2007.04.025, 2007.

Sundman, A., Karlsson, T., Laudon, H. and Persson, P.: XAS study of iron speciation in soils and waters from a boreal catchment, Chem. Geol., 364, 93–102, 10.1016/j.chemgeo.2013.11.023, 2014.

Syvitski, J. and Murray, J.: Particle ~~Interaction~~ interaction in fjord suspended sediment, Mar. Geol., 39, 215–242, 10.1016/0025–3227(81)90073–6, 1981.

Uher, G., Hughes, C., Henry, G. and Upstill–Goddard, R.: Non–conservative mixing behavior of colored dissolved organic matter in a humic-rich, turbid estuary, Geophys. Res. Lett., 28, 3309–3312, 10.1029/2000GL012509, 2001.

van der Zee, C., Roberts, D. R., Rancourt, D. G. and Slomp, C. P.: Nanogoethite is the dominant reactive oxyhydroxide phase in lake and marine sediments, Geology, 31, 993–996, 10.1130/G19924.1, 2003.

Virta, J.: Estimating the water and salt budgets of a stratified estuary, Nord. Hydrol., 8, 11–32, 1977.

Virtasalo, J. J., and Kotilainen, A. T.: Phosphorus forms and reactive iron in late glacial, postglacial and brackish-water sediments of the Archipelago Sea, northern Baltic Sea. Mar. Geol., 252, 1–12, 2008.

Virtasalo, J., Kohonen, T., Vuorinen, I. and Huttula, T.: Sea bottom anoxia in the Archipelago Sea, northern Baltic Sea – Implications for phosphorus remineralization at the sediment surface, Mar. Geol., 224, 103–122, 10.1016/j.margeo.2005.07.010, 2005.

Virtasalo, J. J., Kotilainen, A. T., Räsänen, M. E., and Ojala, A. E. K.: Late-glacial and post–glacial deposition in a large, low relief, epicontinental basin: the northern Baltic Sea, Sedimentology, 54, 1323–1344, 2007.

~~Voipio, A.: The Baltic Sea, Elsevier, Amsterdam, The Netherlands, 1981.~~

Winterhalter, B., Flodén, T., Ignatius, H., Axberg, S., and Niemistö, L.: Geology of the Baltic Sea, in: The Baltic Sea, Voipio, A. (Ed), Elsevier, Amsterdam, The Netherlands, 1981.

Yu, C., Virtasalo, J. J., Karlsson, T., Peltola, P., Osterholm, P., Burton, E. D., Arppe, L., Hogmalm, J. K., Ojala, A. E. K. and ~~Astrom~~Åstrom, M. E.: Iron behavior in a northern estuary: Large pools of non-sulfidized Fe(II) associated with organic matter, Chem. Geol., 413, 73–85, 10.1016/j.chemgeo.2015.08.013, 2015.

Zillen, L., Lenz, C. and Jilbert, T.: Stable lead (Pb) isotopes and concentrations – A useful independent dating tool for Baltic Sea sediments, Quat. Geochronol., 8, 41–45, 10.1016/j.quageo.2011.11.001, 2012.

~~Tables~~Tables

Tables

Formatted: English (United Kingdom)

Formatted: Heading 1

Campaign and ~~Station~~Station code	Co-ordinates (degree-decimal) °N	°E	Water depth (m, sediment ~~station~~Stations only)	Water sampling	Sediment sampling
Mustionjoki ~~transect~~ September 2014; June 2015					
A	60.091617	23.554630	7	Full profile (2015)	4 samples (2014) Full profile (2015)
B	60.079833	23.531167	11	Full profile (2015)	5 samples (2014)
C	60.054300	23.509517	22	Full profile (2015)	5 samples (2014)
D	60.022650	23.474600	39	Full profile (2015)	5 samples (2014) Full profile (2015)
E	60.014033	23.467950	21	Full profile (2015)	5 samples (2014)
F	59.994750	23.452300	8	Full profile (2015)	5 samples (2014)
G	59.961383	23.396730	6	Full profile (2015)	5 samples (2014)
H	59.920117	23.332650	17	Full profile (2015)	5 samples (2014)
I	59.907367	23.326200	21	Full profile (2015)	5 samples (2014)
J	59.855286	23.261780	33	Full profile (2015)	5 samples (2014) Full profile (2015)
K	59.789867	23.335430	47	Full profile (2015)	5 samples (2014)
Paimionjoki ~~transect~~ August-September 2001					
L	60.354667	22.563000	18		Surface (0–2 cm)
M	60.313333	22.509833	46		Surface (0–2 cm)
N	60.140970	22.410722	27		Surface (0–2 cm)
O	60.057288	22.355018	46		Surface (0–2 cm)
P	59.913438	21.753072	35		Surface (0–2 cm)
Q	59.764387	21.706720	107		Surface (0–2 cm)
Mustionjoki ~~transect~~ April-August-October 2011 (water); September 2015 (sediments)					
a	60.095467	23.590867		Surface only	Surface (0–2 cm)
b	60.036650	23.484183		Surface only	

Formatted: Font: Italic

Formatted: Font: Italic

Formatted: Font: Italic

c	59.977800	23.421300	Surface only
d	59.917300	23.324433	Surface only
e	59.855567	23.261967	Surface only
~~F~~f	59.816317	23.271450	Surface only

Table 1. Sampling campaigns and ~~station~~stations (see also Fig. 1).

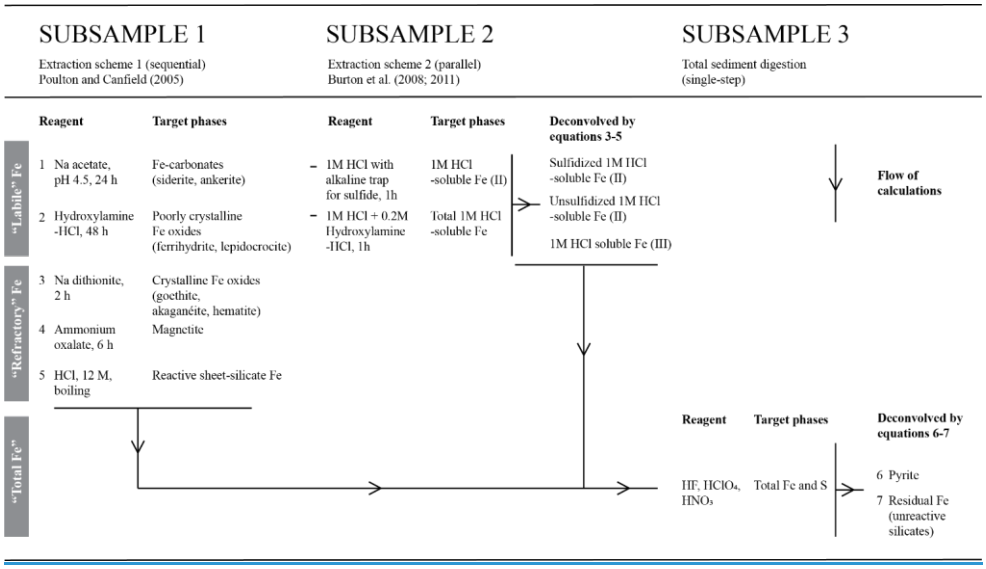

~~Extraction stage~~	~~Reagent~~	~~Nominal target phases (original protocol)~~	~~Interpreted phases (this study)~~
~~1~~	~~Na acetate, pH 4.5, 24 h~~	~~Fe-carbonates (siderite, ankerite)~~	~~Ferrihydrite~~
~~2~~	~~Hydroxylamine-HCl, 48 h~~	~~Poorly crystalline Fe oxides (ferrihydrite, lepidocrocite)~~	~~Ferrihydrite~~

3	Na dithionite, 2 h	Crystalline Fe oxides (goethite, akaganéite, hematite)	Organic Fe (II) complexes
4	Ammonium oxalate, 6 h	Magnetite	Organic Fe (II) complexes, magnetite
5	HCl, 12 M, boiling	Reactive sheet-silicate Fe	Reactive sheet-silicate Fe
6 (sulfide-Fe)	Total digestion + ICP-OES analysis for S		Pyrite
Total Fe	Total digestion + ICP-OES analysis for Fe		All Fe phases in sample
7 Residual Fe	Calculated (Total Fe − Σ[1-6])	Unreactive silicate Fe	Unreactive silicate Fe

Table 2. Stages of the Protocol for sediment Fe sequential extractions employed in for Fe used in this study, . based on the protocol of Poulton and Canfield (2005). The results of the extractions are combined according to equations 3–7 (see text).

	Solubility in Poulton and Canfield (2005) extraction	Solubility in 1M HCl extraction	Allocation in Mössbauer subspectra	Presence in samples of this study
Labile Fe (II) phases				
Fe carbonates (siderite, ankerite)	Stage 1	Yes	Not detected	Unlikely
Acid-Volatile Sulfur (FeS)	Stage 1-2 (inferred)	Yes	Not resolvable	Likely
Labile Fe (II)-OM	Stage 1-2 (inferred)	Yes	Not resolvable	Likely
Fe (II) phosphates	Stage 2 (inferred)	Yes	Not resolvable	Likely
Labile Fe (III) phases				
Poorly crystalline Fe oxides (ferrihydrite, lepidocrocite)	Stage 2	Yes	SP Fe (III)	Likely
Labile Fe (III)-OM	Stage 1-2 (inferred)	Yes	SP Fe (III)	Likely
Refractory Fe (II) and Fe (III) phases				
Goethite (< 14 nm)	Stage 3 (-4 inferred)	No	SP Fe (III)	Likely
Goethite (> 14 nm)	Stage 3 (-4 inferred)	No	Not detected	Unlikely
Hematite	Stage 3	No	Hematite	Likely
Akaganéite	Stage 3	No	Not detected	Unlikely
Amorphous ferric aluminosilicates	Stage 3-4 (inferred)	No	SP Fe (III)	Likely
Wüstite	Stage 3 (inferred)	No	Wüstite	Likely
Magnetite	Stage 4	No	Magnetite ($Fe^{2.5+}$) Magnetite (Fe^{3+})	Likely
Reactive sheet silicate Fe (II)	Stage 5	No	Silicate Fe (II)	Likely
Pyrite	No	No	Not resolvable	Likely
Residual unreactive silicate Fe (II)	No	No	Silicate Fe (II)	Likely

Table 3. Scheme for the interpretation of sedimentary Fe phases based on the extraction protocols and Mössbauer data. Solubilities in the Poulton and Canfield (2005) extraction listed as *inferred* indicate that these were not defined in the original protocol, but have either been investigated by later studies or are assumed for reasons described in the text. SP Fe (III) = superparamagnetic Fe (III).

Mineral Phase	δ[a] (mm/s)	Δ_{EQ}[b] (mm/s)	B_{hf}[c] (T)	Area[d] (%)	Fe(III)/Fe(II)
River bed sediment (Station 'a')					
SP Fe^{3+}	0.34	0.69	-	56	1.27
Silicate Fe^{2+}	1.15	2.57	-	44	
~~Station~~Station A 0–1 cm					
SP Fe^{3+}	0.32	0.67	-	26	[f]
Silicate Fe^{2+}	1.08	2.61	-	18	
Wüstite ~~Magnetite $Fe^{2.5+}$~~	0.78~~[0.67][e]~~	0.83~~[0.00]~~	-~~[46.5]~~	42~~9~~	
Magnetite $Fe^{2.5+}$ ~~Magnetite Fe^{3+}~~	[0.67][e]~~[0.30]~~	[0.00]~~[0.03]~~	[46.5]~~[49.8]~~	9~~5~~	
Magnetite Fe^{3+} ~~Silicate Fe^{2+}~~	[0.30]~~1.08~~	[0.03]~~2.61~~	[49.8]~~-~~	5~~18~~	
~~Undocumented Fe^{2+} ("organic Fe (II)")~~	~~0.78~~	~~0.83~~	~~-~~	~~42~~	
Station A 26–28 cm					
SP Fe^{3+}	0.40	0.73	-	8	[f]
Silicate Fe^{2+}	1.12	2.65	-	15	
Wüstite	0.94	0.76	-	42	
Magnetite $Fe^{2.5+}$	0.66	-0.01	45.5	16	
Magnetite Fe^{3+}	0.26	-0.01	48.6	9	
Hematite	0.35	-0.08	-	10	
Station D 0–1 cm					
SP Fe^{3+}	0.25	0.86	-	51	1.04
Silicate Fe^{2+}	1.19	2.48	-	49	
Station D 26–28 cm ~~*Superparamagn. FeOx Fe^{3+} ("ferrihydrite") 0.32 0.67 – 26*~~					
SP Fe^{3+}	0.36	0.73	-	62	1.63
Silicate Fe^{2+}	1.13	2.58	-	38	
Station J 0–1 cm					
SP Fe^{3+}	0.35	0.75	-	49	1.17
Silicate Fe^{2+}	1.15	2.56	-	46	
Unspecified Fe (III) oxide	0.30	-0.04	50.3	5	

Station J 30–32 cm					
SP Fe^{3+}	0.34	0.69	-	53	1.13
Silicate Fe^{2+}	1.14	2.57	-	47	
Station D					
Silicate Fe^{2+}	1.19	2.48	-	49	
Superparamagn. FeOx Fe^{3+} ("ferrihydrite")	0.25	0.86	-	51	

[a]Isomer or center shift.

[b]Quadrupole splitting. For 6-line spectra (magnetite, hematite and unassigned Fe oxide), values represent quadrupole shift <ε> (same units).

[c]Internal magnetic field.

[d]Subspectral area ratio, to first order proportional to relative amount of total Fe contained in mineral phase. A general uncertainty of ±2% absolute is applied.

[e]Values in square brackets were fixed to values from library spectra during the fitting process.

[f]Values for Fe (III):Fe(II) are only given for those samples unaffected by industrial pollution (see text).

Table 34. Mössbauer parameters corresponding to spectra in Fig. 57 and Supplementary Fig. 2.

Formatted: Font: (Default) +Body (Times New Roman)
Formatted: Font: (Default) +Body (Times New Roman), 10 pt
Formatted: Font: 10 pt
Formatted: Font: (Default) +Body (Times New Roman)
Formatted: Font: (Default) +Body (Times New Roman), 10 pt
Formatted: Font: (Default) +Body (Times New Roman)
Formatted: Font: (Default) +Body (Times New Roman), 10 pt
Formatted: Font: (Default) +Body (Times New Roman)
Formatted: Font: (Default) +Body (Times New Roman), 10 pt
Formatted: Font: (Default) +Body (Times New Roman), 10 pt
Formatted: Font: (Default) +Body (Times New Roman)
Formatted: Font: (Default) +Body (Times New Roman), 10 pt
Formatted: Font: 10 pt
Formatted: Font: (Default) +Body (Times New Roman)
Formatted: Font: (Default) +Body (Times New Roman), 10 pt
Formatted: Font: (Default) +Body (Times New Roman)
Formatted ...
Formatted: Font: (Default) +Body (Times New Roman)
Formatted ...
Formatted ...
Formatted: Font: (Default) +Body (Times New Roman)
Formatted ...
Formatted: Font: 10 pt
Formatted ...
Formatted: Font: 10 pt
Formatted: Font: 10 pt
Formatted: Font: (Default) +Body (Times New Roman)
Formatted: Font: 10 pt
Formatted: Font: (Default) +Body (Times New Roman)
Formatted: Font: (Default) +Body (Times New Roman)
Formatted: Font: 10 pt
Formatted: Font: (Default) +Body (Times New Roman)
Formatted: Font: 10 pt
Formatted: Superscript

Figures

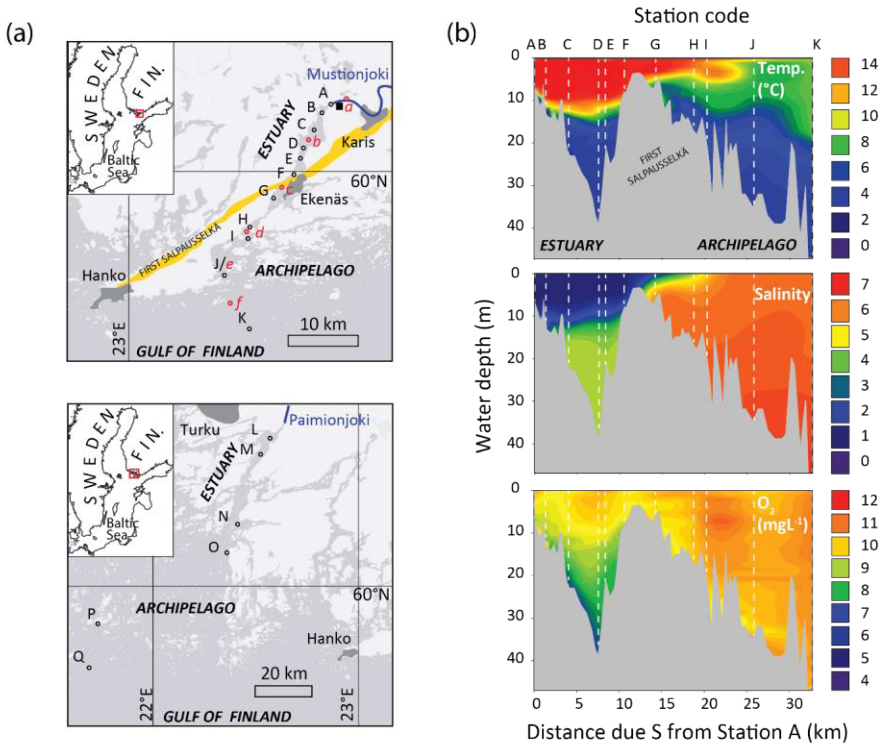

Figure 1. (a) Location of the Mustionjoki estuary transect (top) and the Paimionjoki estuary transect (bottom). In both systems, point-source river inputs discharge into a channel-like estuary, which in turn connects into the archipelago coastline of the Gulf of Finland, northern Baltic Sea. Sediment and water column sampling locations are indicated A–Q (of which L–Q were first reported in Virtasalo et al., 2005). Dissolved organic matter (DOM) sampling locations (Asmala et al., 2014, 2016) are indicated *a-f*. The location of the Åminnefors blast furnace is indicated by the black square. The First Salpausselkä ice-marginal formation is indicated in yellow. (b) Water column characteristics of the Mustionjoki transect during sampling in June 2015. 2D contour plots were generated by extrapolation between the

measured profiles at ~~station~~Stations A–K using Sigmaplot™ software. Distances along transect are reported as distance directly due S from ~~Station~~Station A at the Mustionjoki river mouth.

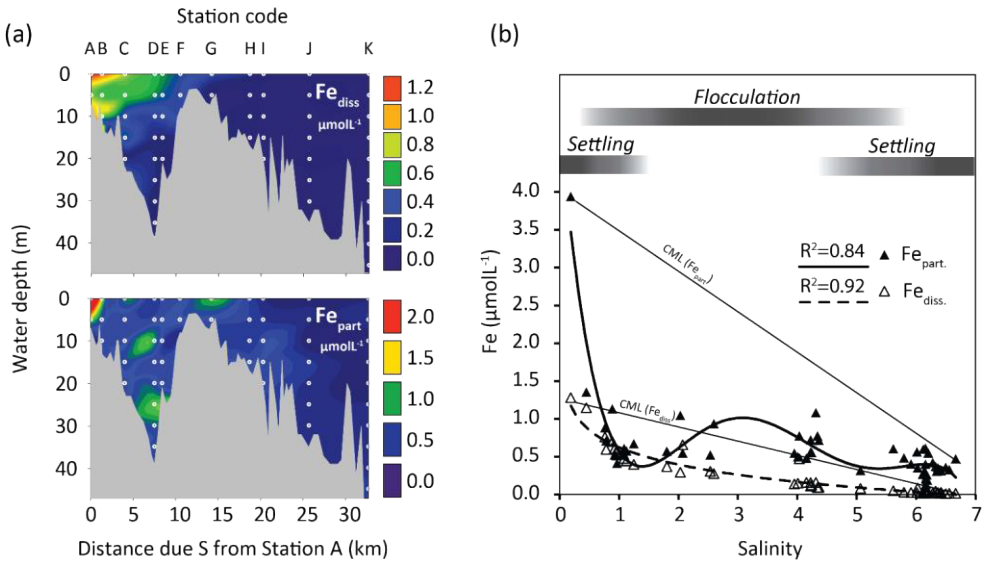

Figure 2. (a) 2D contour plots of dissolved (top) and particulate (bottom) Fe in the water column along the Mustionjoki transect (~~Station~~Stations A–K), operationally defined by filtration at 0.45 µm, June 2015. White circles represent sampling positions (vertical depth resolution = 5m). (b) Data from *a* plotted against salinity, including trendlines for $Fe_{part.}$ (polynomial) and $Fe_{diss.}$ (logarithmic). Linear Conservative Mixing Lines (CML) are drawn between the high- and low- salinity end-member samples for Fe_{part} and Fe_{diss}. The inferred dominant processes controlling Fe_{part} along the salinity transect are indicated by the grey bars.

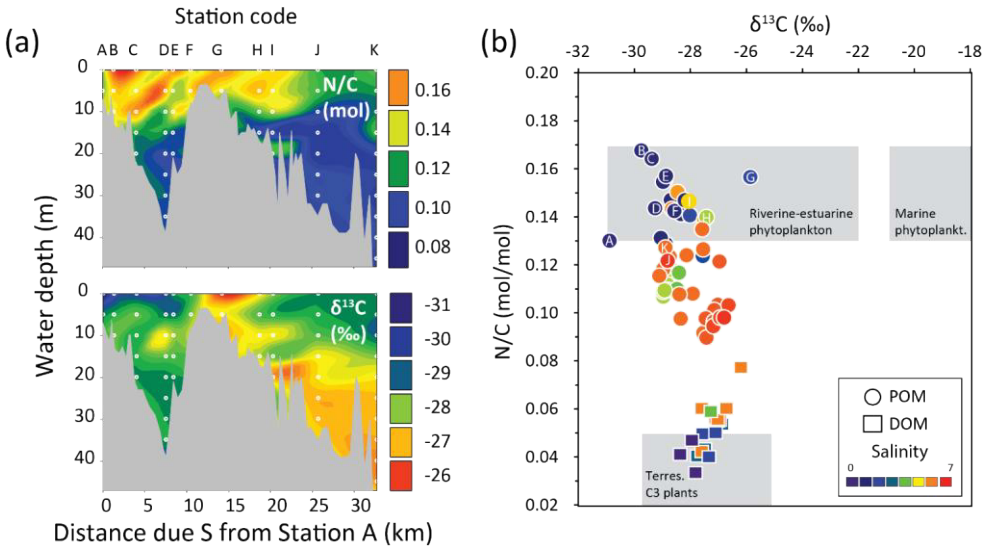

Figure 3. (a) 2D contour plots of molar N/C (top) and $\delta^{13}C$ (bottom) of particulate organic matter (POM) along the Mustionjoki transect, operationally defined by filtration at 0.45 µm, June 2015. White circles represent sampling positions (vertical depth resolution = 5m). (b) Cross plot of molar N/C vs. $\delta^{13}C$ of POM in June 2015 (circles, each representing a single sample from the 2D plot in *a*) and of published data for dissolved organic matter (DOM) from the same transect (squares, surface water only, 6 samples each from campaigns in April, August and October 2011). In-situ salinity at the time and location of sampling is indicated by the color scale. Samples marked with letters indicate surface water samples. Organic matter source fields are taken from Goñi et al. (2003).

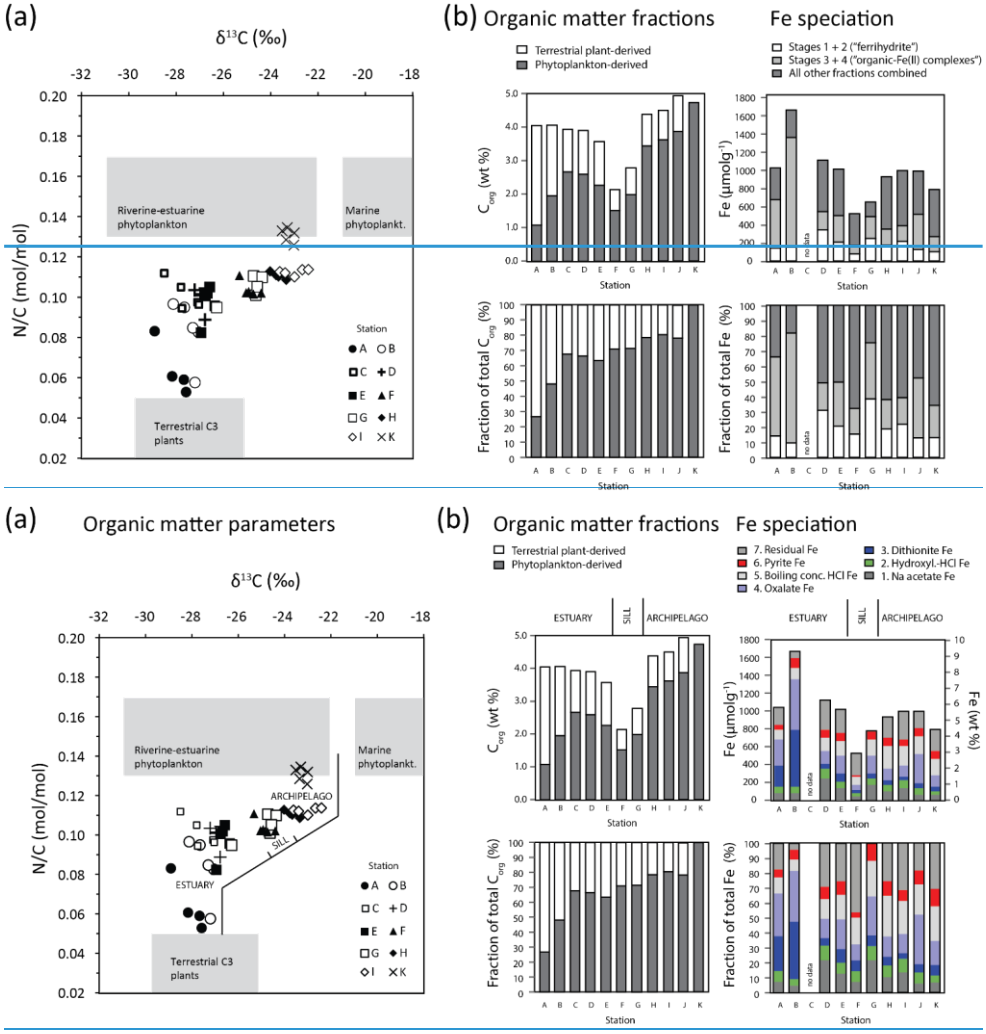

Figure 4. (a) Cross plot of molar N/C vs. $\delta^{13}C$ of sedimentary organic matter along the Mustionjoki transect. ~~Station~~Stations are indicated by the symbols. No isotope data was available for ~~station~~Station J. Four or five samples

are plotted for each ~~station~~Station, representing evenly spaced 2 cm thick slices throughout a GEMAX™ core of 30–60 cm length (e.g. ~~Station~~Station K: 0–2 cm; 8.5–10.5 cm, 17–19 cm, 25.5–27.5 cm, 34–36 cm). (b) Organic matter fractions of the same sediment samples, derived from molar N/C ratios, assuming end-member values of N/C = 0.04 (terrestrial-derived) and 0.13 (phytoplankton-derived). Mean values are reported of the 4 or 5 samples from each core; Operational Fe speciation of surface-sediment samples (0–2 cm)~~, derived from sequential extraction by the method of Poulton and Canfield (2005) and an additional extraction for sulfide-bound Fe~~. No extraction data was available for ~~station~~Station C.

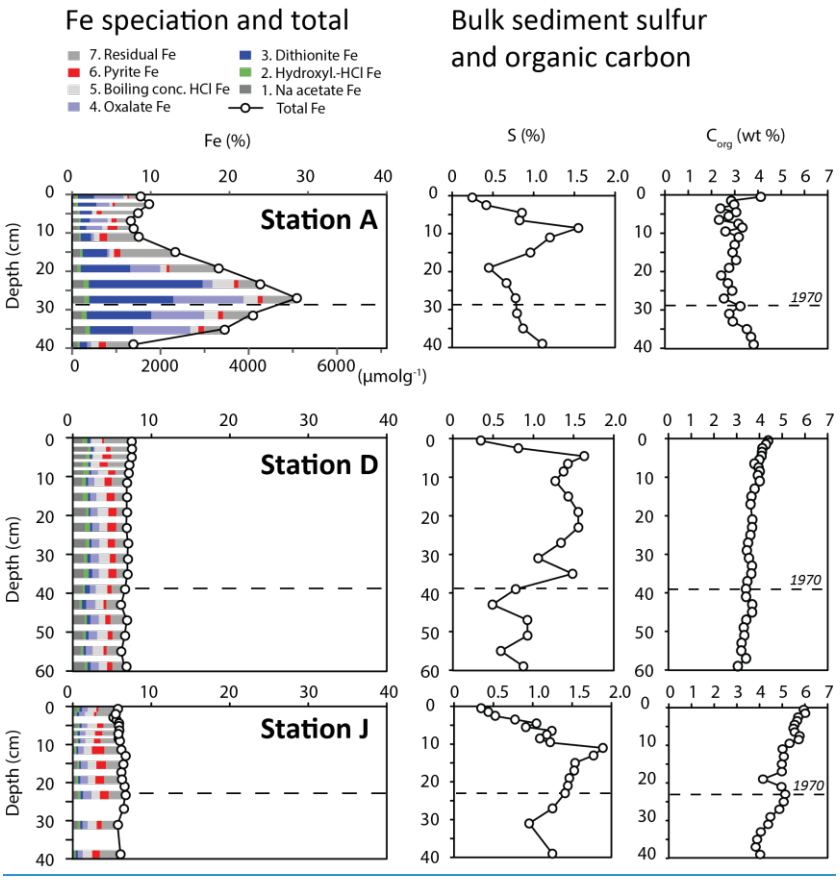

Formatted: Centered

Figure 5. (left) Down-core operational Fe speciation and total sedimentary Fe content for Stations A, D, and J. Thickness of bars corresponds to thickness of sampled interval (i.e. 1 or 2 cm). Note that not all depth intervals were sampled. (right) Bulk chemical profiles from the same cores. The depth interval corresponding to 1970 is estimated from the peak in concentrations of total lead (Pb_{tot}) (see Supplementary Fig. 1).

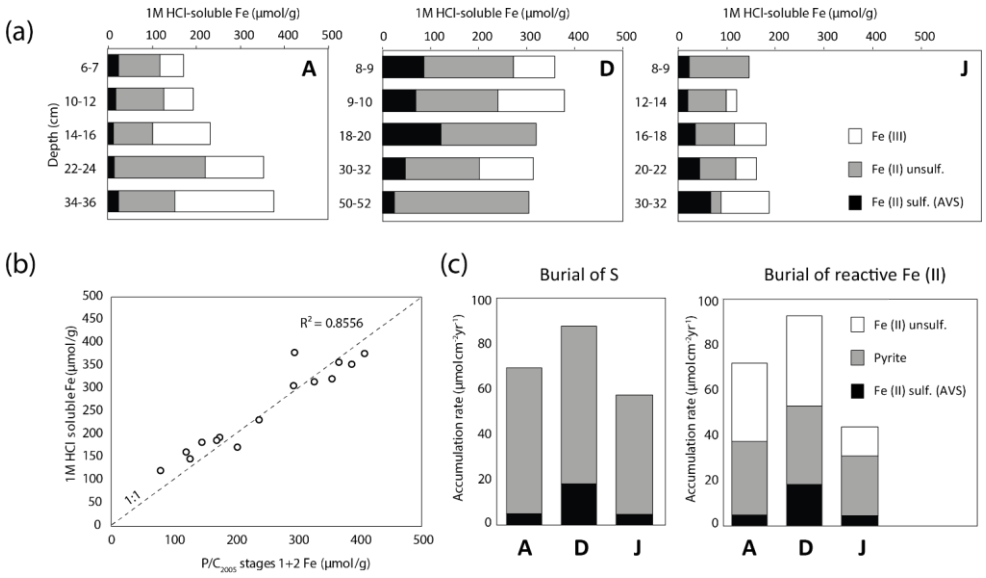

Figure 6. (a) Results of the 1M HCl extraction, carried out on 15 samples (5 each from Stations A, D, J). (b) Comparison of total 1M HCl-soluble Fe and the sum of Stages 1+2-soluble Fe in the Poulton and Canfield (2005) protocol. Where no equivalent sample was available, adjacent samples have been compared (n =4). Dashed line represents 1:1 and the least-squares regression is performed against this line. (c) Depth-integrated rates of burial of S and reactive Fe (II) over the period 1970–2015 at Stations A, D and J.

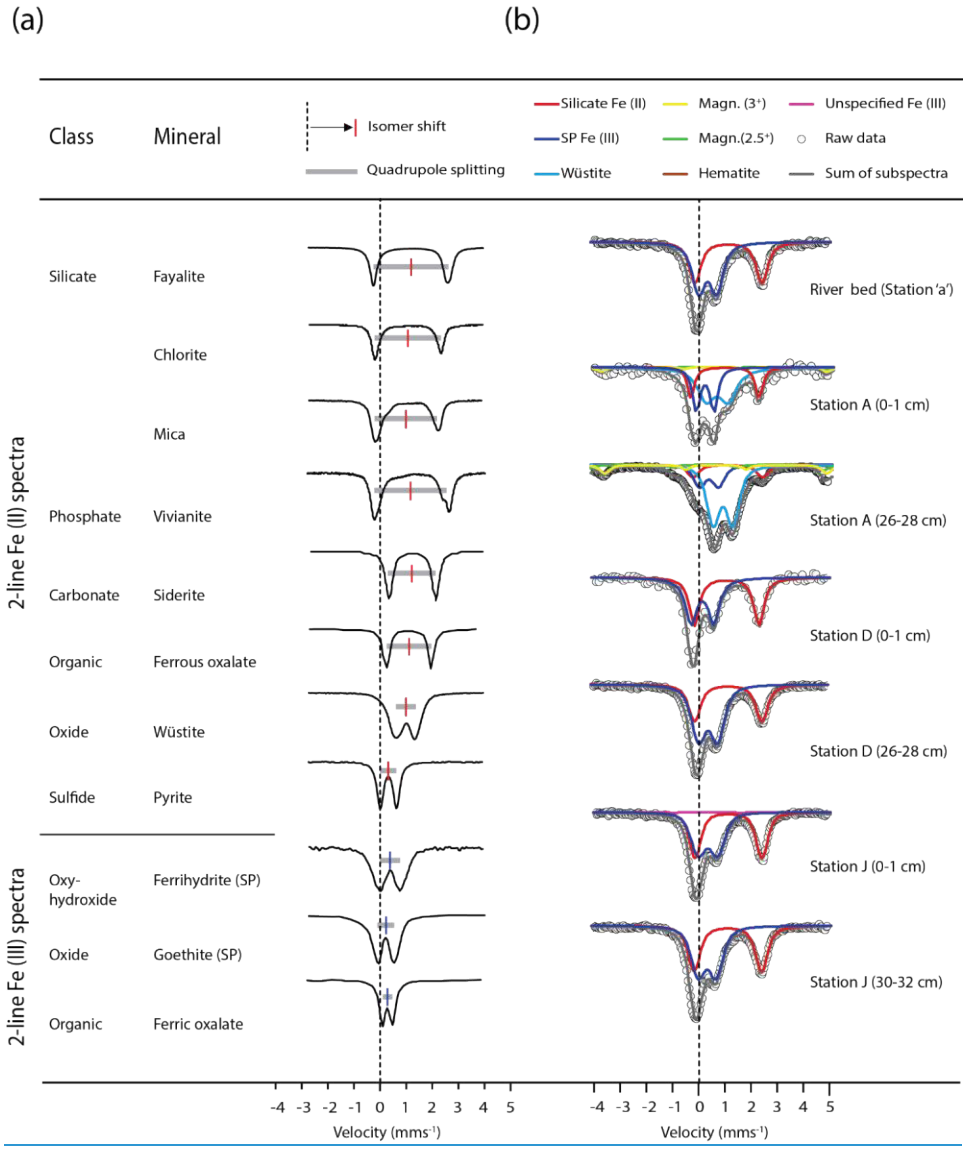

Formatted: Centered

Figure 7. (a) Room temperature (RT) 2-line Mössbauer ^{57}Fe reference spectra from various sources. Spectra have been trimmed and normalized for visual intercomparison. The arbitrary y-axis indicates the intensity of gamma-ray transmission, hence troughs correspond to absorption maxima. Spectra for fayalite, chlorite, mica, vivianite, siderite, wüstite, pyrite and ferrihydrite are reproduced by permission of M. Darby Dyer from the Mineral Spectroscopy Database of Mount Holyoke College. These spectra are previously unpublished with the exception of fayalite (Belley et al., 2009) and vivianite (Dyar et al., 2014). A plot digitization software was used to extract Fe (II) and Fe (III) oxalate spectra from D'Antonio et al. (2009), and a superparamagnetic goethite (goethite SP) spectrum from van der Zee et al. (2003). The isomer shift and quadrupole splitting of each spectrum are indicated. Note that with the exception of pyrite, Fe (II) phases typically show a more positive isomer shift (position of center of doublet relative to zero velocity) and larger quadrupole splitting (distance between two peaks of a doublet on the velocity axis) than Fe (III) phases. (b) RT Mössbauer ^{57}Fe spectra from this study. Spectra have been trimmed and normalized, and all spectra are presented in the same orientation for visual intercomparison. Spectra from Station A 0–1 cm and Station D 0–1 cm were collected in backscatter mode, hence the troughs correspond to backscatter emission maxima. All other spectra were collected in transmission mode. See Supplementary Fig. 2 for complete original spectra in true orientation, including 6-line standards. The subspectra used in the model fit for each bulk spectrum are shown in the legend. Relative spectral areas of each component are given in Table 4.

Formatted: Superscript

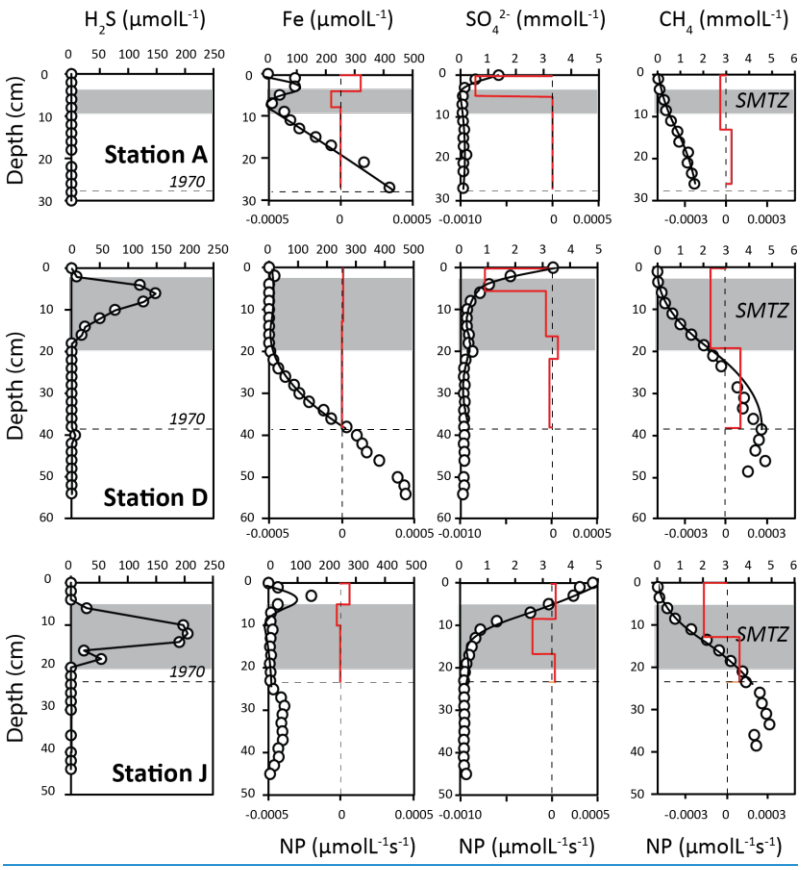

Formatted: Centered

Formatted: Left

Formatted: Subscript

Figure 8. Pore water data from Stations A, D and J. Hydrogen sulfide (H_2S) data are connected point-by point. The depth of the H_2S peak is used to define the sulfate-methane transition (SMTZ). Where no H_2S is present (i.e., at Station A), the SMTZ is defined by the corresponding minimum in pore water Fe. For all other parameters, parabolic best fit lines were generated using PROFILE. These fits were used to determine the zones, and instantaneous rates, of net production (NP) of each species within the depth interval 1970–2015 (red lines). The rate of net production is

determined from the change in gradient of the concentration as described by equation 8. Negative rates indicate net consumption.

Formatted: Centered

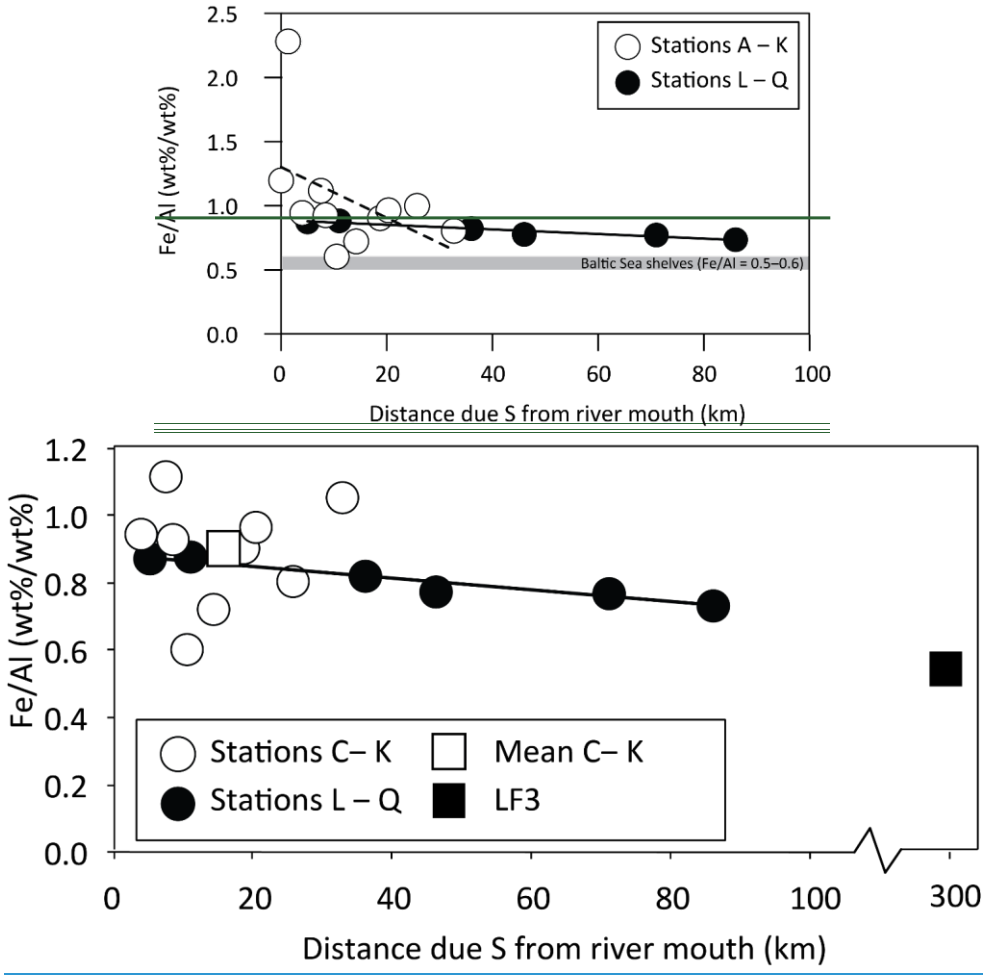
Stations A – K
Stations L – Q
Fe/Al (wt%/wt%)
Baltic Sea shelves (Fe/Al = 0.5–0.6)
Distance due S from river mouth (km)
Stations C– K
Mean C– K
Stations L – Q
LF3
Fe/Al (wt%/wt%)
Distance due S from river mouth (km)

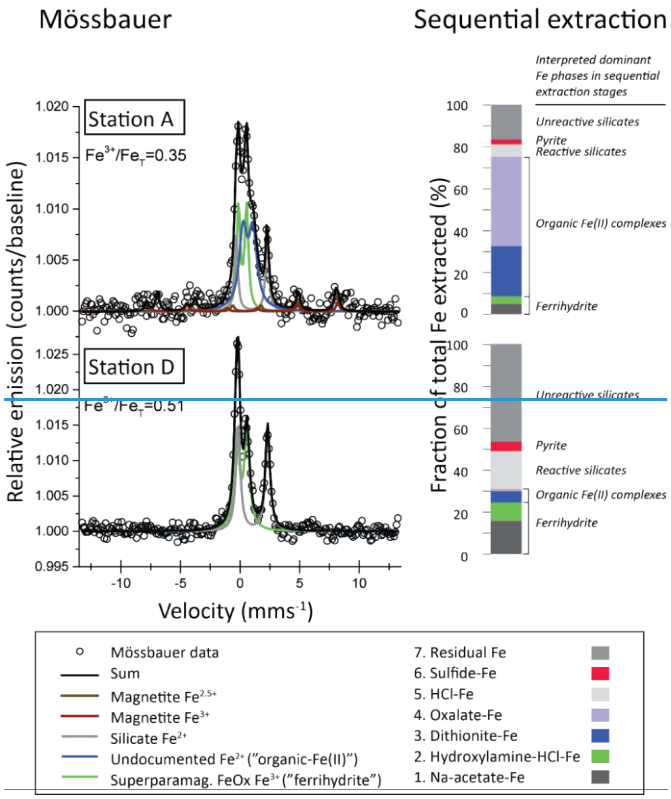

Figure 9. Fe/Al weight ratios for surface sediment samples along the Mustionjoki transect (0–2 cm; Stations C–K) and Paimionjoki transect (0–1 cm; Stations L–Q), plotted against distance from the respective river mouth. Stations A and B have been removed from the analysis due to the influence of industrial Fe pollution (see text). Linear regression line is shown for the Paimionjoki transect. Typical values from a site on the Baltic Sea shelves (LF3, Eastern Gotland basin Fe/Al =0.5–0.6, Lenz et al., 2015) are shown for comparison. LF3 is given an arbitrary distance of 300 km from the river systems of the southern coast of Finland, although Fe at this site may be sourced from more proximal landmasses.

~~**Figure 5. (left) Mössbauer spectra of powdered surface sediments (0–1 cm) from Stations A and D, sampled in 2015 (0.0 and 7.5 km respectively from the river mouth of the Mustionjoki transect). Sub-spectra of Fe-bearing sedimentary components (colored lines) were combined using a linear combination fitting (LCF) routine to generate a sum spectrum**~~

(black line) with the closest fit to the raw data (circles). Concentrations of each component, and Fe^{2+}/Fe_t ratios, were estimated from the LCF model. Mössbauer fitting parameters are listed in Table 3. (right) Sequential extraction results from the same samples, showing the complete speciation of Fe according to the method of Poulton and Canfield (2005) and an additional extraction for sulfide-bound Fe. The interpreted dominant Fe phases in each stage of the sequential extraction are given in the right column.

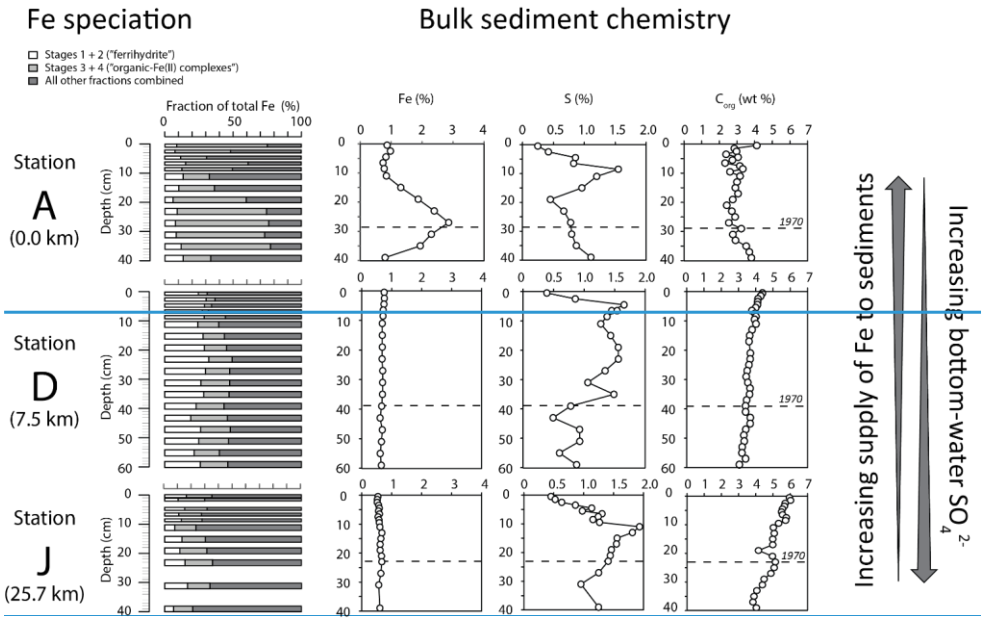

Figure 6. (left) Down-core operational Fe speciation for Stations A, D, and J (0.0, 7.5 and 25.7 km respectively from the river mouth of the Mustionjoki transect), derived from sequential extraction by the method of Poulton and Canfield (2005) and an additional extraction for sulfide-bound Fe. Thickness of bars corresponds to thickness of sampled interval (i.e. 1 or 2 cm). Note that not all depth intervals were sampled. (right) Down-core bulk chemical profiles from the same cores. Total Fe and S were determined by ICP-OES analysis of powdered sediments digested by $HF+HClO_4+HNO_3$, while C_{org} was determined by thermal combustion of powdered sediments (see text for further details). The depth interval corresponding to 1970 is estimated from the peak in concentrations of total lead (Pb_{tot}) as determined by ICP-OES (see Supplementary information).

Supplementary information

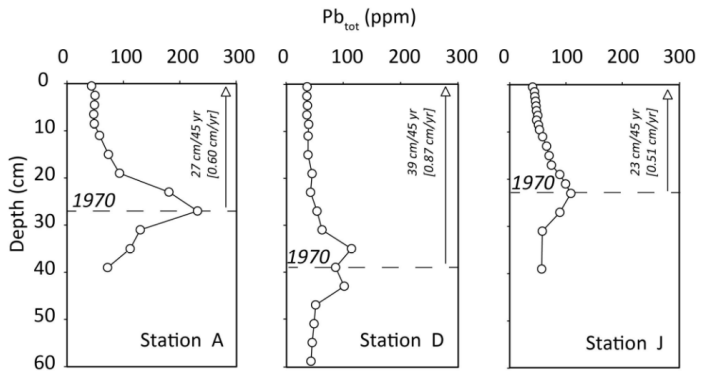

Supplementary Figure 1. Total lead (P_{tot}) concentrations in sediment cores from stations A, D and J in 2015, determined by ICP-OES. The peak in P_{tot} is assumed equivalent to the year 1970 (Zillen et al., 2012). Mean sedimentation rates for each core were estimated for the interval 1970-2015 as indicated in the panels.

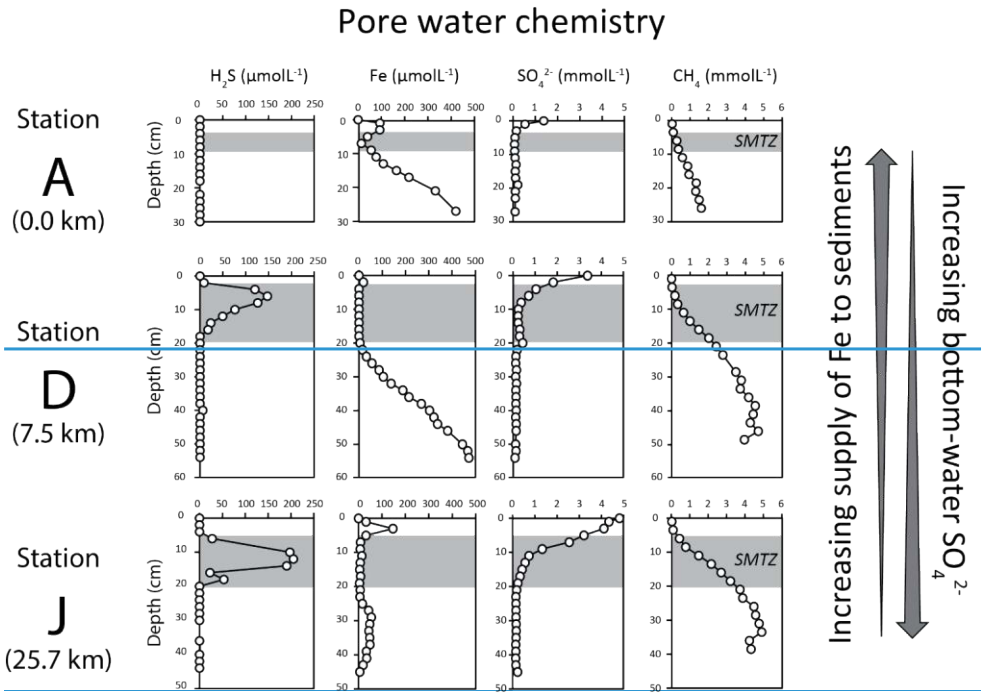

~~Figure 7. Pore water chemical profiles from Stations A, D and J (0.0, 7.5 and 25.7 km respectively from the river mouth of the Mustionjoki transect). See text for methodological details. SMTZ = Sulfate-Methane Transition Zone.~~

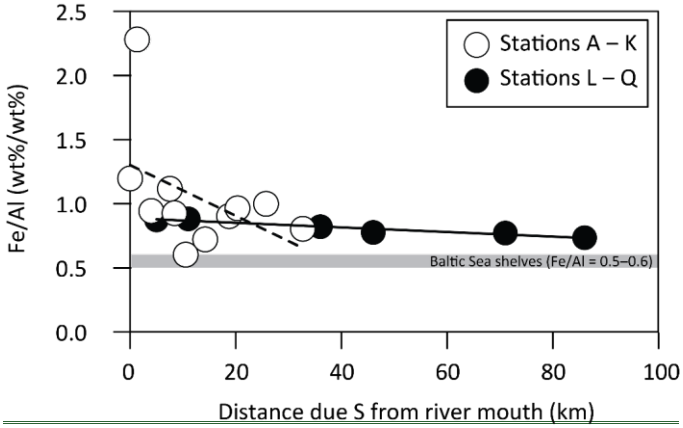
Stations A – K
Stations L – Q
Baltic Sea shelves (Fe/Al = 0.5–0.6)
Fe/Al (wt%/wt%)
Distance due S from river mouth (km)
2.5
2.0
1.5
1.0
0.5
0.0
0
20
40
60
80
100

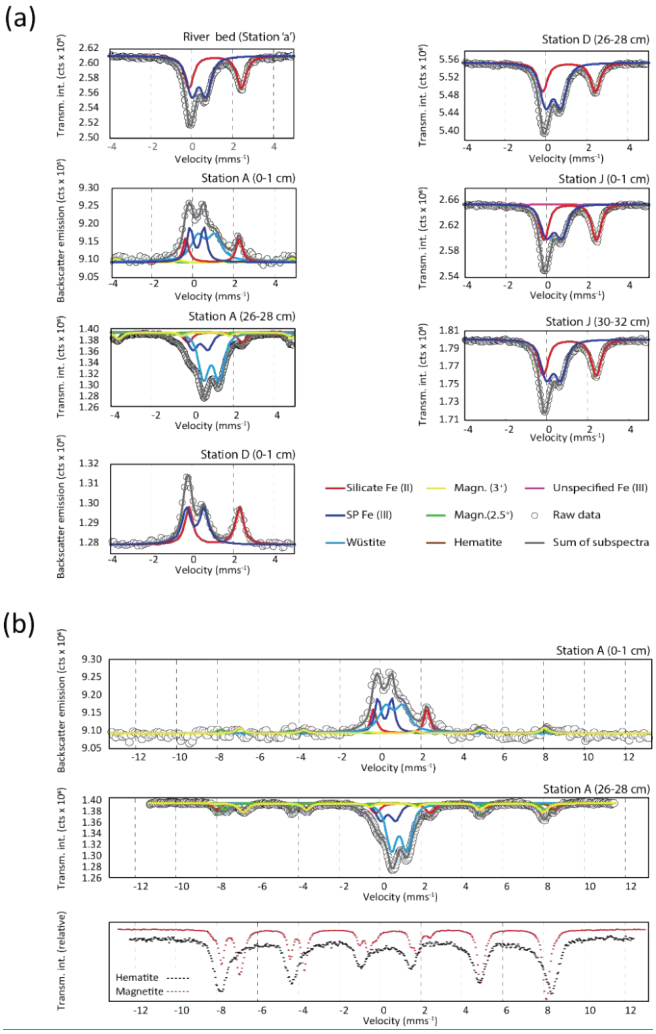

Formatted: Centered

Supplementary Figure 2. (a) Mössbauer spectra from all samples presented in true orientation. Samples from Station A (0-1 cm) and Station D (0-1 cm) were analyzed in backscatter mode. All other samples were analyzed in transmission

mode. (b) Expanded spectra from Station A, showing sextet components. Reference spectra for magnetite and hematite are reproduced by permission of M. Darby Dyer from the Mineral Spectroscopy Database of Mount Holyoke College.

~~Figure 8. Fe/Al weight ratios for surface sediment samples along the Mustionjoki (0–2 cm; Stations A–K) and Paimionjoki (0–1 cm; Stations L–Q) transects. Linear regression lines are shown for each transect. Typical values for surface sediments of the Baltic Sea shelves (Fe/Al =0.5–0.6, Eastern Gotland basin, Lenz et al., 2015) are shown for comparison.~~